Joint Centre for Mesoscale Meteorology, Reading, UK

Contributions to the Poster Session at the 1998 UWERN Annual Science Meeting

K. A. Browning, J.- P. Chaboureau
S. Clough, A. C. L. Deveson, R. S. Dixon
R. Forbes, T. D. Hewson, A. Illingworth
N. Keeley, H. Lean, C. Liu
A. Montani, M. Pedder, N. Roberts
N. Robertson, I. Roulstone, A. Semple
G. J. Shutts, O. Stiller, S. J. Swarbrick
A. J. Thorpe, A. White, G. Winter

Internal Report No. 105

August 1999

Met Office Joint Centre for Mesoscale Meteorology Department of Meteorology
University of Reading PO Box 243 Reading RG6 6BB United Kingdom
Tel: +44 (0)118 931 8425 Fax: +44 (0)118 931 8791
www.metoffice.com

Designed and produced by the Met Office © Crown copyright 2001 01/0240 The Met Office logo is a registered trademark.

Contributions to the Poster Session

at the

1998 UWERN Annual Science Meeting

by

K A Browning, J-P Chaboureau, Sid Clough, A C L Deveson, R S Dixon, Richard Forbes, T D Hewson, Anthony Illingworth, N Keeley, Humphrey Lean, Chun-Lei Liu, Andrea Montani, Mike Pedder, Nigel Roberts, Nicola Robertson, Ian Roulstone, Adrian Semple, G J Shutts, Olaf Stiller, S J Swarbrick, A J Thorpe, Andy White and G Winter

Assembled by

A A White

JCMM / Meteorological Office

August 1999

Summary

This Report records the scientific content of the JCMM/Met Office and Reading University contributions to the poster session of the Second UWERN Annual Science Meeting (UWERN = Universities WEather Research Network) held in Reading on September 7th and 8th, 1998.

Contents

Introduction	A A White	1
Mesoscale Prediction of Precipitation	Nicola Robertson and Mike Pedder	2
Differentiation of Hail and Rain Using Radar	Anthony J Illingworth and Chun-Lei Liu	6
Radar Measurements of the Developing Boundary Layer	Anthony Illingworth	11
Shear Production by Convection in the Absence of Large Scale Forcing	Olaf Stiller	16
Evidence of Sublimation-Driven Structure in FASTEX IOP 16	Sid Clough, Richard Forbes, Humphrey Lean and Nigel Roberts	24
FASTEX Secondary Wave Cyclone Development	J-P Chaboureau and A J Thorpe	28
The Christmas Eve Storm and its Associated Cloud Head – an NWP Representation of its Dynamics	R S Dixon, K A Browning and G J Shutts	36
Diagnostic Study of a Polar Low	G Winter and K A Browning	40
Conceptual Models of Cyclogenesis – a Unified Perspective	Adrian T Semple	48
A Classification Scheme for FASTEX Cyclones	A C L Deveson, K A Browning and T D Hewson	52
Use of Qualitative Structural Models in Quantitative Weather Prediction	Ian Roulstone, Adrian Semple and Andy White	59
Application of PV Inversion and Water Vapour Imagery in NWP	S J Swarbrick	67
Control Tests of PV Inversion on the UM Global Grid	N Keeley and A A White	71
Use of ECMWF Singular Vectors for Targeting during FASTEX	Andrea Montani and Alan J Thorpe	78
Whatever Happened to Stability Theory?	Andy White	83

Introduction

The second UWERN Annual Science Meeting was held in Reading on September 7th and 8th, 1998. The consensus in JCMM afterwards was that – during a successful and lively meeting – the poster session had been too short. There had not been time to give all the posters the attention they required, or to justify the effort that had gone into producing them. It was decided to assemble some sort of compendium, at least of the JCMM contributions, for local use and record.

To have produced an Internal Report which faithfully miniaturised the poster session material would have been expensive (principally because of the cost of colour copying) and would not necessarily have been a scientifically useful enterprise: the poster board and the A4 page are different modes of presentation. The aim, rather, has been to convey the science of the posters, using reduced original material where appropriate and newly-drafted material where necessary. Contributors were invited to provide an A4 version of their posters, subject to an upper limit of 8 pages for each paper; both portrait and landscape page orientations were declared acceptable. There was an exhortation to include colour diagrams only when absolutely necessary – and no undertaking that material submitted in colour would be included in colour.

The order of presentation reflects many considerations, of which the physical scale of the relevant phenomena is the most important. We start with the perspective of individual cumulonimbus clouds and rainfall catchments, and then work up through the mesoscale structure of mid-latitude weather systems to the scale of the weather systems themselves. Deviations from this order may be observed, and can be ascribed to various causes and influences; but papers on similar subjects generally do appear together.

When I began assembling material for this report, my intention was to complete its production within a few weeks of the UWERN meeting. Various factors – not least my unexpected departure from JCMM – made this intention wildly unrealistic (as, indeed, some wise colleagues foresaw at an early stage). Nearly a year has passed before I have found the time for the final production tasks. I regret this delay, and offer my apologies to contributors – especially to those (a clear majority) who submitted material in the requested form and met the original deadline! One may reasonably hope, however, that the appearance of this collection of poster papers a full month ahead of the 1999 UWERN Annual Science meeting (to be held in Aberystwyth on September 6th and 7th) will be timely as well as tardy.

A A White
Met Office
Bracknell
July 1999

Nicola Robertson and Mike Pedder
Department of Meteorology
University of Reading, RG6 6BB, UK
email swr97nr@met.reading.ac.uk

MESOSCALE PREDICTION OF PRECIPITATION

INTRODUCTION

The overall objective of this research project is to quantify and improve understanding of the factors influencing the accuracy of predicted precipitation on the mesoscale. This is investigated from an atmospheric water balance perspective using mesoscale model data and an observational dataset.

The observational data are from a dense network of rain gauges covering a small river catchment in Somerset. The raingauges were set up as part of HYREX (HYdrology and Radar EXperiment) run by the Institute of Hydrology. These data are used as a verification tool for assessing the accuracy of precipitation predicted by the mesoscale version of the UKMO Unified Model.

Model data are averaged over a single grid box (17km x 17km) which is slightly larger than the Brue river catchment. However both datasets have a time resolution of 15 minutes allowing reasonable comparison.

The data analysis presented here is from an example case study of a cold front producing significant precipitation across the British Isles on 6th November 1996.

Figure 1 - Location of Brue catchment

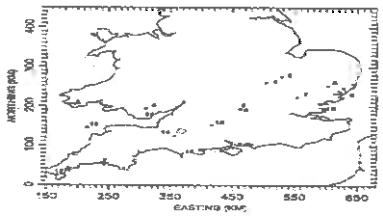

MOISTURE BUDGET THEORY

For a precipitating atmosphere, we assume the simplified form of the atmospheric water balance equation:

$$\underline{P} = \frac{\partial}{\partial t}\bar{q} + \overline{\nabla\bullet(\underline{v}q)}$$

where $\underline{P}$ is surface precipitation rate (kg m^{-2} s^{-1}), q the specific humidity and $\underline{v}$ the horizontal wind velocity (ms^{-1}); the overbar indicates vertical integration through the whole of the atmospheric column. (This ignores terms involving evaporation, changes in liquid storage and liquid water advection.)

The moisture flux divergence term can be written as the sum of advection and wind divergence terms:-

$$\overline{\nabla\bullet(\underline{v}q)} = \overline{\underline{v}\bullet\nabla q} + \overline{q\nabla\bullet\underline{v}}$$

Moisture budget analysis involves looking at the relative magnitudes of these components, both as time series of column integrals and also as vertical profiles averaged over the peak precipitation period.

6th NOVEMBER 1996

The synoptic situation at 00z on 6th November featured a low centred just west of northern Scotland with a long cold front curving through Scotland and out towards the Atlantic. The front passed over the Brue catchment at approximately 0415. Figure 2 shows the distribution of rain intensity across the model subdomain at this time. Fronts are most easily identified from sharp gradients in wet bulb potential temperature (theta w). The 900mb field shows the front clearly (Figure 3).

Figure 2

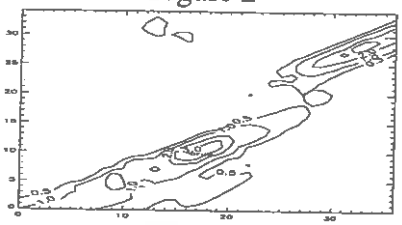

Figure 3

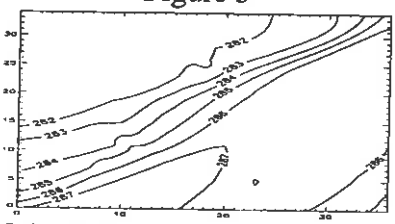

In order to assess the accuracy of the timing and intensity of the model predicted precipitation, rain intensity time series were plotted for both the Brue catchment (from rain gauge measurements) and for the model grid box centred on the Brue catchment.

Figure 4

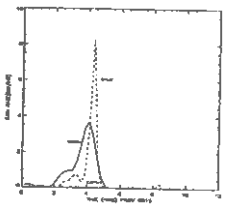

In this case the model has tended to spread the precipitation in time i.e the predicted rain was less intense but of longer duration than the observed rain at Brue. This agrees with results from another case studied by Pedder et al. (1997). Note also that the precipitation is almost entirely a result of large scale dynamical processes and the convective component of the model precipitation is negligible.

Figure 5

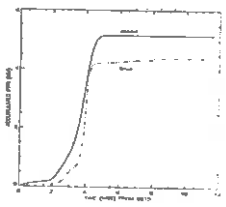

The model predicted the total rainfall to be just over 5mm which is a slight overprediction of approx. 0.7mm compared with the Brue data. However this example shows that the model is capable of predicting catchment rainfall totals to a reasonable degree of accuracy.

MOISTURE BUDGET ANALYSIS

The moisture budget equations mentioned earlier are for a fixed frame of reference with the x and y axes pointing eastwards and northwards respectively. In order to investigate the across/ along frontal components for a diagonally orientated front, it is necessary to rotate these axes so that the y axis lies parallel to the major frontal axis. Also, it is of more use to look at the components in a frame of reference moving with the system to eliminate any large advection terms due to changes in air mass across the front. This was done by subtracting an estimated system velocity from the cross frontal component of velocity in the moisture budget equations.

Below is a time series plot of the moisture budget contributions vertically integrated through the atmospheric column.

Figure 6

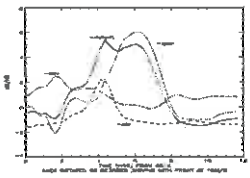

The advection term dominates Dq/Dt before the onset of rain and the wind divergence term is convergent only during precipitation. The local tendency term in the post-frontal period is significant showing a decrease in specific humidity as the cold dry air moves in behind the front.

The moisture advection and wind divergence contributions are then split between the across and along front components.

Figure 7

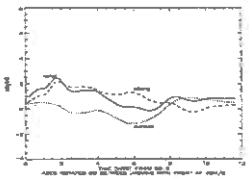

The across front component is negligible throughout the frontal passage. However there is a significant contribution from moisture advection along the front just prior to the onset of rain, suggesting that southerly moisture advection is 'feeding' the precipitation system. This agrees with current conceptual models of frontal cyclones such as those by Browning (1995) or Young (1994) which feature a warm conveyor belt (high theta w) moving approximately parallel to the front.

Figure 8

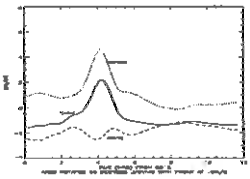

The frontal precipitation coincides almost exactly with the across front wind convergence component. However the total convergence is reduced by an along front divergent component. Because of this reduction, the contribution as a column integral is comparable in magnitude to the advection contribution.

Since fronts are inclined in the vertical, the components directly related to frontal dynamics are confined to the lower layers of the atmosphere. Column integrals may therefore be misleading and vertical profiles of the contributions are clearly necessary for a detailed analysis. These have been averaged over a 90 minute period coinciding with the peak rainfall.

Figure 9

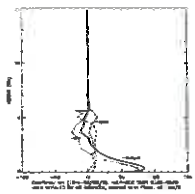

In contrast to the column integral time series, these vertical profiles highlight the variations in relative magnitudes of the moisture budget components within different layers of the atmosphere. This profile shows that the largest contribution is from the horizontal wind divergence term and is confined mainly to the lowest 1.5 km of the atmosphere. High vertical resolution within the boundary layer is therefore crucial to accurate precipitation forecasting.

Figure 10 shows that the advection component across the front is insignificant (in a system-following frame of reference) and the total moisture advection profile is entirely dependant upon variations in the along front
moisture gradient.

This contribution is significant throughout the lowest 4 km although figure 9 showed the Dq/Dt contribution to be confined to the lowest 1.5 km. This is due to the dominance of the wind convergence component which is confined to a shallower depth. The wind convergence is dominant in the across front direction, as might be expected. However there is significant along front wind divergence throughout the lowest 2km, reducing the total contribution.

Figures 10 and 11

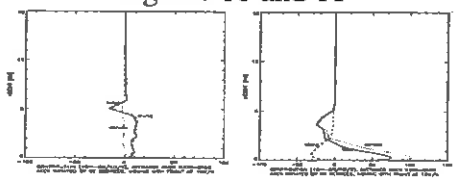

These contributions can be converted into units of equivalent precipitable water and plotted as vertical profiles of column integrals.

Figure 12

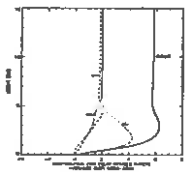

The contributions to precipitable water by the advection, wind convergence and local tendency terms are all approximately equal above 5 km. However, in the lowest 2 km where frontal processes dominate, the wind convergence term clearly provides the major contribution. Note that in a fixed frame of reference, the contribution from moisture advection becomes insignificant due to cancellation by the cross-frontal advection of the drier air mass.

SUMMARY OF OBSERVATIONS

- Catchment scale precipitation can be predicted numerically to a reasonable degree of accuracy for predominantly large scale precipitation processes.
- The largest contribution to frontal precipitation is from cross-frontal wind convergence in the lowest 1.5 km of the atmosphere, implying high boundary layer resolution is essential for accurate precipitation forecasting.
- In a system-following frame of reference, moisture advection is important just prior to the onset of rain, decreasing throughout the precipitation period. This is in a direction parallel to the front and is consistent with warm conveyor belt theories.
- The wind convergence provides a shallow but large contribution to precipitation whereas moisture advection provides a smaller contribution extending over a greater depth. As column integrals they are of comparable magnitude.

FURTHER WORK

The short-term aim is to carry out a number of case studies in order to assemble a composite model representing frontal precipitation. This model will then be used to perform a sensitivity analysis on the various components of the moisture budget to assess which factors have the greatest influence on the accuracy of predicted precipitation.

References

Browning, K.A. and Roberts, N.M., 1996, Variation of frontal and precipitation structure along a cold front, *Q.J.R. Meteorol. Soc.*, **122**, pp1845-1872.

Pedder, M.A., Haile, M. and Thorpe, A.J., 1997, Short period forecasting of catchment-scale precipitation. Part I: The role of numerical weather prediction, *HYREX Special Issue, Hydrology and Earth Systems Science.*

Differentiation of Hail and Rain Using Radar

Anthony J. Illingworth and Chun-Lei Liu

JCMM, Dept. of Meteorology, University of Reading
Reading RG6 6BB, UK

1. THE PROBLEM

Radars measure radar reflectivity, Z, but we often want the rainfall rate R.

$Z = \sum N D^6$ where N is the concentration of raindrops of size D.

Z measured in $mm^{-6}m^3$ or dBZ=10logZ.

Converting Z to R depends on raindrop size distribution but use an empirical relationship of the form $Z = 200R^{1.6}$.

Echo of Z=60dBZ (=10^6 $mm^{-6}m^3$) could be:
Rainfall of 200mm/hr — risk of flash flooding.
OR One cm sized hailstone per cubic meter — low rainfall.

2. SOLUTION

A radar which can transmit (and receive) vertically and horizontally polarised radiation, provides two parameters related to the shape of the hydrometeors — and then exploit the fact that large raindrops are oblate spheroids falling with their minor axis in the vertical, and hailstones are oblate but tend to tumble as they fall. Two validation examples observed with the Chilbolton S-band radar are presented here.

3. THE TWO NEW PARAMETERS

i) Differential reflectivity $Z_{DR} = 10\log\left(\frac{Z_H}{Z_V}\right)$

The difference in reflectivity measured with horizontal (Z_H) and vertical polarisation (Z_V).

For heavy rain, large oblate raindrops $Z_H > Z_V$, so Z_{DR} is positive. (and magnitude of Z_{DR} provides an estimate of the mean D of the rain)
For tumbling hail $Z_H = Z_V$ so Z_{DR}=0.

D=1mm	D=3mm	D=6m
Z_{DR}=0dB	Z_{DR}=1.54dB	Z_{DR}=4.43dB

SO Can we recognise hail from high Z but zero Z_{DR} whereas rain has high Z and positive Z_{DR} ?

BUT This will fail if we have a mixture of rain and hail AND hail tends to be oblate thus proving it doesn' t tumble completely randomly as it falls so that Z_{DR} may not be quite zero.

ii) Specific differential phase shift K_{DP}

In heavy rain the oblate raindrops result in the speed of the horizontally polarised radar wave being slower than that of the vertically wave.

If our radar is Dopplerised then the phase of the horizontally polarised wave (ϕ_H) lags more and more behind that of the vertically polarised wave (ϕ_V) as the wave moves through heavy rain.

If we define K_{DP} as the increase in (ϕ_H - ϕ_V) in degrees per kilometre then we find that K_{DP} is related to the rainfall

$$K_{DP} = 0.0122\, R^{1.38}$$ (for a 10cm radar)

If hailstones tumble then they have the same effect on ϕ_H and ϕ_V and so do not contribute to K_{DP} in theory.

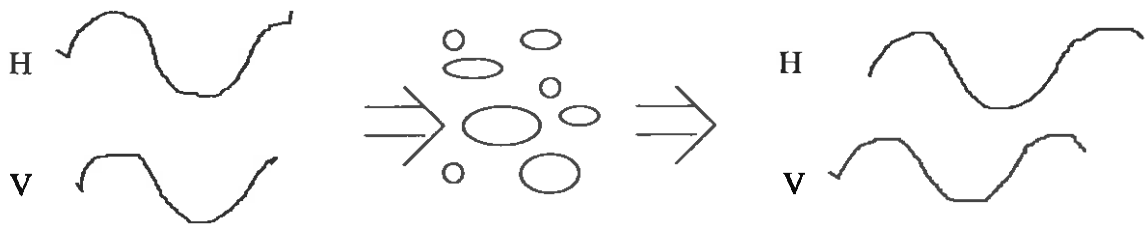

4. USE Z_{DR} AND K_{DP} TO DETECT HAIL

Both Z_{DR} and K_{DP} depend upon oblate raindrops - that is their size. Much recent research has concentrated on combining Z_{DR}, K_{DP} and Z to provide better estimates of R. Z_{DR} and K_{DP} providing information on the raindrop size distribution.

It transpires that Z_{DR} and K_{DP} are not independent. Naturally occurring raindrop size distributions can be described by a gamma function of the form:

$$N(D) = c\,D^{m}e^{-LD} \qquad \text{where } L = \frac{3.67+m}{D_o}$$

It might be thought that with the three variables Z, Z_{DR} and K_{DP} one could deduce the three unknowns in the spectra c (related to the total concentration), D_o (the mode volume diameter) and m (the shape of the distribution).

But in fact it turns out that K_{DP}/Z is an unique function of Z_{DR}. This is a coincidence which occurs because of the precise shape of naturally occurring raindrops.

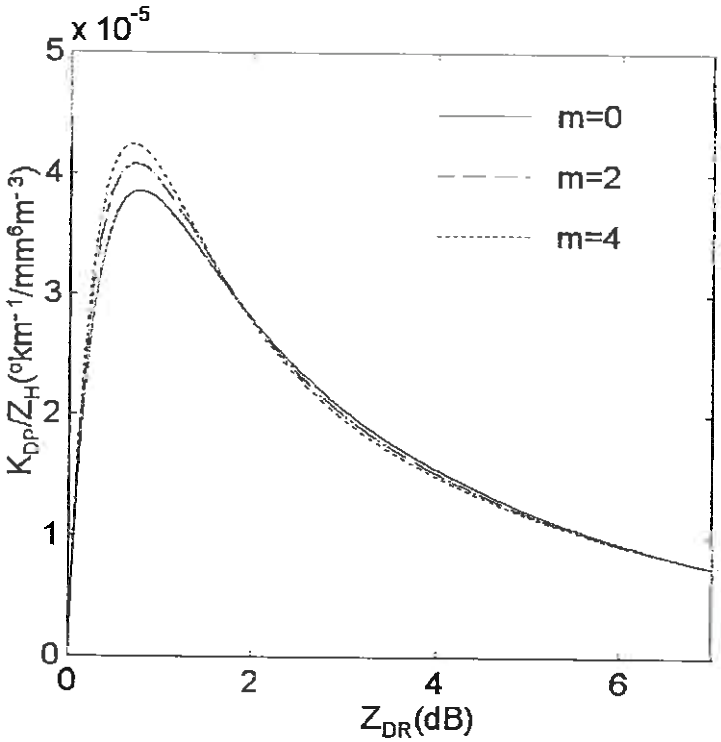

The detection algorithm, then, exploits this redundancy:

i) Using the observed value of Z and Z_{DR} at each gate calculate K_{DP} at that gate.

ii) Add up the phase shift at each gate from the theoretical K_{DP} and calculate the total differential phase shift along the ray.

iii) Compare the theoretical total phase shift with the observed value. This is 'DIF' in figures. If they agree it is rain; where they diverge hail is present. Where 'DIF' rises from 0° to 15° in figures identifies hail

Case I: **10 July 95** **Hail Storm**

High Z region > 60dBZ —— 200mm/hr Rain or Hail ?
'DIF' is theoretical rain phase shift compared to observed shift.
'DIF' changes from 0 ° to 15° (black) at 34km N / 27km E, the place around the Tilehurst, Reading, where ground truth confirms the present of hails with the typical size of 2cm in the major axis.

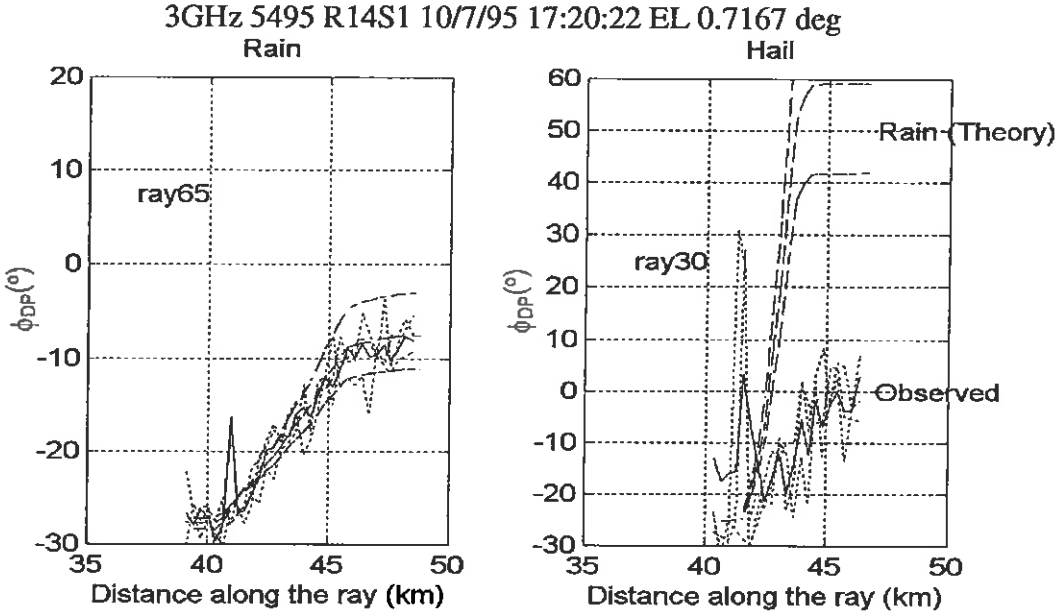

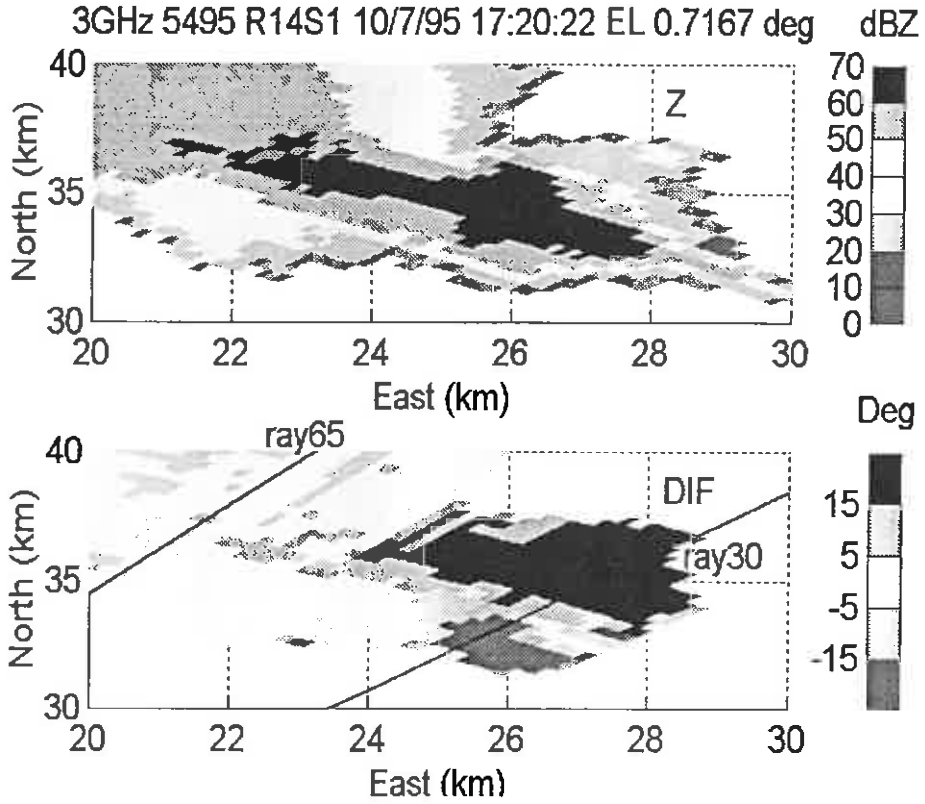

Case II: **The Reading Tornado Storm —— 13 June 98**

Black Z ~ Very Heavy Rain or Hail ?
'DIF' goes from 0 ° to 15° at 32km N / 28km E.
∴ Hail over M4 service at 16:57 GMT.

The storm was moving from west to east. At 17:10 GMT, 150mm/hr rainrate was recorded in the Meteorological Departmet, University of Reading. The observations of hails are reported via an email survey. The typical size of the hail is less than the pea size. In the plot, 'H'=hails observed, 'R'=rain only, '*'=Reading university campus, and 'o'=Reading city centre.

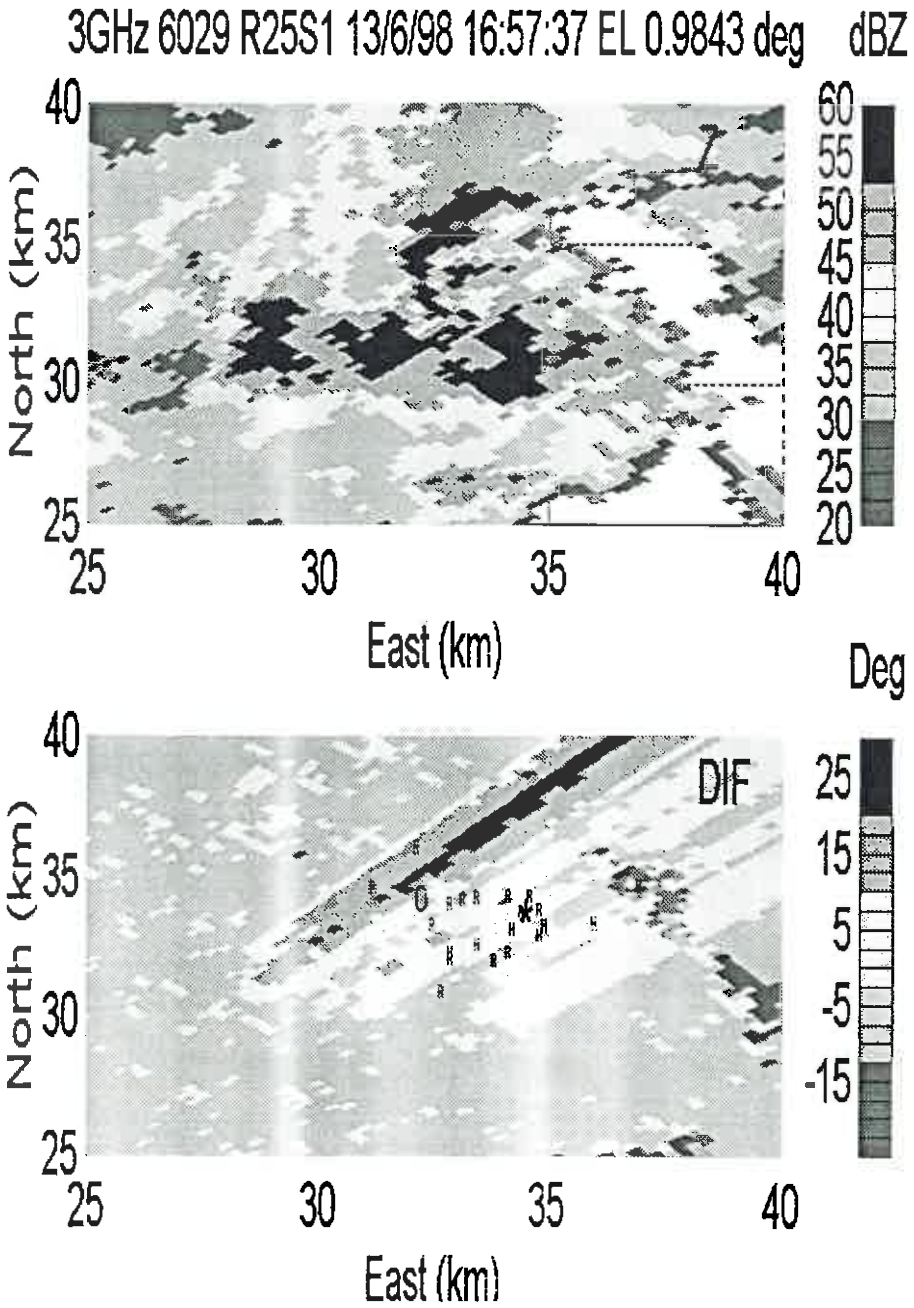

RADAR MEASUREMENTS OF THE DEVELOPING BOUNDARY LAYER.

ANTHONY ILLINGWORTH

JCMM, DEPT OF MET, U OF READING.

CLEAR AIR RADAR.

CLEAR AIR RADAR ECHOES RELY ON BRAGG SCATTERING FROM INHOMOGENEITIES IN REFRACTIVE INDEX ON THE SCALE OF HALF OF THE RADR WAVELENGTH.

THESE INHOMOGENEITIES ARE DUE TO FLUCTUATIONS IN TEMPERATURE.

RADAR CROSS SECTION PER UNIT VOLUME η GIVEN BY:

$$\eta = 0.38 \; C_N^2 \; \lambda^{-1/3} \qquad m^{-1}$$

where C_N^2 , the structure constant, is a measure of the index fluctuations.

WIND PROFILERS OPERATING AT 450 OR 950MHZ (75 or 35cm) RELY ON BRAGG SCATTERING WHICH IS ALWAYS PRESENT IN THE FREE ATMOSPHERE.

PRECIPITATION RADAR

THIS SHOULD BE CONTRASTED WITH THE RADAR CROSS SECTION PER UNIT VOLUME DUE TO RAYLEIGH SCATTERING BY PRECIPITATION:

$$\eta = \pi^5 \; \lambda^{-4} \; Z \qquad m^{-1}$$

where $Z = \Sigma \, N \, D^6$.

FOR CM WAVELNGTH RADAR THIS SIGNAL USUALLY DOMINATES.

CHILBOLTON RADAR

10CM WAVELENGTH CHILBOLTON RADAR CAN DETECT BOTH BRAGG SCATTERING AND RAYLEIGH SCATTERING FROM PRECIPITATION.

BRAGG ECHOES CAN BE DETECTED IN THE SUMMER TIME BOUNDARY LAYER.

TWO COLOUR PICTURES SHOW DEVELOPING BOUDARY LAYER ON 17 JULY 1992 LOOKING EAST FROM CHILBOLTON.

* ECHO INTENSITY MUCH BELOW THAT OF PRECIPITATION.

* TOP OF THE BOUNDARY LAYER IS IN GREEN ECHO Z ABOUT 0dBZ.

* TOP OF THE B L HAS WAVES WITH LAMBDA ABOUT 5KM.

* TOP OF THE B L AT 2KM - RISES DURING THE DAY.

* DOPPLER SHOWS INCREASING WESTERLY WIND WITH HEIGHT

* ABOVE THE BL WEST WIND ABOUT 20 M/S

* BELOW THE BOUNDARY LAYER 10 M/S

* HORIZONTAL SHEAR: 10M/S IN 2KM i.e. 0.005 /S

* POLARISATION ECHO SHOWS SOME AREAS OF HIGH ZDR (p14)

* ZDR = 10 LOG (ZH/ZV)

ZH IS REFLECTIVITY FOR HORIZONTAL POLARISATION
ZV IS REFLECTIVITY FOR VERTICAL POLARISATION

* BLACK ZDR: ZH>>ZV WINGED INSECTS GIVE ZH>>ZV

* BLUE ZDR = 0dB ZH = ZV - FROM ISOTROPIC TURBULENCE.

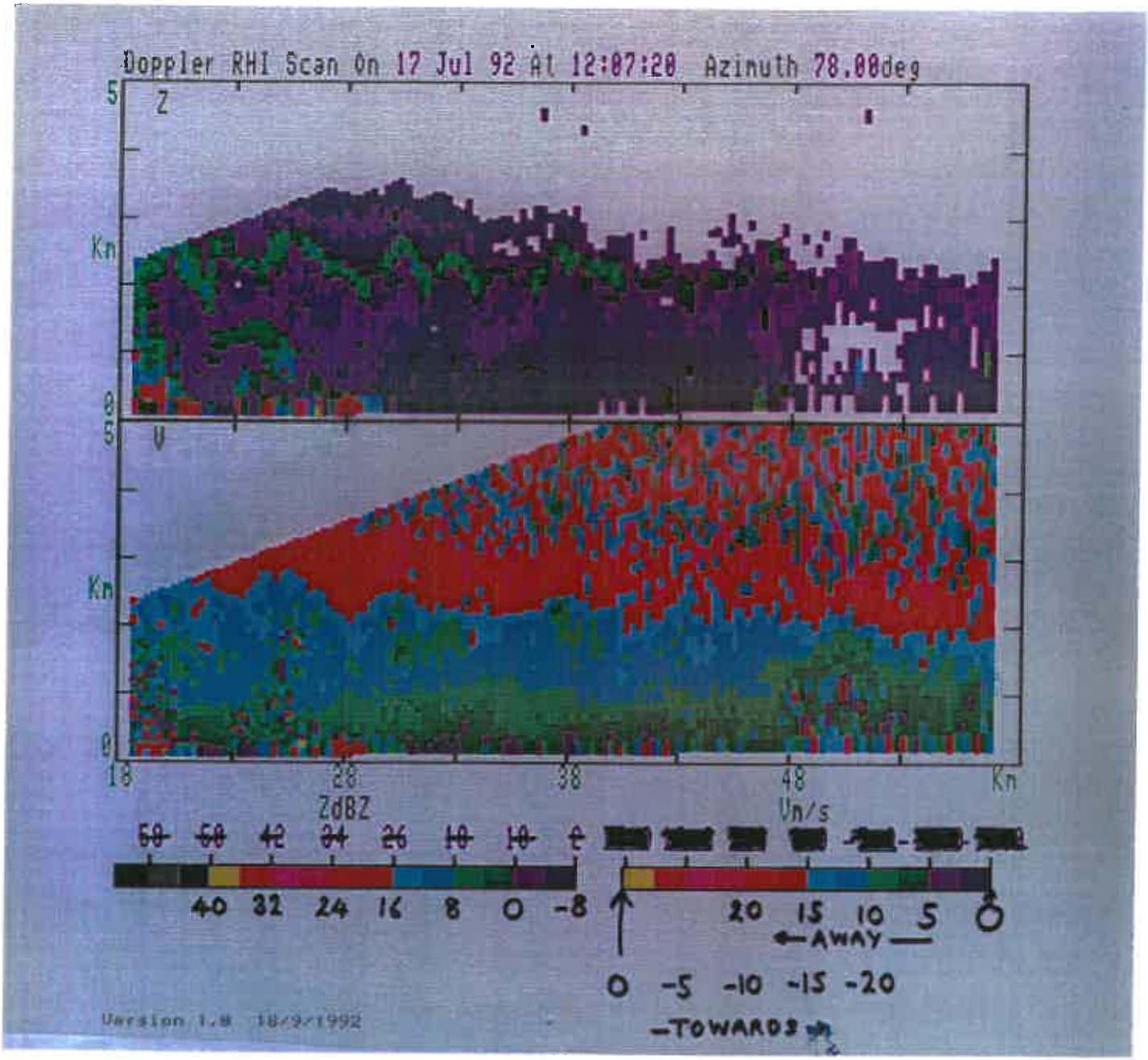
Doppler RHI Scan On 17 Jul 92 At 12:07:20 Azinuth 78.00deg
Z
Km
V
Km
18
28
38
48
Km
ZdBZ
Vm/s
40 32 24 16 8 0 -8
20 15 10 5 0
AWAY
0 -5 -10 -15 -20
TOWARDS
Version 1.8 18/9/1992

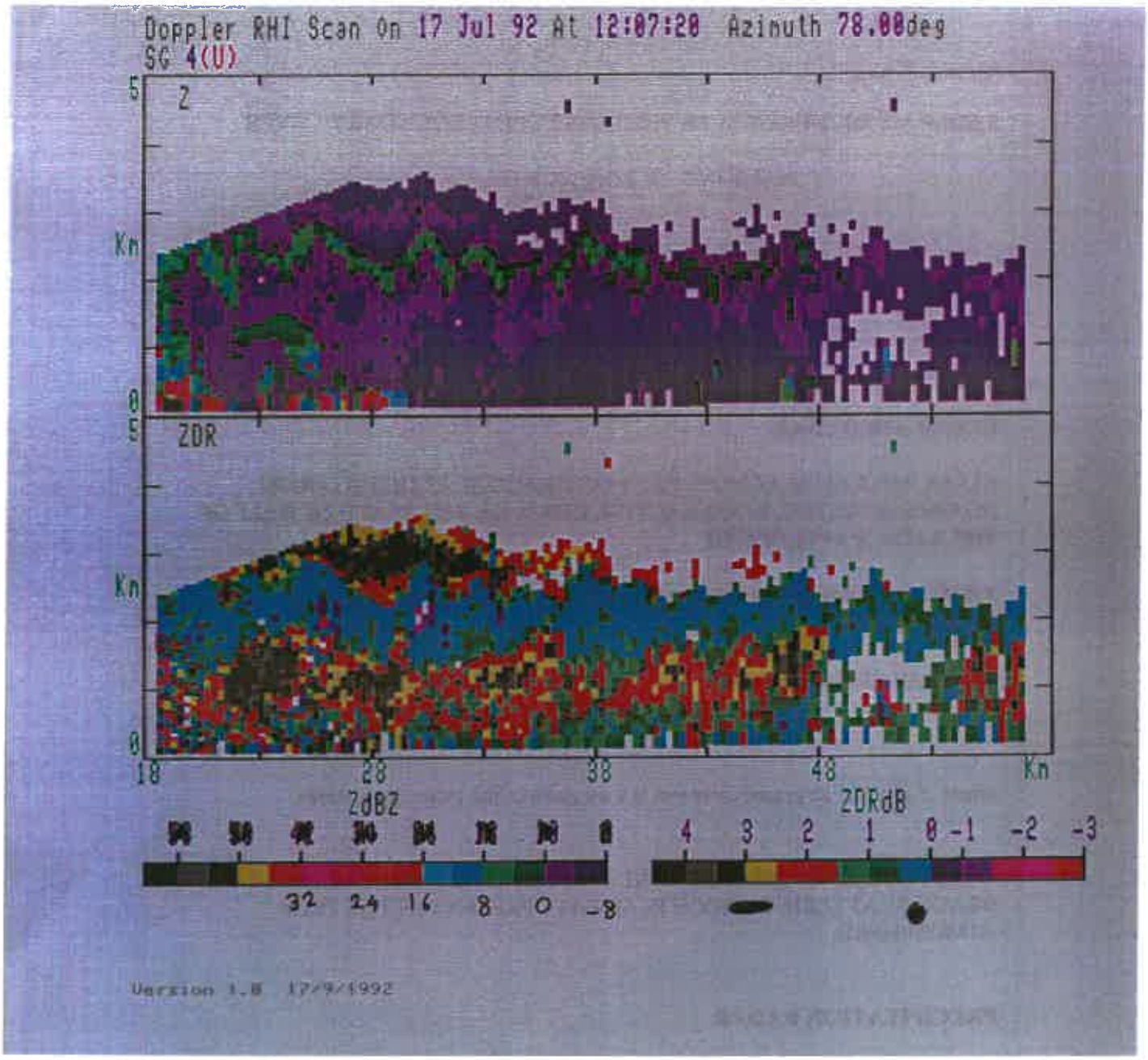
Doppler RHI Scan On 17 Jul 92 At 12:07:20 Azimuth 78.00deg
SC 4(U)
Z
Kn
ZDR
Kn
18
28
38
48
Kn
ZdBZ
32 24 16 8 0 -8
ZDRdB
4 3 2 1 0 -1 -2 -3
Version 1.8 17/9/1992

CHILBOLTON RADAR IS A POWERFUL TOOL FOR STUDYING THE DEVELOPMENT OF THE BOUNDARY LAYER ON SUMMER DAYS OVER SOUTHERN ENGLAND.

POSSIBLE PROJECTS:

* COMPARE HEIGHT OF BL WITH HEIGHT IN UNIFIED MODEL.

* COMPARE HEIGHT VARIATIONS AND TOPOGRAPHY FOR DIFFERENT WIND FIELDS.

* ?????

FOR A UKMO PILOT PROJECT CALLED 'DROP' THIS AUGUST AND SEPTEMBER THE CHILBOLTON RADAR IS TAKING TIME SERIES SEQUENCES OF VERTICAL SCANS THROUGH THE DEVELOPING BOUNDARY LAYER.

IS THERE A B L EXPERT WHO WOULD LIKE TO LOOK AT THIS DATA?

IF SO CONTACT EMAIL a.j.illingworth@reading.ac.uk

Shear production by convection in the absence of large scale forcing

by Olaf Stiller, Department of Meteorology, University of Reading

Summary

This poster yields results from a 3d study using the Met. Office large eddy model to investigate the effect of convection on the horizontal momentum budget. While a lot of attention has been paid to highly organized systems with strong wind shear like squall lines or convective storms this study focuses on systems with no or weak shear. As a striking feature we observe a zigzag instability that leads to a strongly oscillatory transport of horizontal momentum. The production of large-scale shear (which has been observed by earlier investigations) therefore appears as a slow systematic tendency of a strongly fluctuating quantity. These strong fluctuations make it difficult to trace back cause and effect of the large-scale shear production.

The first part of the poster illustrates the zigzag instability which actually is a common feature of many types of buoyancy-driven motion. The second part shows some results from simulations of convection in a weak-shear environment. Observed is a systematic increase of the low-level shear while the net tendency in the upper levels is obscured by the oscillatory nature of the momentum flux.
So far most simulations were performed in an atmosphere that is 98% saturated everywhere (initial condition). When repeating some runs with a dryer upper troposphere, convection is found to stop at lower levels (which might be expected from the stronger loss of buoyancy through mixing) while the zigzag instability appears to be unchanged or even enhanced in a dryer environment.

Zig Zag Instability creates vertical shear on a small scale

Buoyancy driven rising or falling objects do not always move on a straight line. A frequent phenomenon is the zigzag instability which for falling paper (Fig. 1) or buoyant bubbles (Fig. 2) can be shown to scale with an appropriately defined Froude or Reynolds number, respectively. The same kind of instability is observed in our simulations of a warm bubble imposed in an atmosphere which is weakly unstable to moist convection (Fig. 3a and b). The instability seems to be enhanced when the environment is dryer so that mixing processes lead to a stronger loss of buoyancy (Fig. 4).

Objectives:
How does this zigzag instability affect mixing processes?
How does the zigzag instability depend on Reynolds number, moisture, microphysics? Is there a simple scaling law?

Fig. 1: Vortices behind a falling strip of paper (from A. Belmonte, H. Eisenberg and E. Moses, Physical Review Letters 81 pp. 345-358, 1998).

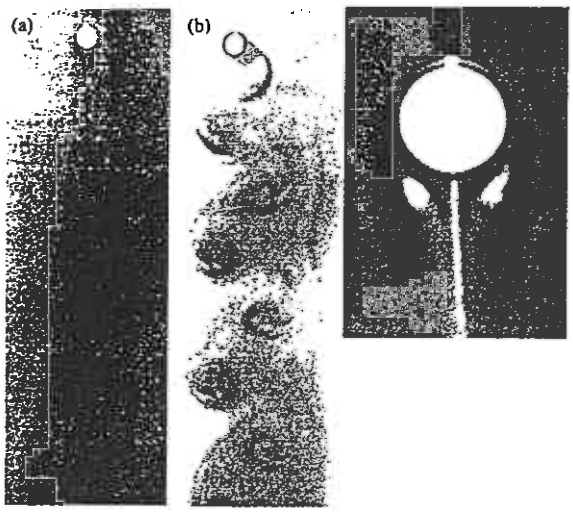

Fig. 2: Wake structure behind rising bubbles for Reynolds numbers where the motion is stable (a,c) and unstable (b) with respect to zigzag instability. (from E. Kelley and M. Wu Physical Review Letters 79 pp. 1265-1268, 1997).

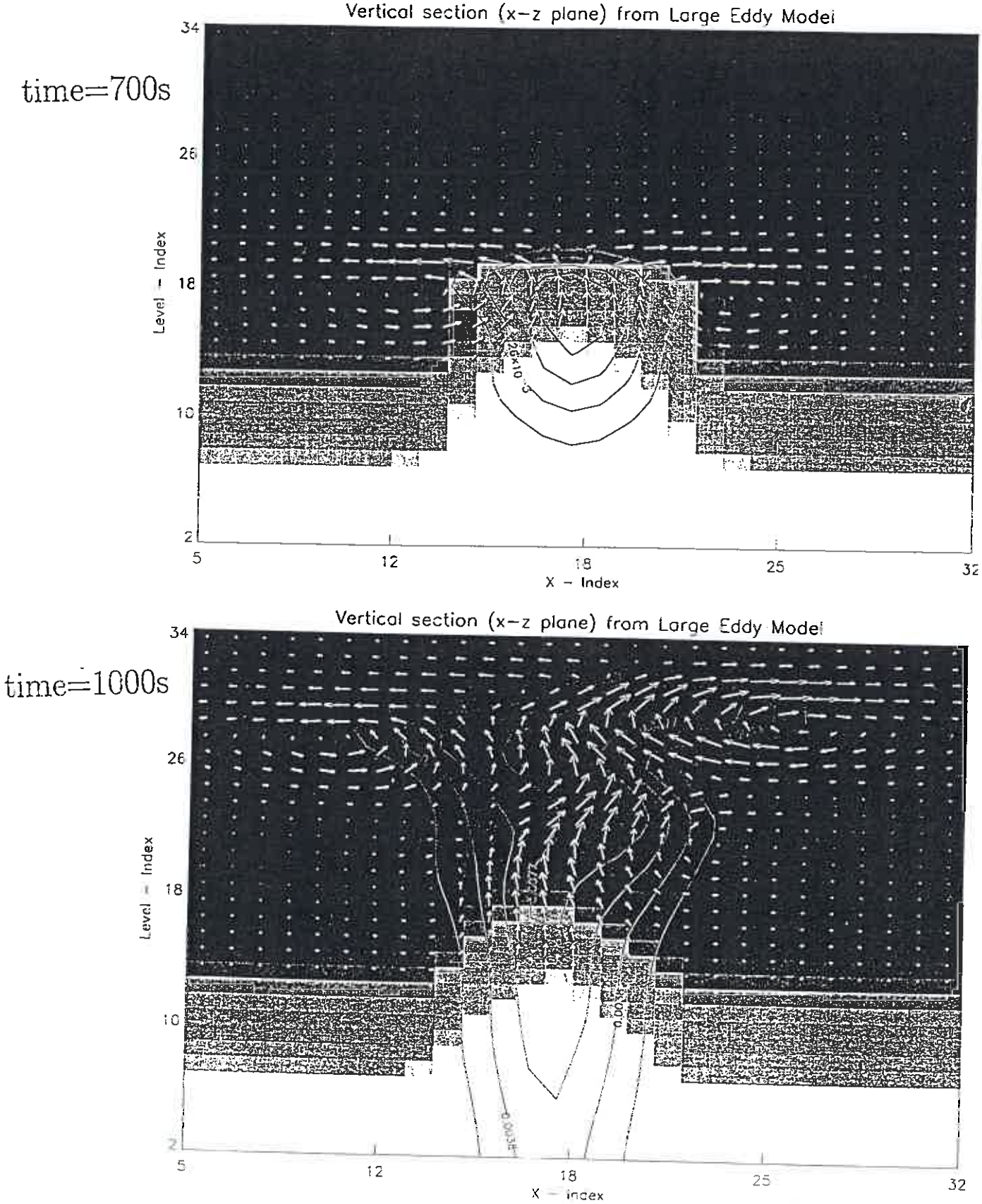

Fig. 3: Zigzag instability occuring in a (simulated) moist atmosphere (relativehumidity: 98%). Colours show the total water content, arrows the velocity field. Contours the mixing ratio of rain drops.

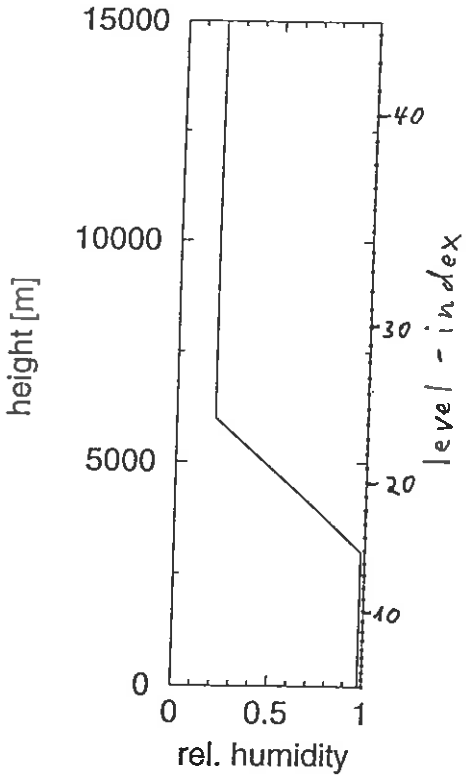

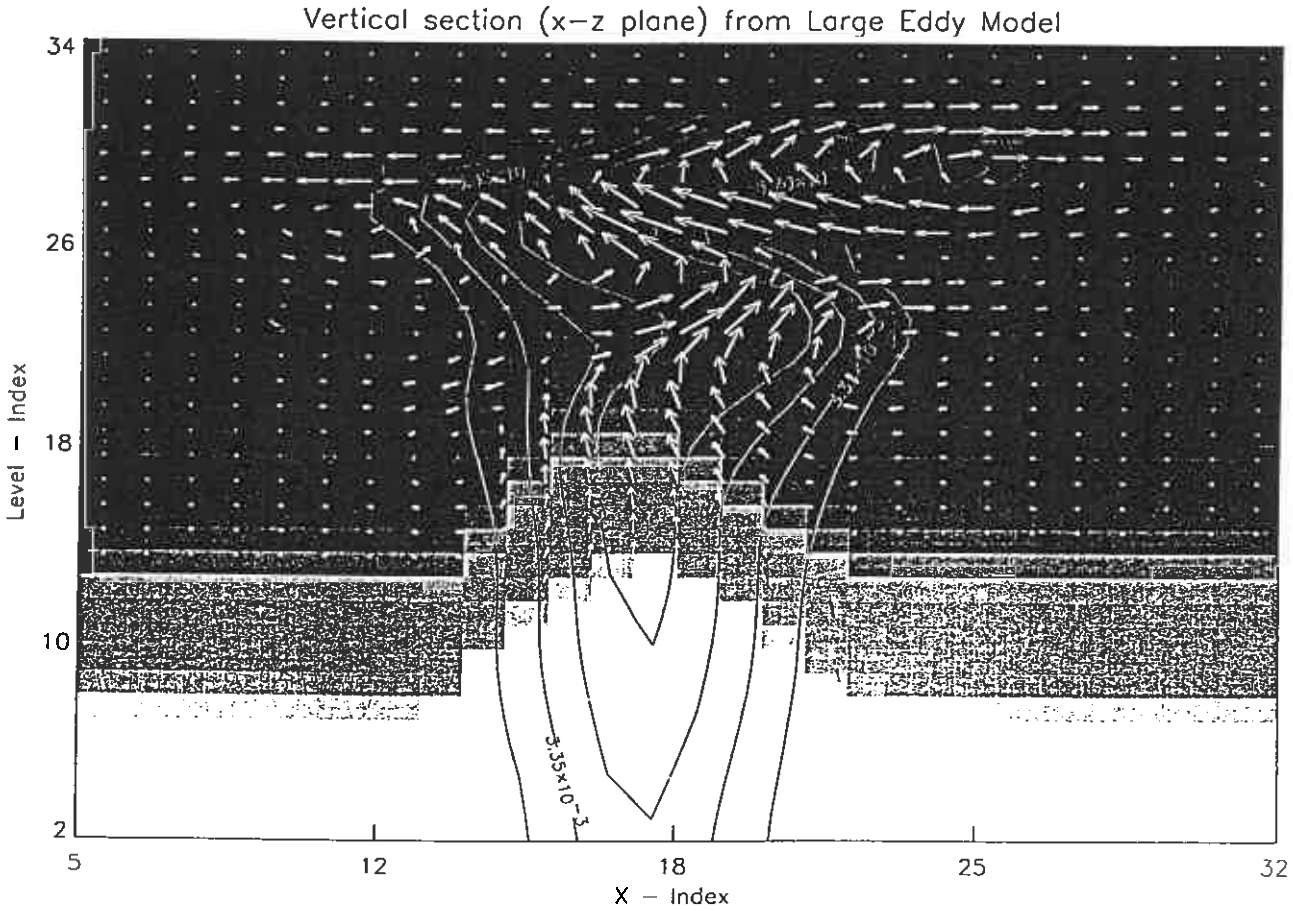

Fig. 4: As Fig. 3a but for a dryer atmosphere (see top figure for the humidity profile): The zigzag instability appears to be enhanced.

Effect on large scale shear

In 2D and 3D simulations of moist-convective equilibrium, large scale shear was observed to develop spontaneously (see Figs. 5 and 6). This indicates that the vertical transport of horizontal momentum exhibits some degree of organization that contradicts the naive picture of random mixing which would decrease any kind of shear. While for some (almost) stationary convective systems with strong shear the conversion of vertical into horizontal momentum is largely understood the momentum budget for extended systems with no or weak shear has not been systematically studied. This task is made more difficult by the presence of the zigzag instability that leads to a strongly oscillatory momentum flux. Figure 7 shows a typical picture with a strong zigzag motion of the updraft at the upshear side of the cloud. Also the downdrafts exhibit a largely oscillatory motion in the middle part but become more systematic (shear enhancing) near the surface. As seen in Figs. 9 and 10 (top) the surface velocity is systematically accelerated by this effect.

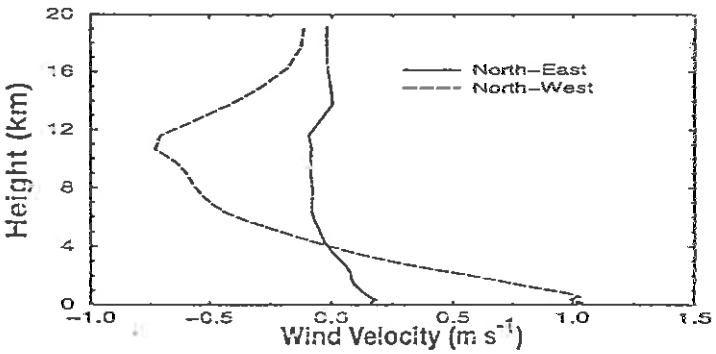

Fig. 5: Horizontally averaged horizontal velocities. From a 3D simulation of Adrian Tompkins (PhD thesis, University of Reading, 1997).

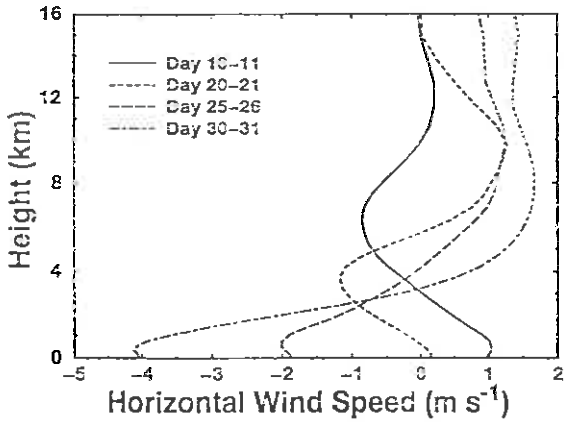

Fig. 6: Evolution of the horizontally averaged velocity from a 2D simulation. From Adrian Tompkins, PhD thesis, University of Reading, 1997.

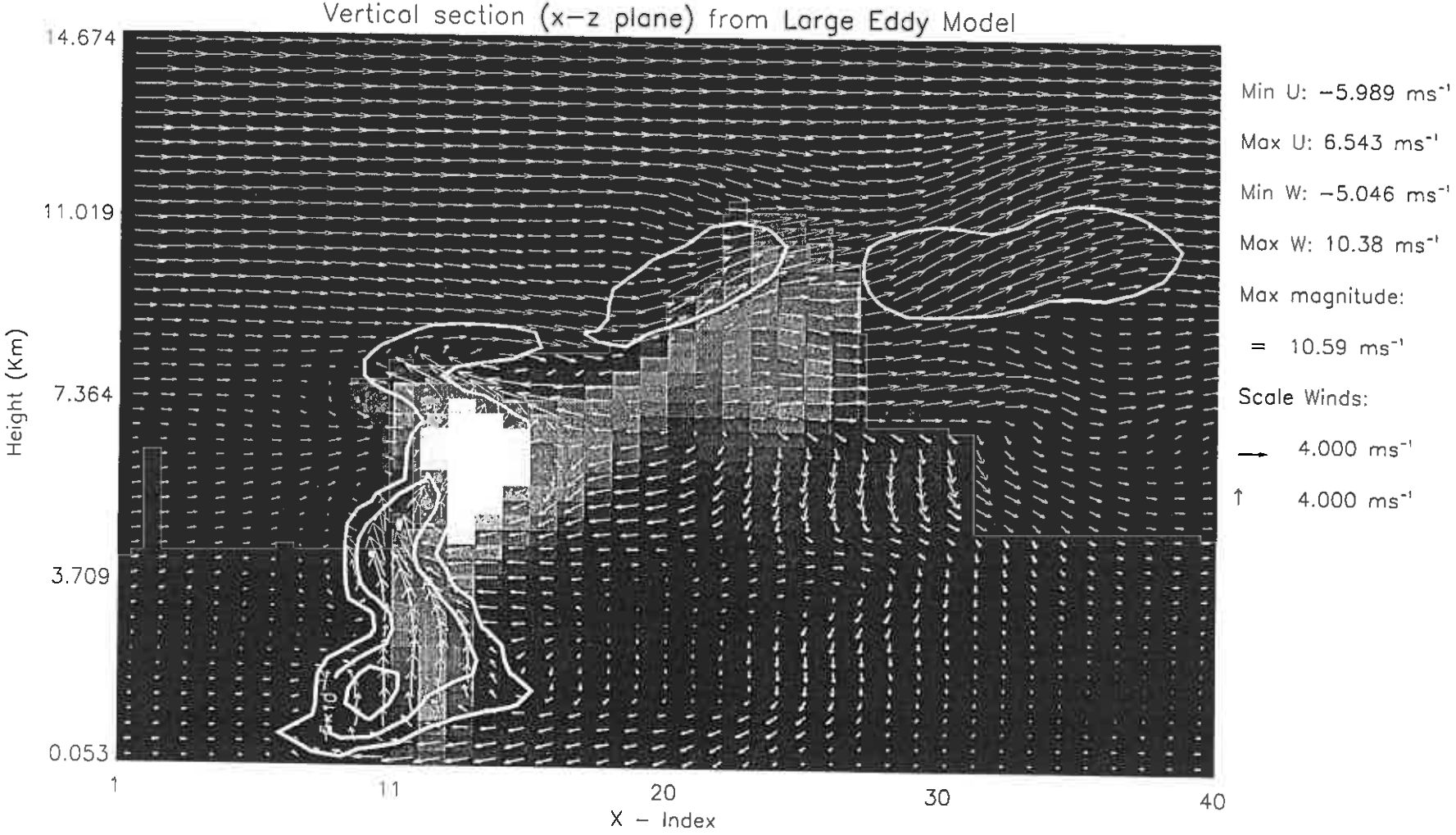

Fig. 7: Time=2000s after initialisation of a heat bubble in th lowest 1000m. The initial wind shear corresponds to the bold line in Fig. 8. Grey scales represent the mixing ratio of rain drops (black= no rain). Contours (0.0, 1e-4, 5e-4, 1e-3) show the content of cloud water.

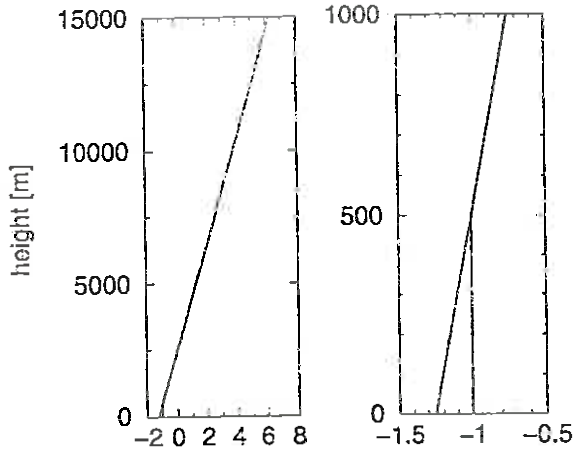

Fig8: initial velocity profiles

Vorticity

In 2D the y-component η_y of $\vec{\eta} = \frac{rot\vec{U}}{\rho}$ is a globally conserved quantity that can only be changed by boundary fluxes. In 3D, however, η_y can also also be changed by vortex tilting. The systematic increase of the volume integrated (and area averaged) η_y shown in Figs. 9 and 10 (bottom) appears to be caused by vortex tilting since surface fluxes are most likely to decrease the vorticity (y-component).
Figures 9 and 10 suggest that the increase of η_y is largely connected to the increase of lowlevel velocity (shear).

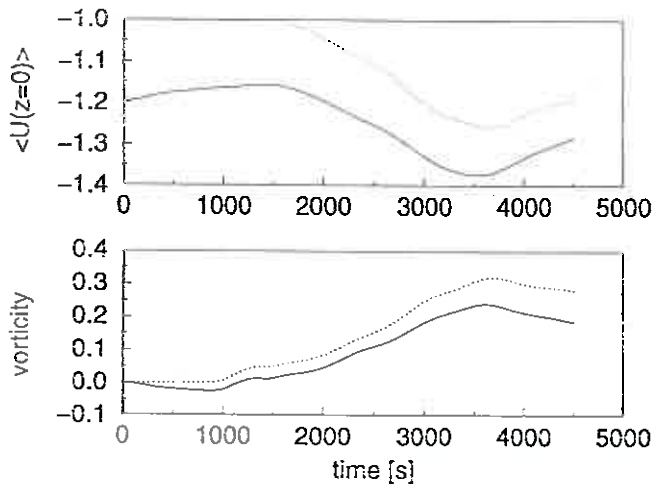

Fig. 9: Time series from runs with 98% humidity and different inititial velocity profiles (see left)
top: mean surface wind.
bottom: changes of η_y (compare text).

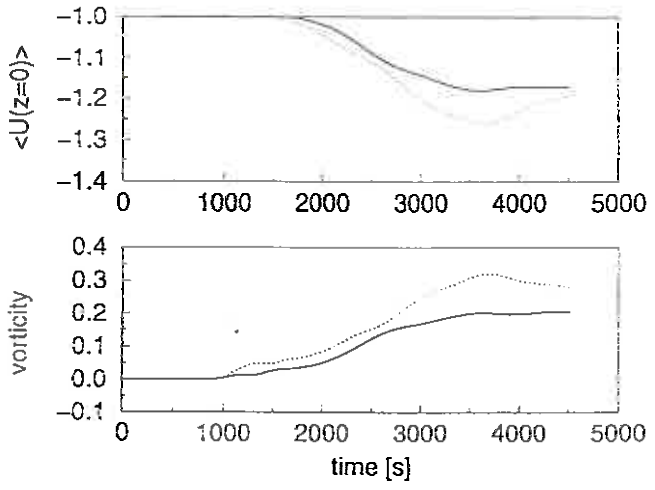

Fig. 10: The same as Fig.9 but for different humidity profiles (The bold solid line corresponds to the dryer profile shown in Fig. 4, top).

The influence of humidity

Figures 10 and 11 illustrate some aspects of the influence of humidity. Figure 11 illustrates that a dryer environment (solid line) generally decreases the mass flux of a given updraft as well as the height reached by the updraft. The slower increase of vorticity (solid line in Fig. 10) appears to be consistent with the smaller mass flux.
The bottom graphs in Fig. 11 however show that

$$\langle U' \rangle_{upd} = \frac{\langle UW \rangle}{\langle W \rangle} \tag{1}$$

[where $\langle\rangle$ indicates the average over all updrafts with $W > 1ms^{-1}$ at a given height and $U' = U - \bar{U}$ is the difference of U from its mean $\bar{U}$ at that height]
reaches similar or even higher values (though at a smaller altitude) in a dry atmosphere. The strength of the zigzag instability thus seems to be the same (or even stronger) in a dryer atmosphere.

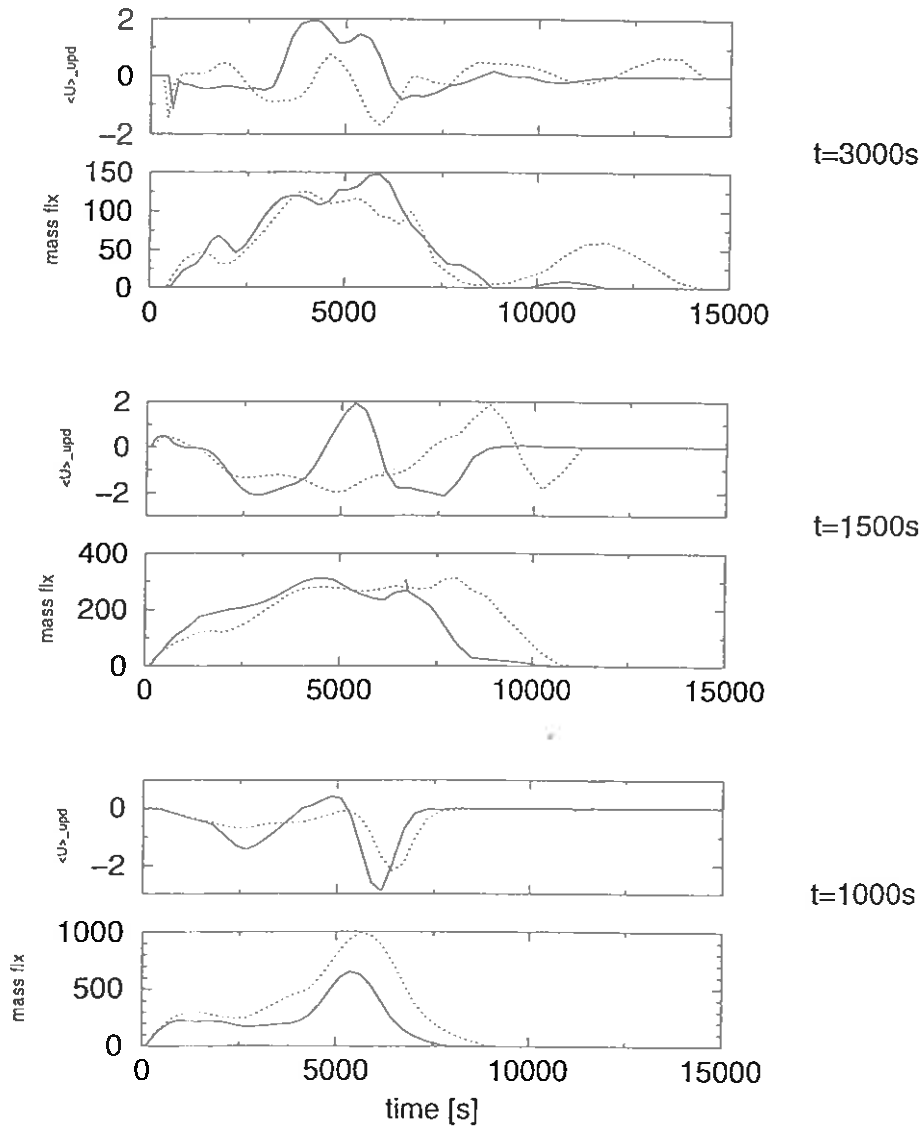

Fig. 11: Vertical profiles at three different times.
Initial condition for dotted and solid lines are the same as in Fig. **10**
Top graphs: The typical updraft value $\langle U \rangle_{upd}$ of U'. U' is the differenz of U from its horizontal mean at a given height.
$\langle U \rangle_{upd} = \frac{\langle U'W \rangle}{\langle W \rangle}$ where $\langle\rangle$ is the mean over all updrafts with $W > 1m/s$.
Bottom graphs: The mass flux of updrafts with $W > 1m/s$.

Evidence of sublimation-driven structure in FASTEX IOP 16

Sid Clough, Richard Forbes, Humphrey Lean and Nigel Roberts

JCMM (Met Office), University of Reading

Sublimation of snow is a rapid and powerful process, so much so that latent heat released in mid-troposphere during baroclinic development is removed from the atmosphere with an attendant generation of mesoscale circulations. The underlying hypothesis of the present work is that this process largely gives rise to mesoscale structures such as rainbands and hyperbaroclinic zones.

Most of the previous background to the work is in Harris (1977; JAS, **34**, 651-72) and Clough and Franks (1991, QJ, **117**, 1057-80) who respectively considered sub-cirrus radar observations of dry convection and the role of sublimation in mesoscale dynamics. The latter emphasised sublimation as a rapid and powerful process and proposed it as an essential player in the occurrence of rainbands by permitting slantwise descent through layers of depth limited by the quantity of precipitation available.

The observations show:

1) an instance of slantwise descent in an upper tropospheric front;
2) formation of layers of weak and strong static stability in mid-upper troposphere extending over 400 km or more across the main front;
3) a strong tendency for relative humidity to approach ice saturation across a wide range of temperatures

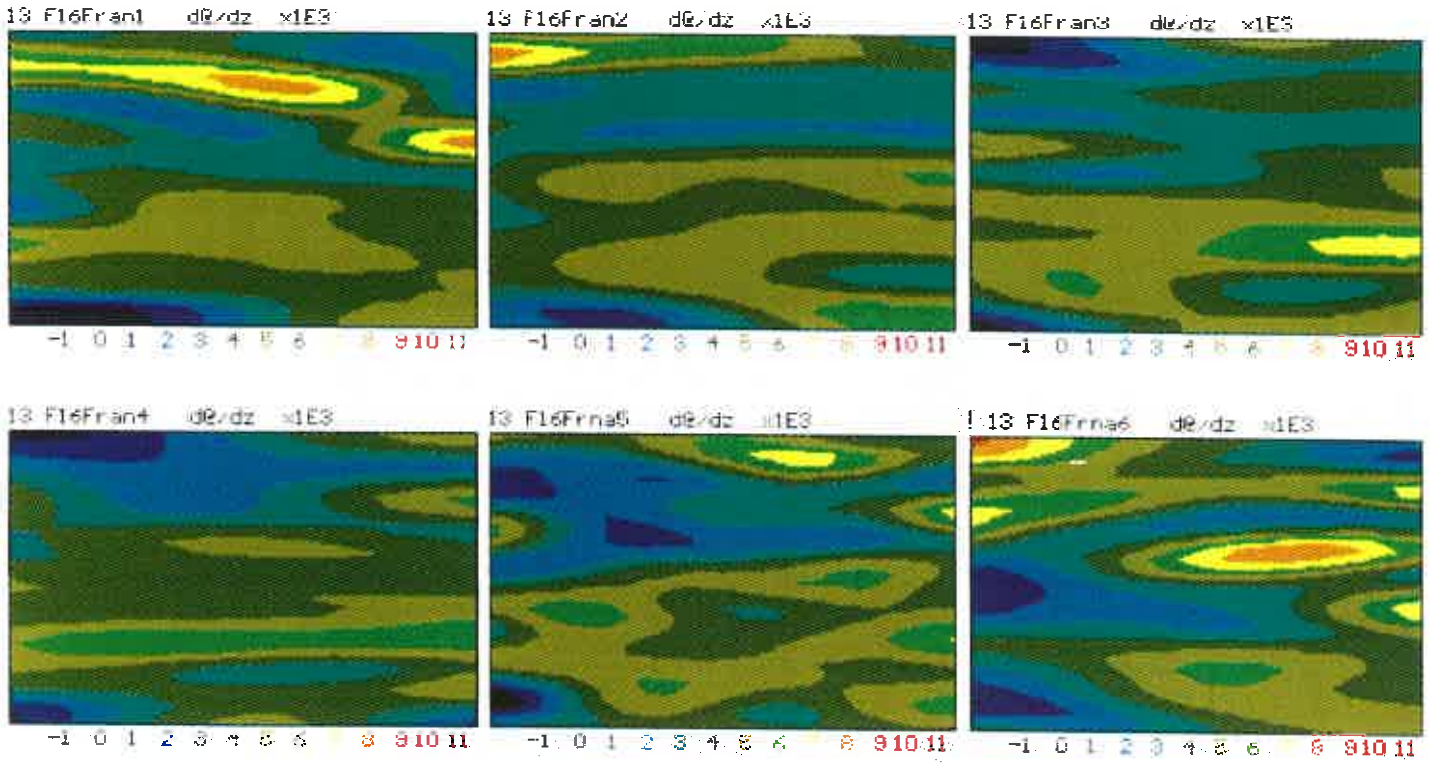

Cross-sections of dry static stability dθ/dz from all six runs (43 sondes). The vertical ranges from 950 to 400 hPa, the horizontal extends around 400-450 km in all cases. Note the large scale of the layering, which reduces in later runs as the lower level circulation develops. Model experiments are confirming that the layering is strengthened by sublimation from the upper cloud shield.

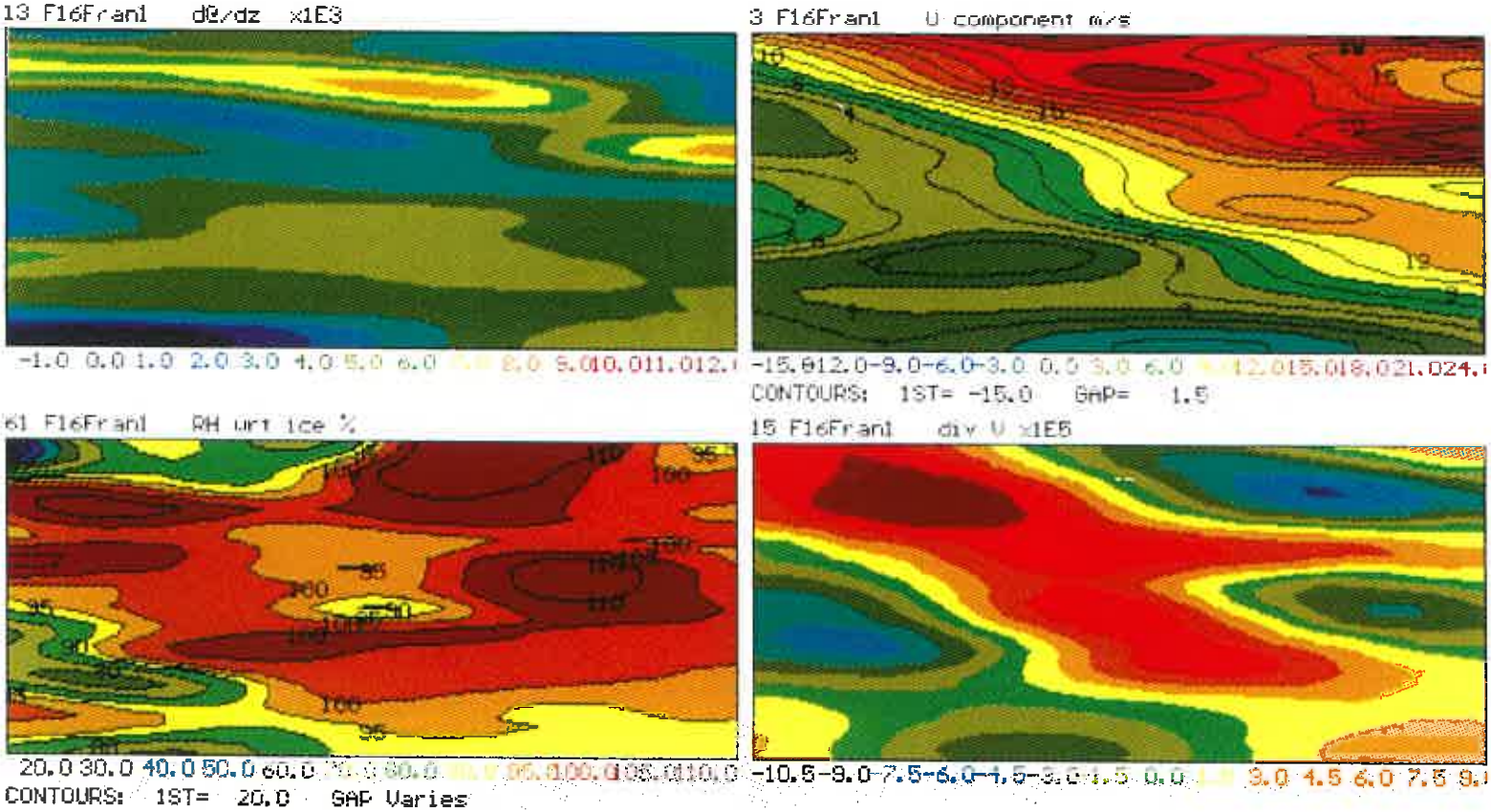

An upper front is evident in run 1. It is accompanied by a strong forward - i.e. descending - flow just above the frontal surface. This run is close to a trough which extends through the troposphere; the circulation is thus driven by larger scale dynamical processes. However, model experiments show that the response is greatly strengthened by sublimation, which enables moist rather than dry adiabatic descent through the precipitating layer. Hence the descent is approximately doubled and a shallow intense forward flow results.

The results thus confirm Clough and Franks's predictions and make more precise its conclusions and their practical relevance. The results clearly indicate :

1) The importance of sublimation to the dynamics of mesoscale structure. PV values of -1PVU were obtained with inclusion of sublimation, -0.5 PVU without.

2) AND the necessity of adequate microphysical parametrization to NWP. Removal of sublimation cooling led to local wind errors up to 10 m/s in a 9 hr simulation.

3) The over-riding role of buoyancy to mesoscale dynamics rather than 'mesoscale dynamical instability' such as CSI. Structure such as rainbands and fronts are dominantly produced by local variations of temperature and moisture driven by latent heat transfers of condensation and sublimation. Vertical motions and hence horizontal currents are induced in response to the horizontal gradients. Ice precipitation is an essential and quantitative agency in this process, which essentially is the solution to the rainband problem.

4) The effect of sublimation is essentially local modulation of the buoyancy frequency. Another process is required to provide the structure of the underlying dynamical organisation. There are strong indications that this process is critical layer instability, by extension of Bretherton's (1966; Quarterly Journal, 92, p325-334) original suggestion.

This study is still ongoing and involves dropsonde and C130 aircraft observations and simulations using the Unified Model, described in Humphrey Lean's paper (Abstract No 33).

FASTEX Secondary Wave Cyclone Development

J.-P. Chaboureau and A. J. Thorpe

Department of Meteorology
University of Reading

Summary

Two major mechanisms of frontogenesis are important in frontal wave cyclone development. **Horizontal deformation** can suppress the non-linear wave development. Using an analytic model, Bishop and Thorpe (1994) showed that large strain rates inhibit any wave slope amplification. For real cases, this ambient strain can be measured using the vorticity-divergence attribution method developed by Bishop (1996). This technique permits us to confirm the crucial role of such strain on the evolution of Fronts and Atlantic Storm Track Experiment (FASTEX) cases.

Horizontal shear, in the presence of an along-front thermal gradient, is also important. Using an Eady model, Joly and Thorpe (1991) showed that in cases of large along-front thermal gradient, frontal waves have growth rates smaller than the front itself, and thus would not develop. The Bishop method is here extended to a geopotential field partition. This leads, via a non-linear balance condition, to the estimation of the ambient along-front potential temperature gradient and its role is discussed.

Selected FASTEX IOPs

Non-developing cases

Low	IOP	date
19a	5	20-21 Jan
22b	7	25-26 Jan
27	9	2-3 Feb
41 rear	17	18-19 Feb
46	19	26-27 Feb

Developing cases

Low	IOP	date
19b	5	21-22 Jan
33	11a	7-8 Feb
34a	12	9 Feb
39a	16	16-17 Feb

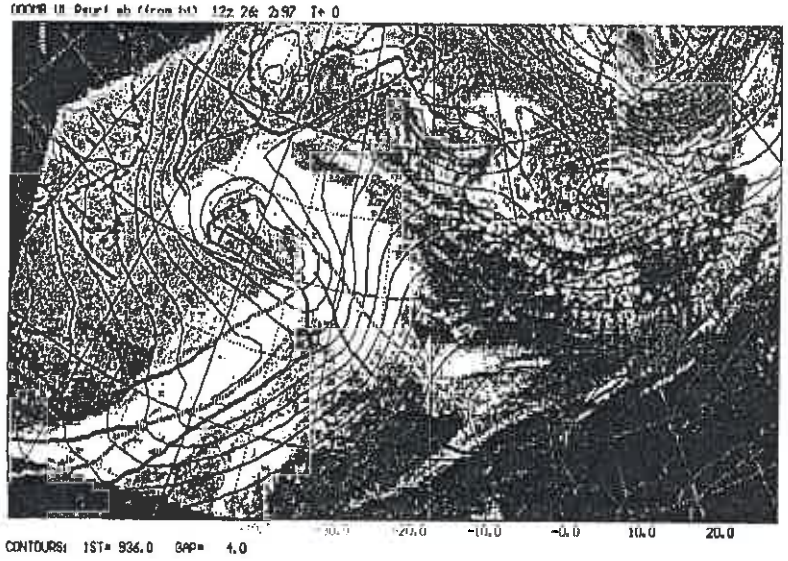

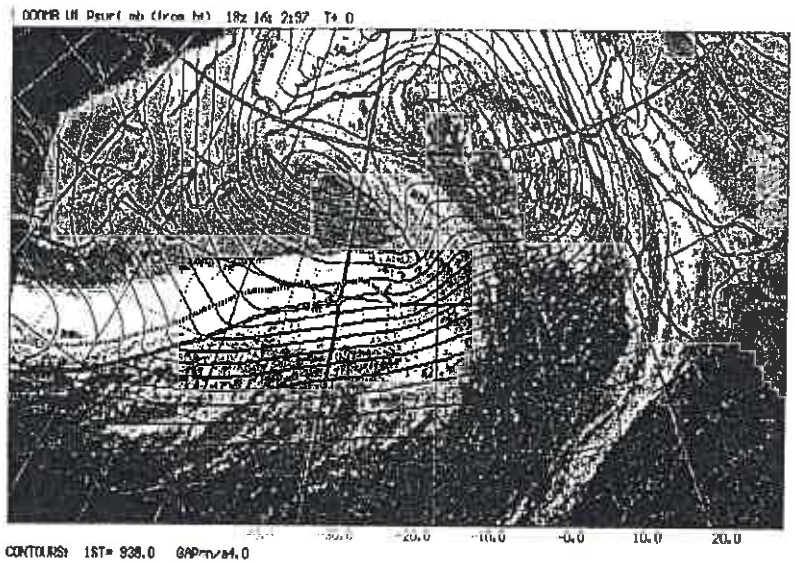

Deformation frontogenesis

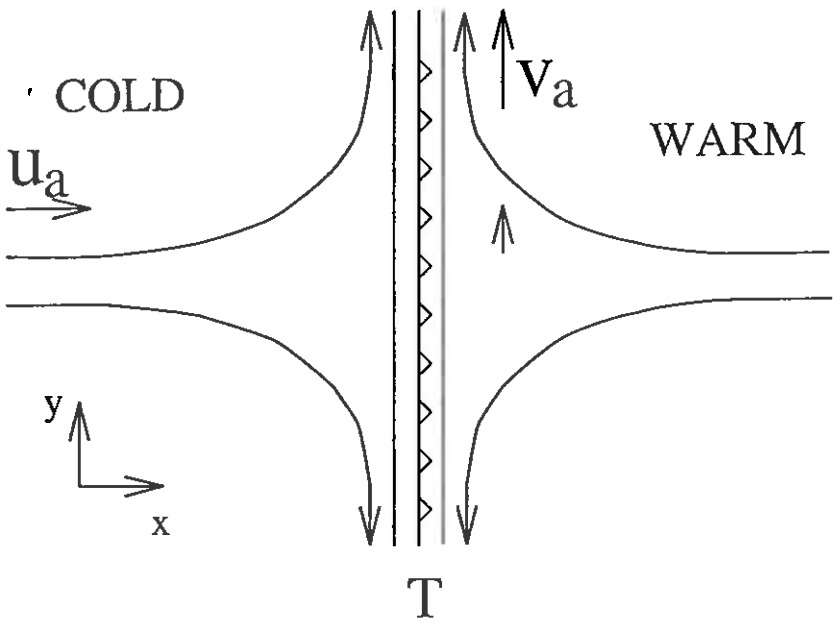

Action on wave development
(Bishop and Thorpe 1994)

- Deformation Flow
→ increases along-front wavelength
→ wave growth reduced

+ Induced ageostrophic convergence
→ increases vorticity in time
→ increases potential instability

If deformation ceases
and potential for instability strong enough,
⇒ frontal wave free to develop along the front

Key parameter: $\partial v_a / \partial y$

Shear frontogenesis

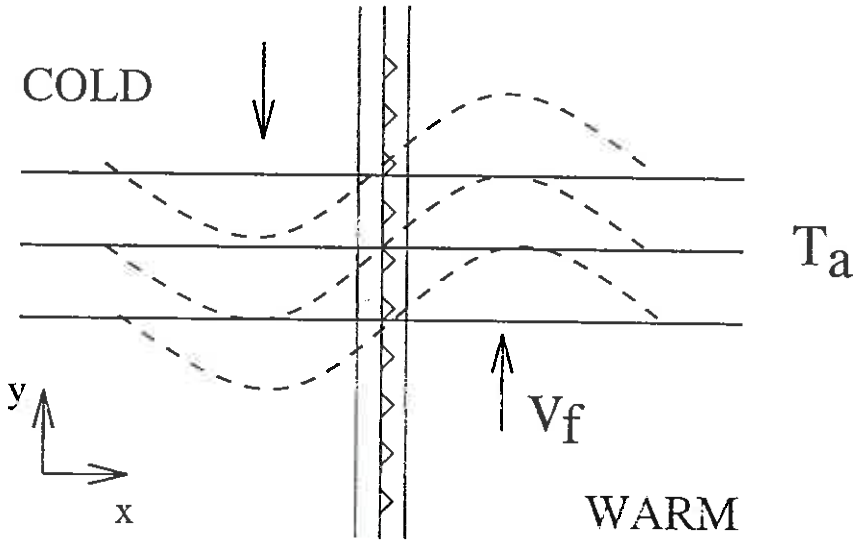

Action on wave development

(Joly and Thorpe 1991)

- Large ambient vertical shear

→ growth of 2-dim front is larger than that of a wave

+ Smaller ambient vertical shear

→ growth of wave is larger

Key parameter: $\partial\theta_a/\partial y$

Domain-independent Attribution

Frontal flow and Temperature Partition

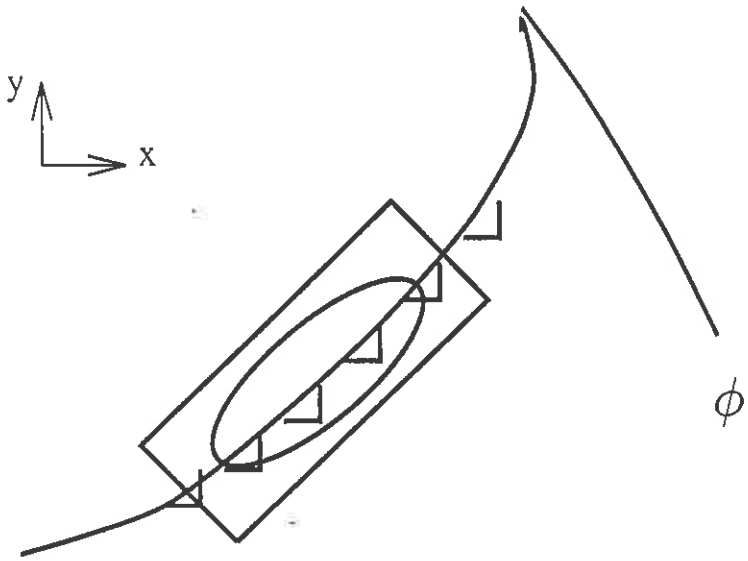

$$\vec{u} = \vec{u_a} + \underbrace{\vec{u_f}}$$

due to vorticity/divergence sources inside the box

$\rightarrow$ $\partial v_a/\partial y$ related to the strain

$$\phi = \phi_a + \underbrace{\phi_f}$$

due to pseudo-vorticity sources inside the box

$\rightarrow$ $\partial \theta_a/\partial y$ related to the shear

Normalized Vertical Shear versus Normalized Strain

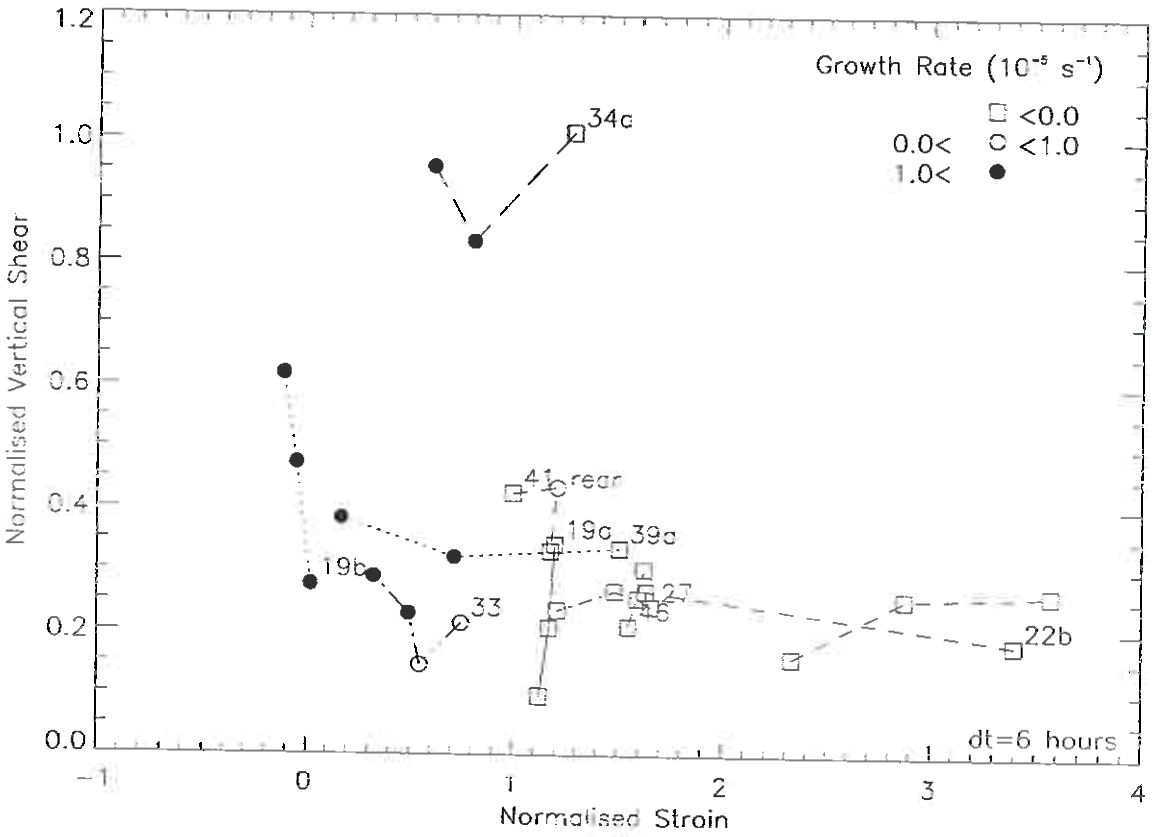

Symbols indicate the range of growth rates (rate of change of the vorticity waviness calculating by differencing the 6 hourly sampled values of different FASTEX cases).

Conclusion

Role of deformation on frontal wave is confirmed

- ☞ strong deformation: no development is possible
- ☞ weak deformation: development is allowed

Role of the shear is less discriminating

- ☞ most of the cases have relatively "low" shear allowing wave growth
- ☞ except 2 developing cases (lows 19b & 34a)

The Christmas Eve Storm and its associated cloud head – A NWP representation of its dynamics

R.S.Dixon, K.A.Browning and G.J.Shutts

Introduction

The storm that hit the United Kingdom on Christmas Eve 1997 was notable for the damaging winds gusting up to 90mph over Western Britain. It also gave a striking example of a 'cloud head', a feature first noted by Böttger *et al.* (1975) as a precursor to the rapid development of cyclones.

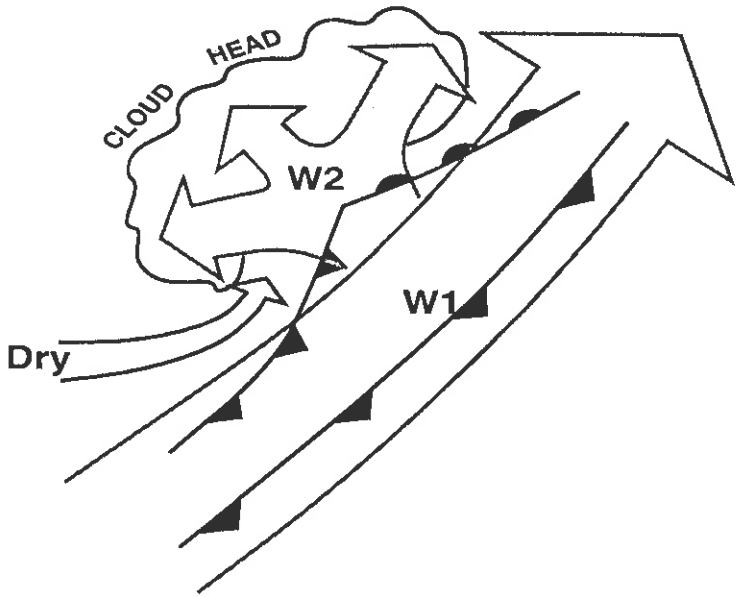

Figure 1 Schematic of a cloud head

The cloud head has been noted by other authors (Browning and Roberts (1994), Young *et al.* (1987)), and Bader *et al.* (1995) devised the schematic of the airflows typical to a developing cloud head shown in **figure 1**.

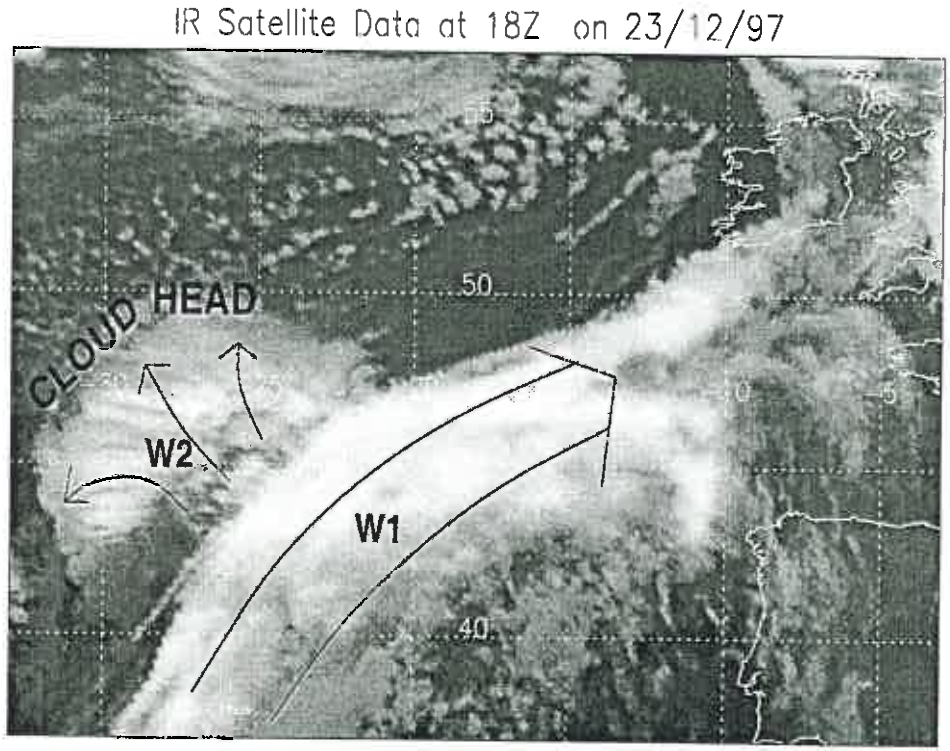

Figure 2 IR satellite image – 18Z 23/12/97

Case Study

The satellite imagery at 18Z on 23rd December (**figure 2**), some 24 hours before the low hit the United Kingdom and also just before the onset of rapid deepening of the system, highlights the above flows.

The 'W1' flow is what is traditionally known as the 'warm conveyor-belt' flow, linked with a pre-existing polar front. The 'W2' flow is identified as the flow associated with the development of the cloud head.

Trajectories

Trajectories can be used to identify the main flows within the cloud head. Adopting the method developed by and described in Wernli (1997), trajectories are selected according to specific criteria. The forecast run of the Met. Office's 50km resolution Limited Area Model (LAM) starting at 06Z, 23rd December 1997 is used to look at the development of the cloud head.

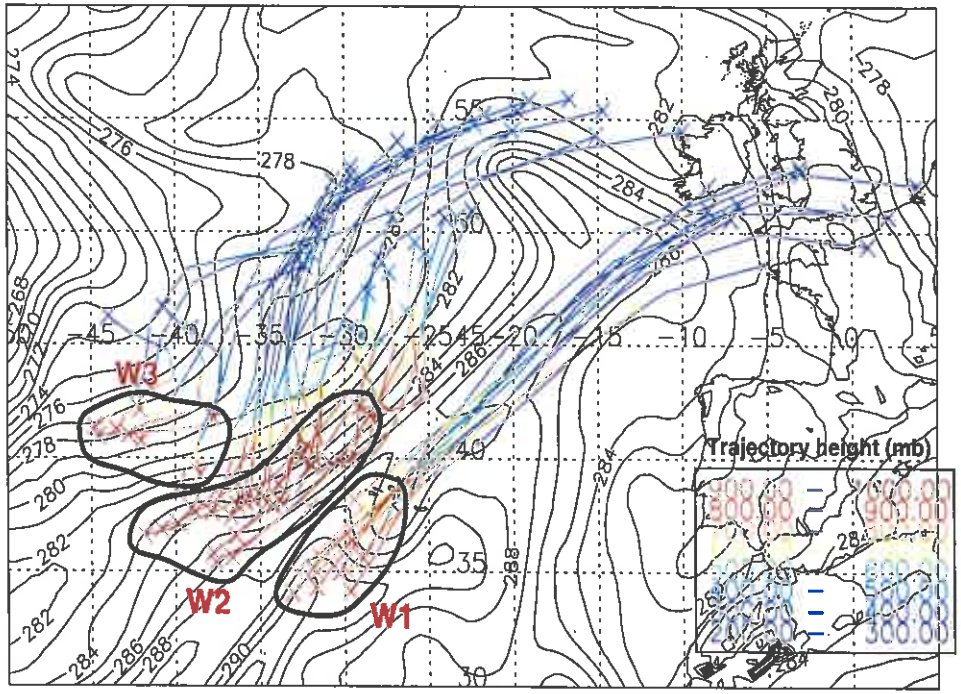

Figure 3 900mb θ_w (23/12/97, 06Z) and trajectory positions from 06Z, 23/12/97 to 06Z, 24/12/97

Figure 3 shows motion of those trajectories that start within the confines of the above domain and ascend more than 300mb in the following 24 hours. The parcels initially appear bunched together on the baroclinic zone at low levels; however, with time a splitting of the trajectories in the horizontal as they ascend into the middle-to-upper troposphere can be noticed. From this splitting, the parcels that contribute to the W1 and W2 flows can be distinguished. Also a second, smaller cloud head and 'W3' flow is seen to the west of W2, but is not studied here.

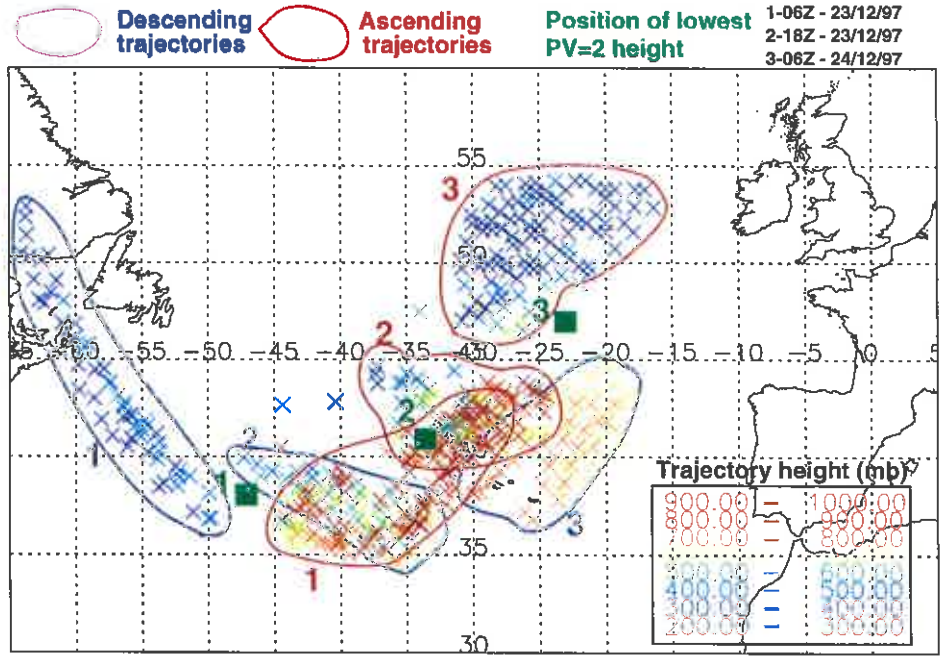

Figure 4 Positions of ascending and descending trajectories from 06Z 23/12/97 to 06Z, 24/12/97

We can also look at the origins of the dry-intrusion and cloud-head air by applying back trajectories and picking parcels that descend more than 200mb over 24 hours. **Figure 4** shows the positions of the descending dry air and the ascending W2 air parcels at 12-hour intervals.

Cross-sections

To accompany the trajectory analysis, cross-sections show an interesting structure. **Figure 6** shows vertical cross sections at 06Z on 23rd December and 00Z on 24th December, an 18-hour forecast. One feature to note is the tilting of the θ_w lines from an upright position in the cloud head's formative stage to a slanting orientation some 18 hours later. The ascent along θ_w surfaces thus changes from upright to slantwise. Also one can note the upper level PV anomaly marking the boundary between the dry (no shading) descending air and the moist ascending air.

Summary and Future Work

- The cloud-head-producing W2 flow is seen, through the use of trajectories, as a separate entity from the polar front cloud band W1 flow.
- Dry descending trajectories move from far upstream behind the upper level PV anomaly into the dry slot. The moist W2 trajectories ascend ahead of the anomaly.
- Viewed relative to the PV anomaly, the envelopes of the trajectories show the pivotal role of the PV anomaly in the production of the cloud head W2 flow and the dry slot.
- Cross-sections through the developing cloud head show the PV anomaly as the boundary between the dry slot and moist ascending W2 air. They also reveal a tilting of the θ_w surfaces as the cloud head develops with time.

Speculation in the past (e.g. Shutts (1990)) has pointed to the potential role of symmetric instability in the development of cloud heads. Thus a high resolution modelling study is being developed. This will utilise the Met. Office's 'Large Eddy Model' to examine the role, if any, of slantwise instability in the development of cloud heads.

References

Bader, M.J., Forbes, G.S., Grant, J.R., Lilley, R.B.E. and Waters, A.J. (Eds.) (1995) *Images in weather forecasting*, Cambridge University Press

Böttger, H, Eckhardt, M. and Katergiannakis, U. (1975). Forecasting extratropical storms with hurricane force intensity. *J.Appl. Met.*, **14**, 1259-1265

Browning, K.A and Roberts, N.M. (1994). Structure of a frontal cyclone. *Q. J. R. Meteorol. Soc.*, **120**, 1535-1557

Shutts, G.J. (1990). Dynamical aspects of the October Storm 1987: a study of a successful fine mesh simulation. *Q. J. R. Meteorol. Soc.*, **116**, 1315-1347

Wernli, H. (1997). A Lagrangian-based analysis of extratropical cyclones. I: The method and some applications. *Q. J. R. Meteorol. Soc.*, **123**, 467-489

Young, M.V., Monk, G.A. and Browning, K.A. (1987). Interpretation of satellite imagery of a rapidly deepening cyclone. *Q. J. R. Meteorol. Soc.*, **113**, 1315-1347

DIAGNOSTIC STUDY OF A POLAR LOW

G. Winter and K. A. Browning
Reading University / JCMM

A dry intrusion plunged down to below 3 km over the Irish Sea in the Easter 1998 Polar Low (14 April). Was it stratospheric air ?

• The MST radar gave an anomalous power signature [not presented here] from 17Z to 20Z on 14 April, indicating dry upper-level air plunging down below 3km. A zoomed view of the MST radar [not presented here] showed that strong wind gusts accompanied this feature.

Fig **A3:** The 17Z Meteosat VIS image showed an archetypal cyclone cloud signature associated with the Polar Low. The MST radar-detected anomaly was associated with a dry slot due to dry-intrusion air penetrating between the cloud head and the cold front cloud.

Fig **B1:** The Polar Low and surface trough travelled SE-wards. The Low was over the Isle of Man at 09Z where there was a 10 cm fall of snow.

Fig **B2:** Weather radar showed precipitation associated with the cloud head of the Polar Low.

Fig **B3:** IR imagery showed the high cloud of the cloud head and lower cloud along the cold front.

WV imagery showed a dark zone indicative of a dry intrusion north of the cloud head.

Figs **C1-C3:** Sequence of Meteosat WV images showing a dark zone travelling towards and over the MST radar at Aberystwyth (A). The increasing area and warmth of the dark zone indicates the descent of the dry-intrusion air. From 15Z to 1830Z the dry intrusion can be seen entering the circulation of the Polar Low as a dry slot.

Fig **D1:** The Polar Low was cold core at and below 800mb; it was warm core at and above 700mb [not shown].

Fig **D2:** The Polar Low vortex was strongest at 800 and 700 mb, with strong north winds ("V component") over the Irish Sea.

Fig **D3:** A small cut-off blob of dry air centred at 800mb engaged with the Polar Low circulation as it approached Wales.

Figs **E1-E3:** The cross-sections are along YY′ in Fig D3 at 09, 12 and 15Z.
Thin contours and grey scale show relative humidity (black = dry).
White (on black) and black (on white) lines show PV = 1 and PV = 2.
Two parts of the dry intrusion are identified:
LSDI (lower stratospheric dry intrusion, close to PV2);
UTDI (upper tropospheric dry intrusion, close to PV1, part of which gets cut off).
The MST radar "sees" the **UTDI**.

A3

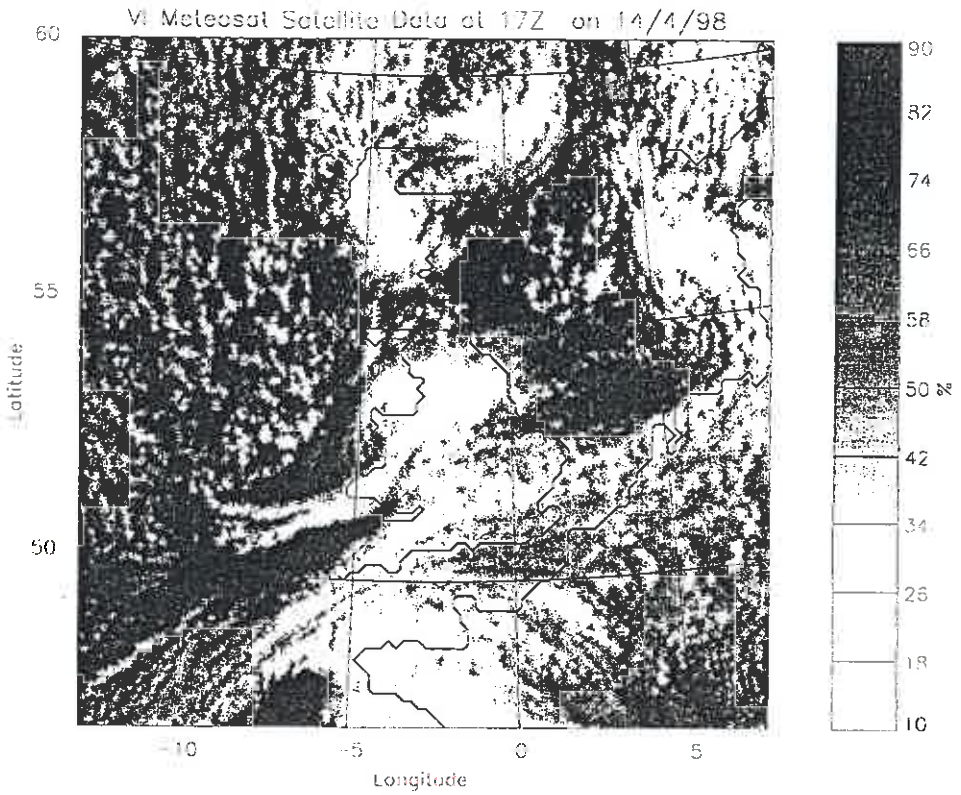
VI Meteosat Satellite Data at 17Z on 14/4/98
60
55
50
Latitude
-10
-5
0
5
Longitude
90
82
74
66
58
50 %
42
34
26
18
10

B1

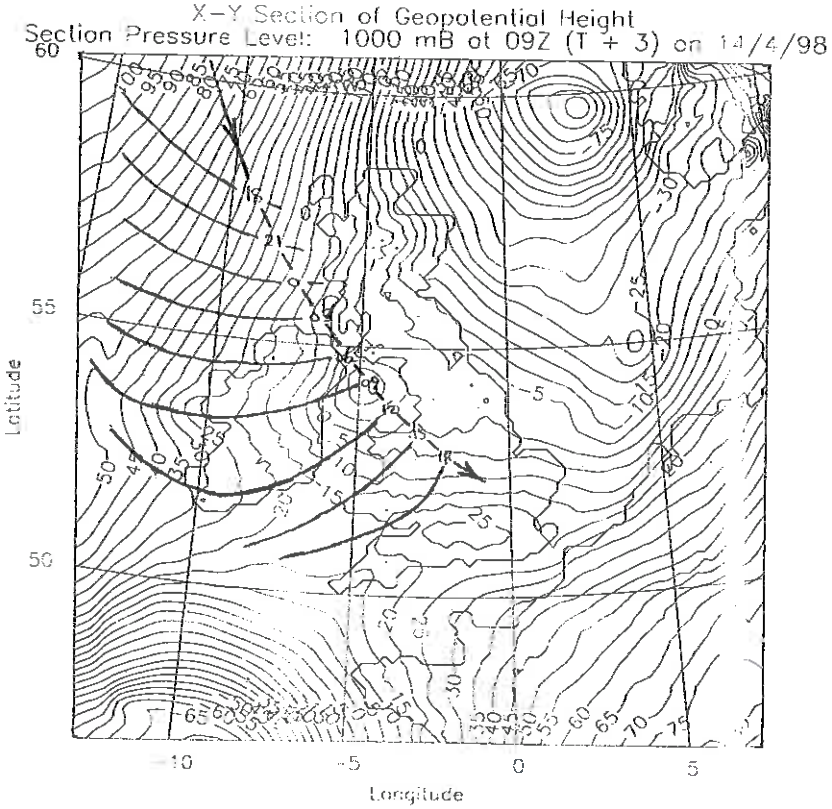
X-Y Section of Geopotential Height
Section Pressure Level: 1000 mB at 09Z (T + 3) on 14/4/98
60
55
50
Latitude
-10
-5
0
5
Longitude

B2

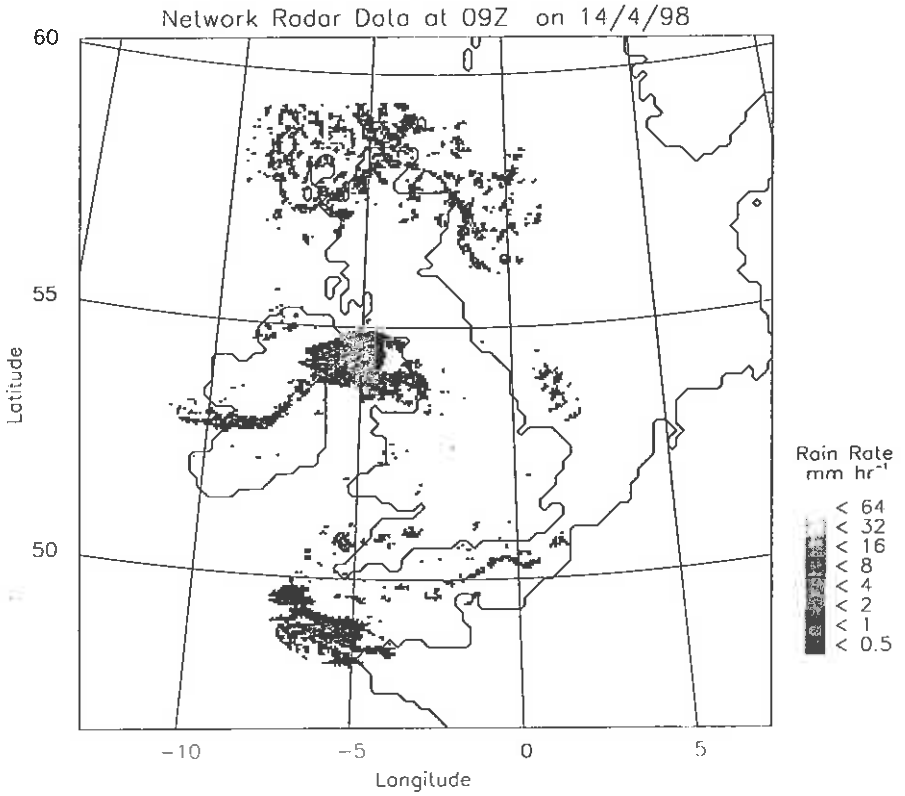
Network Radar Data at 09Z on 14/4/98
60
55
50
Latitude
−10
−5
0
5
Longitude
Rain Rate
mm hr⁻¹
< 64
< 32
< 16
< 8
< 4
< 2
< 1
< 0.5

B3

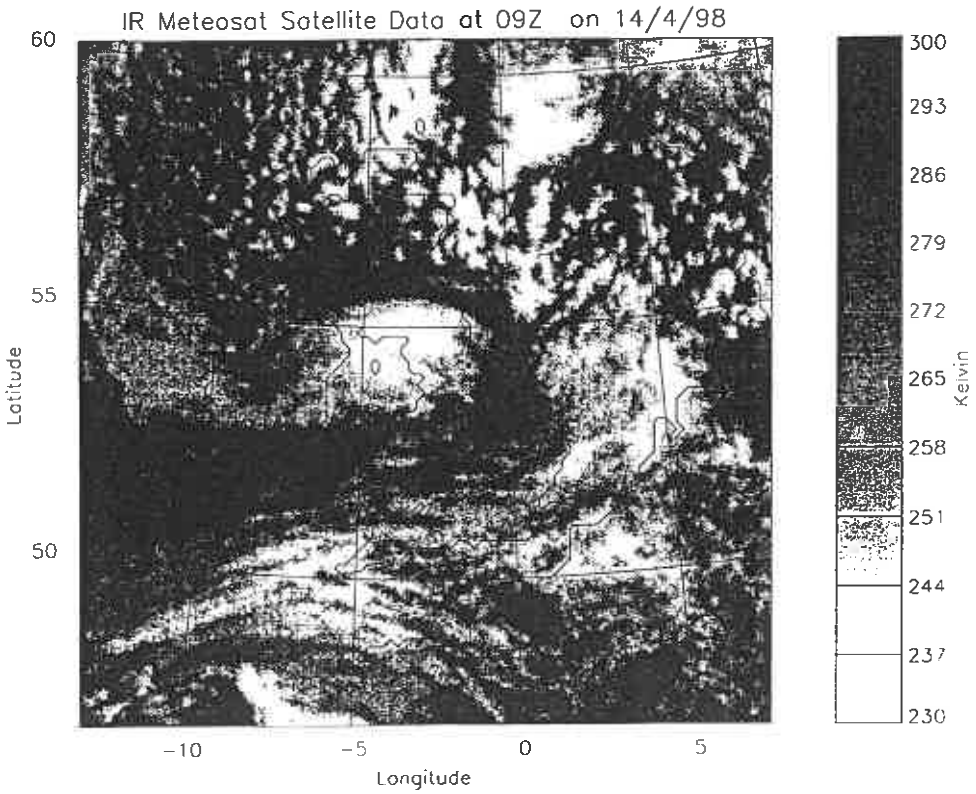
IR Meteosat Satellite Data at 09Z on 14/4/98
60
55
50
Latitude
−10
−5
0
5
Longitude
300
293
286
279
272
265
258
251
244
237
230
Kelvin

C1

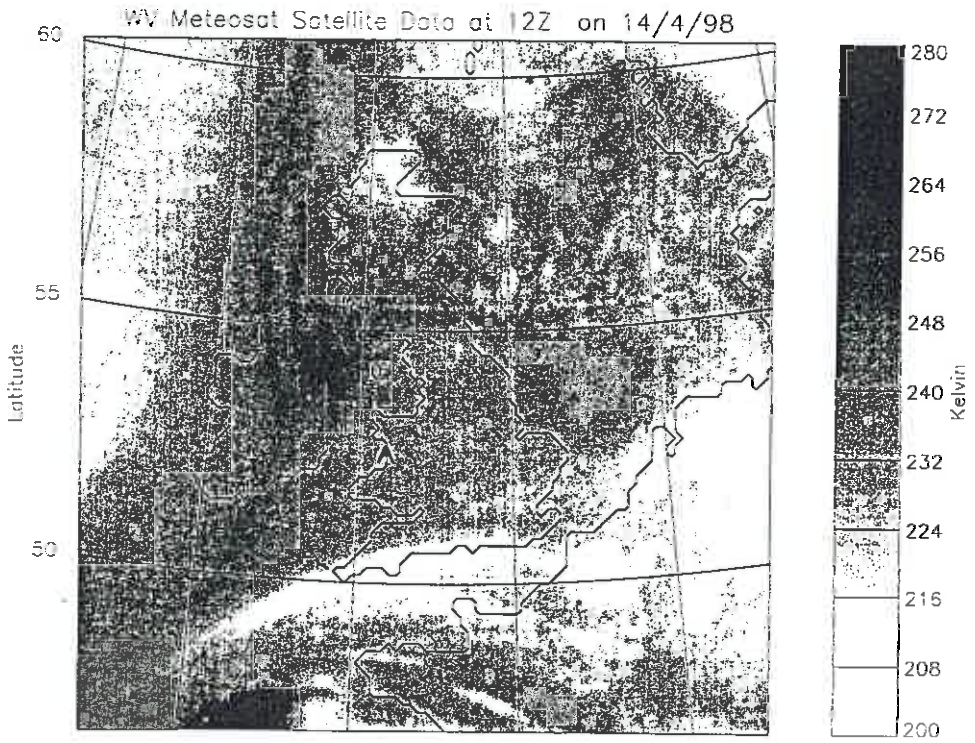
WV Meteosat Satellite Data at 12Z on 14/4/98
60
55
50
Latitude
280
272
264
256
248
240
232
224
216
208
200
Kelvin

C2

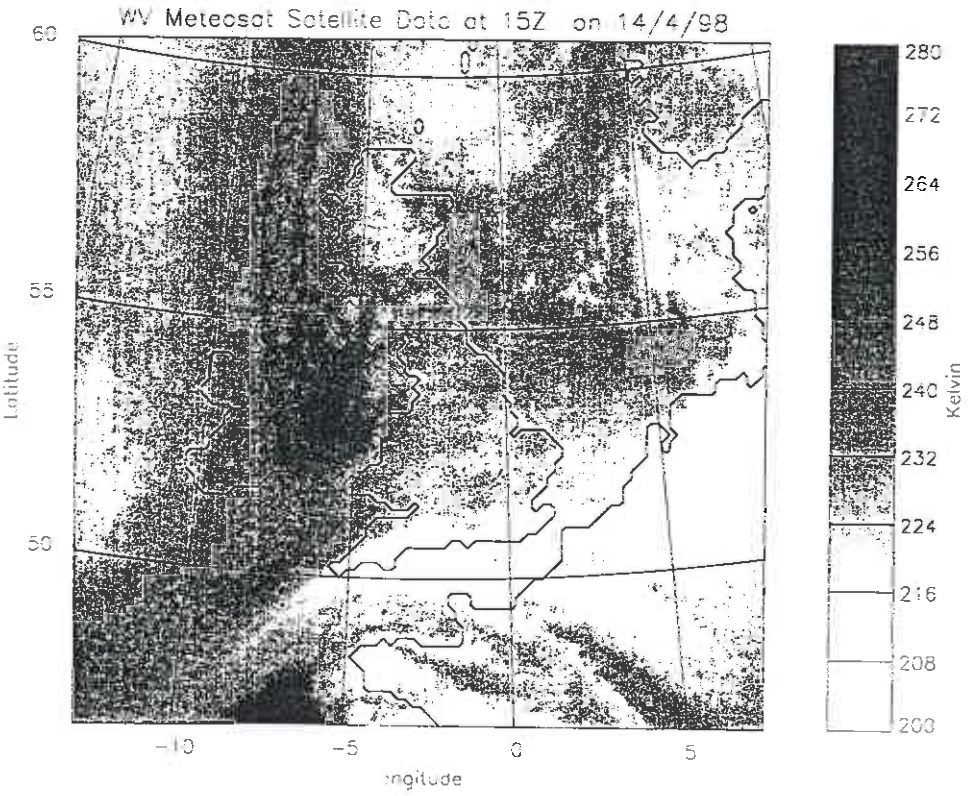
WV Meteosat Satellite Data at 15Z on 14/4/98
60
55
50
Latitude
-10
-5
0
5
ngitude
280
272
264
256
248
240
232
224
216
208
200
Kelvin

C3

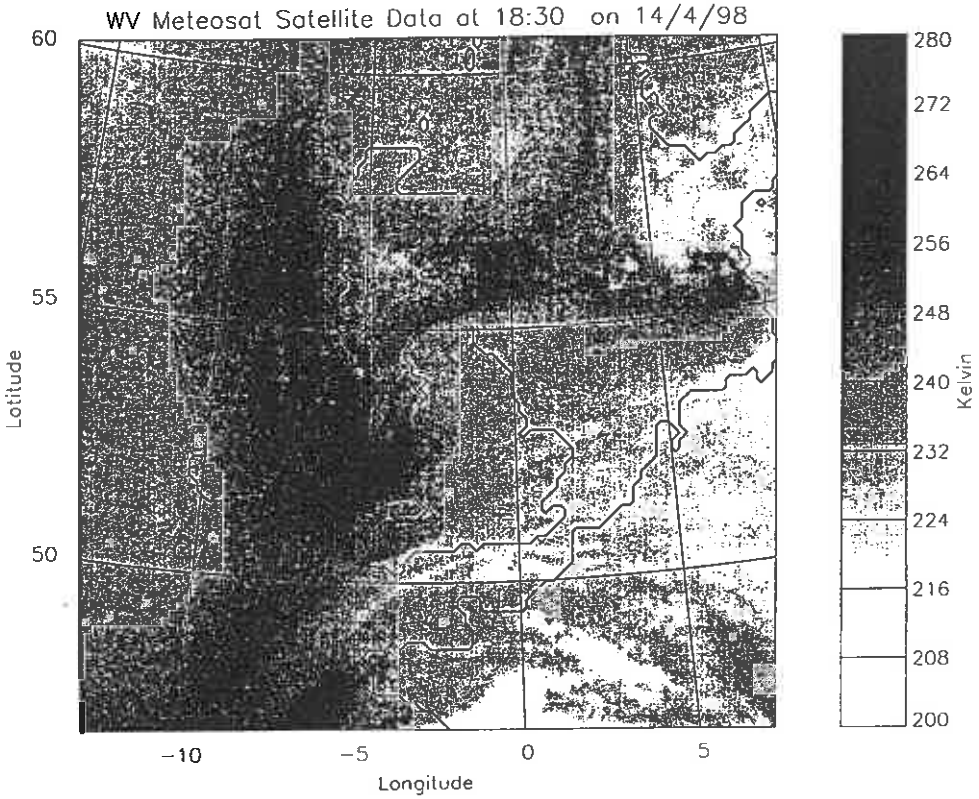
WV Meteosat Satellite Data at 18:30 on 14/4/98
60
55
50
Latitude
-10
-5
0
5
Longitude
280
272
264
256
248
240
232
224
216
208
200
Kelvin

D1

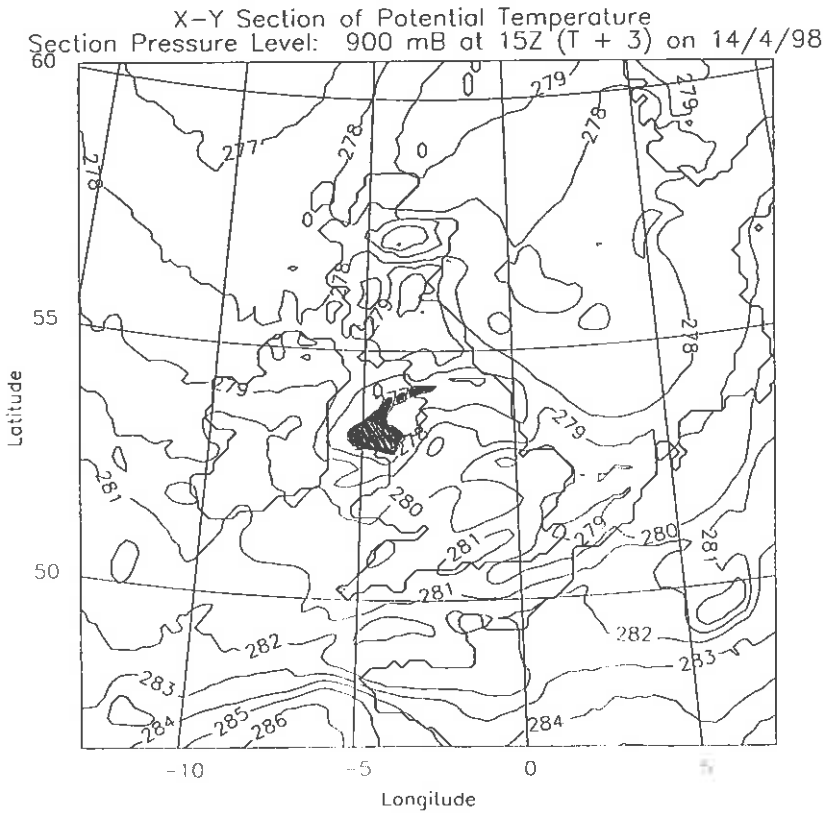
X-Y Section of Potential Temperature
Section Pressure Level: 900 mB at 15Z (T + 3) on 14/4/98
60
55
50
Latitude
-10
-5
0
Longitude

D2

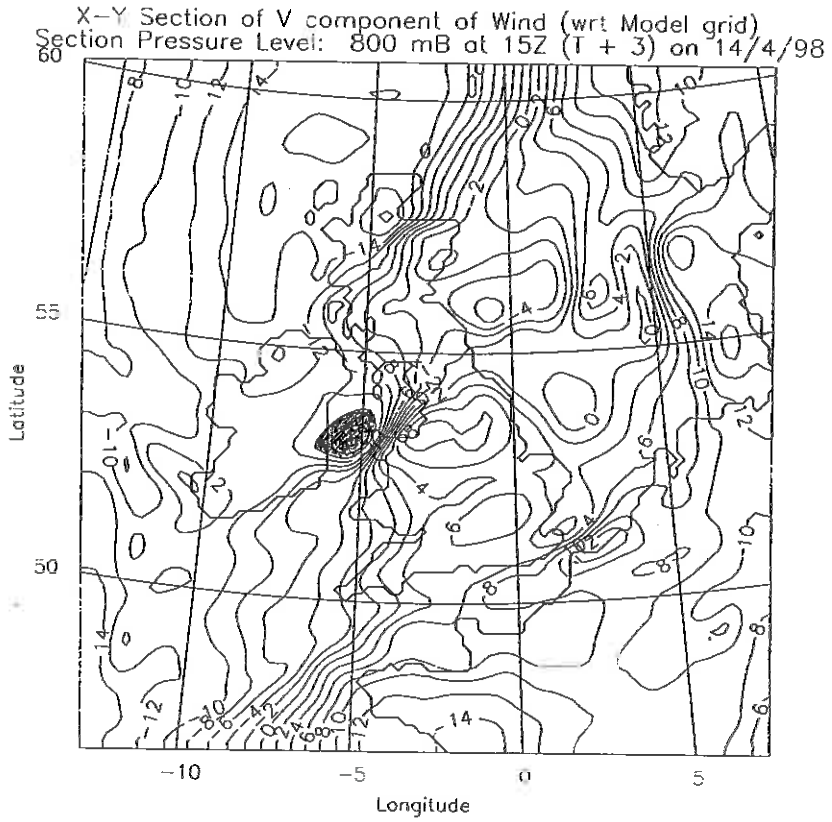
X–Y Section of V component of Wind (wrt Model grid)
Section Pressure Level: 800 mB at 15Z (T + 3) on 14/4/98
60
55
50
Latitude
−10
−5
0
5
Longitude

D3

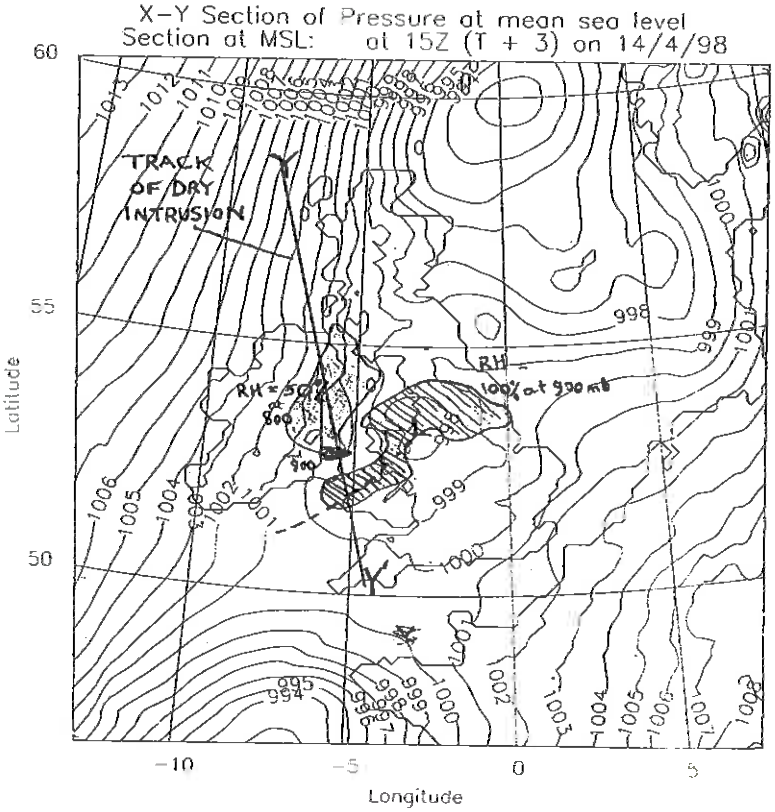
X–Y Section of Pressure at mean sea level
Section at MSL: at 15Z (T + 3) on 14/4/98
60
55
50
Latitude
TRACK OF DRY INTRUSION
RH = 50% at 800 mb
RH = 100% at 930 mb
−10
−5
0
5
Longitude

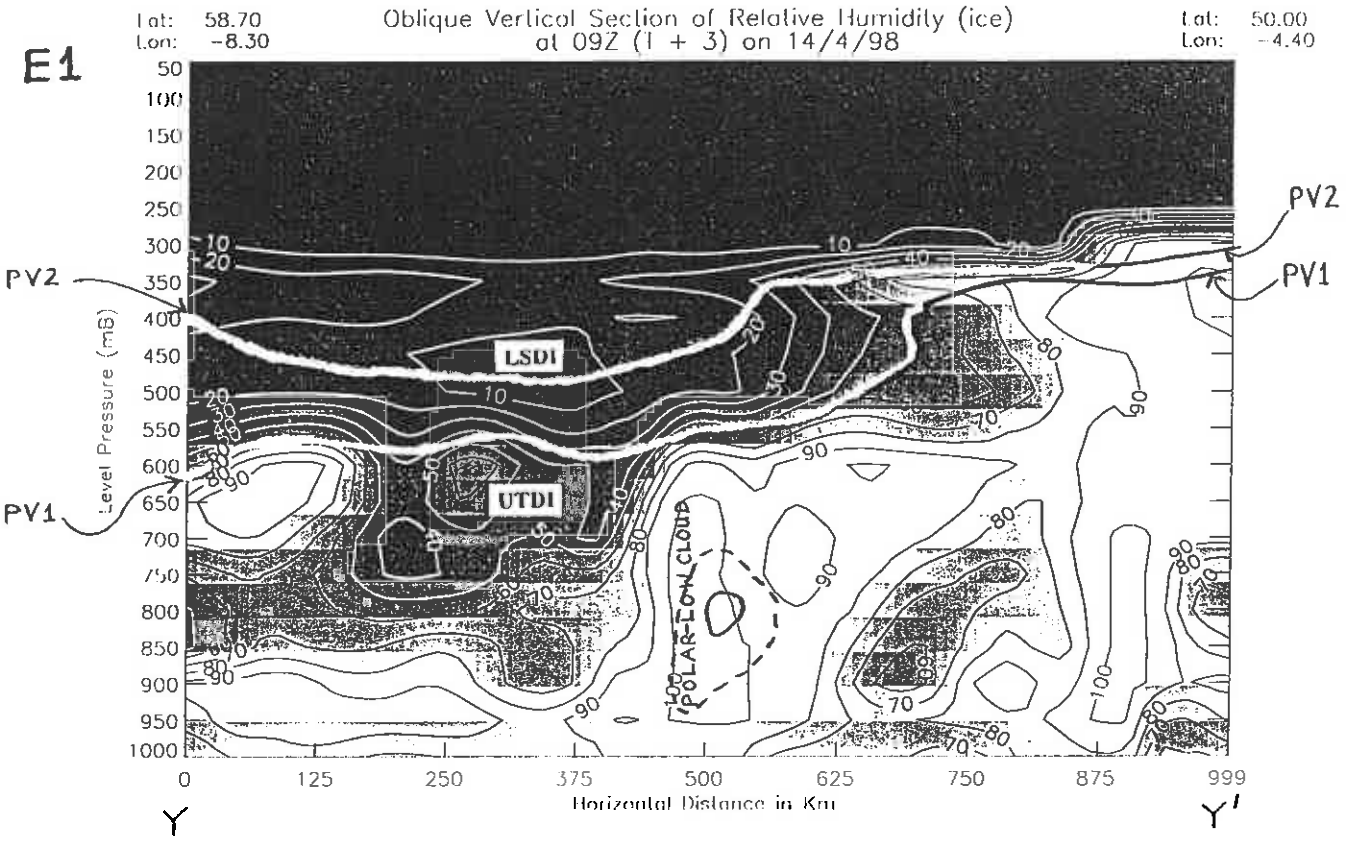
E1
Lat: 58.70
Lon: -8.30
Oblique Vertical Section of Relative Humidity (ice)
at 09Z (T + 3) on 14/4/98
Lat: 50.00
Lon: -4.40
PV2
PV1
PV2
PV1
LSDI
UTDI
POLAR-LOW CLOUD
Level Pressure (mB)
Horizontal Distance in Km
Y
Y'

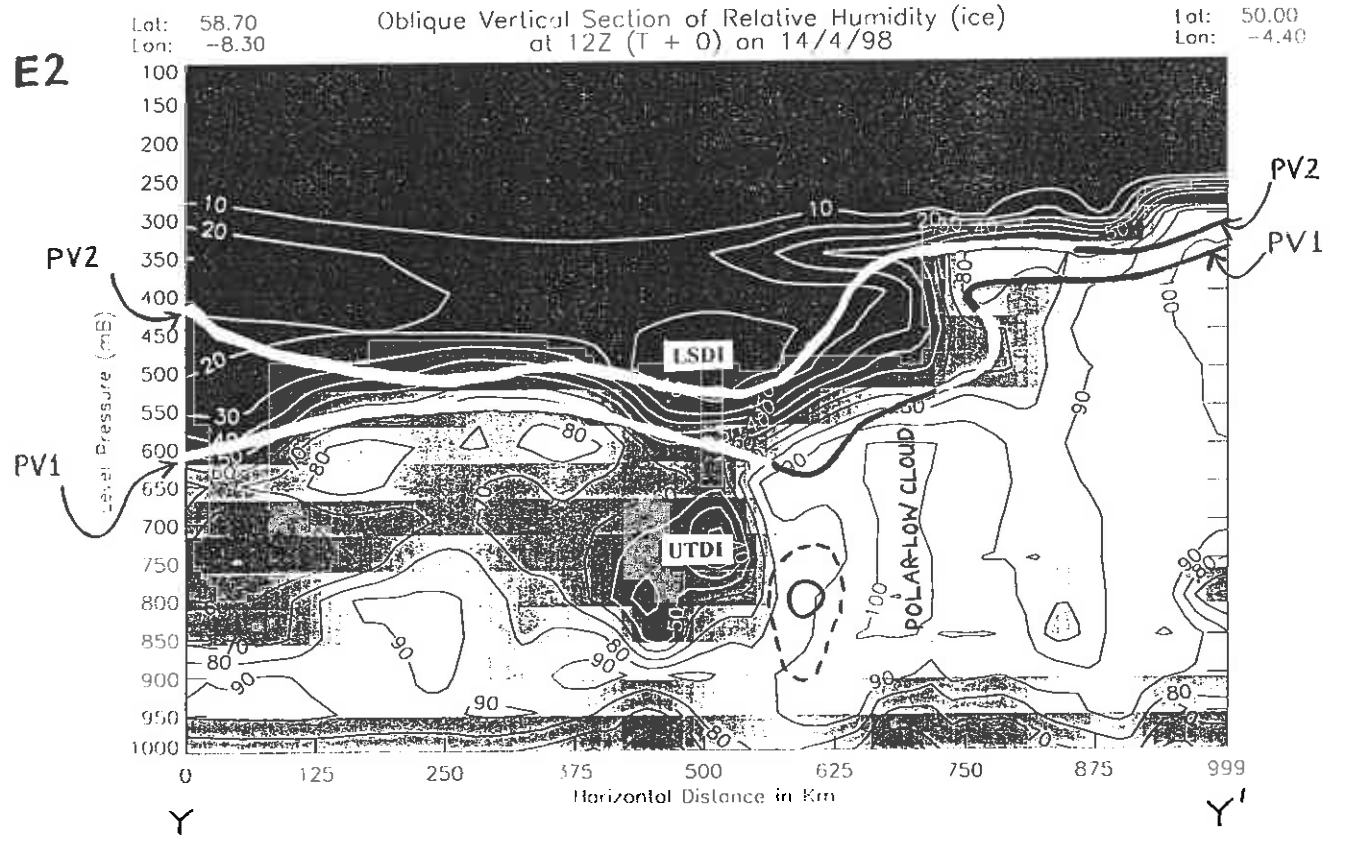
E2
Lat: 58.70
Lon: -8.30
Oblique Vertical Section of Relative Humidity (ice)
at 12Z (T + 0) on 14/4/98
Lat: 50.00
Lon: -4.40
PV2
PV1
PV2
PV1
LSDI
UTDI
POLAR-LOW CLOUD
Level Pressure (mB)
Horizontal Distance in Km
Y
Y'

E3

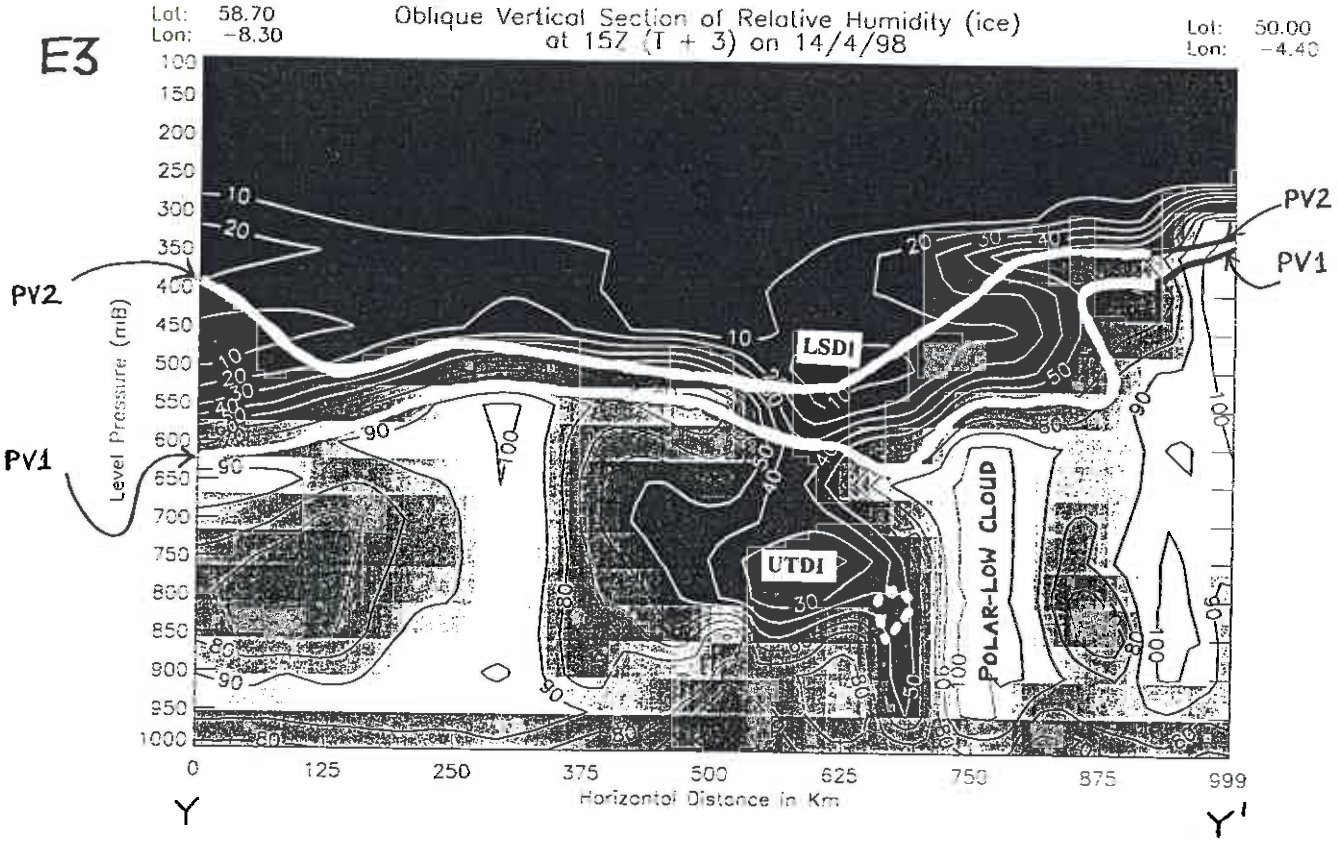
Lat: 58.70
Lon: -8.30
Oblique Vertical Section of Relative Humidity (ice)
at 15Z (T + 3) on 14/4/98
Lat: 50.00
Lon: -4.40
PV2
PV1
PV2
PV1
LSDI
UTDI
POLAR-LOW CLOUD
Level Pressure (mB)
100
150
200
250
300
350
400
450
500
550
600
650
700
750
800
850
900
950
1000
0
125
250
375
500
625
750
875
999
Horizontal Distance in Km
Y
Y'

Conceptual Models of Cyclogenesis - a Unified Perspective

Adrian T Semple

U.K. Meteorological Office (JCMM)

1) The synoptic setting

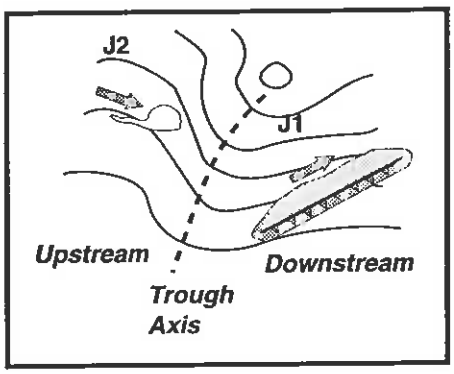

The possibility for the onset of cyclogenesis is intimately connected to the properties of the upper troposphere. Cyclones are commonly induced on the leading edge of synoptic scale upper troughs where there are regions of ascent and upper level forcing in the vicinity of frontal zones. Jet streaks J1 and J2 may often be identified within the trough system and together constitute two fundamental elements of a mid-latitude cyclone.

2) Early development - the leaf cloud

As the cold air associated with the upper trough advances, warm air is forced to ascend in the form of a 'warm conveyor belt' (WCB) and a frontal cloud band develops.

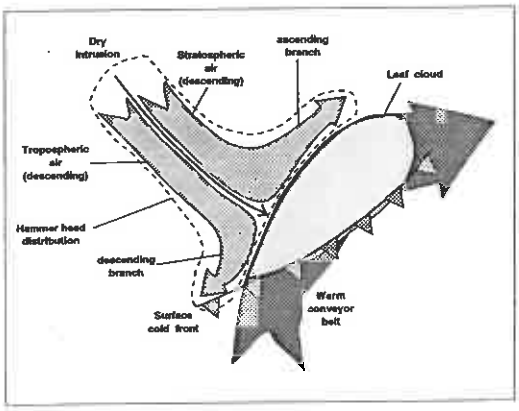

If J1 cuts into the polar front cloud band, a convex-poleward bulge often develops and the cloud evolves into a baroclinic leaf. By the time J1 has initiated the development of the leaf cloud, J2 has often approached the rear of the system.

J2 is the origin of the dry intrusion airstream and has a history of descent originating from the upper troposphere/lower stratosphere.

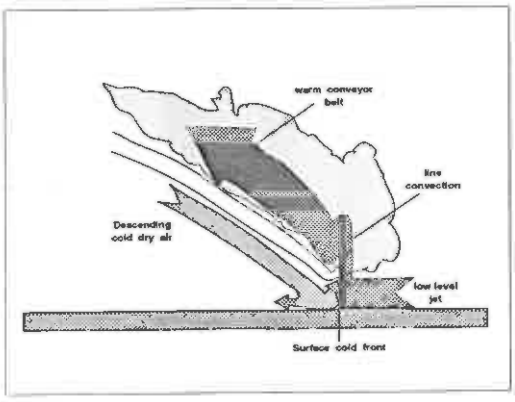

Air at the left exit of J2 is primarily of stratospheric origin and turns cyclonically and ascends.

Air at the right exit of J2 is primarily of tropospheric origin and turns anticyclonically and descends.

The bifurcation of the airflow produces a characteristic hammer-head distribution for the dry intrusion which can be present several hours before leaf cloud formation is complete.

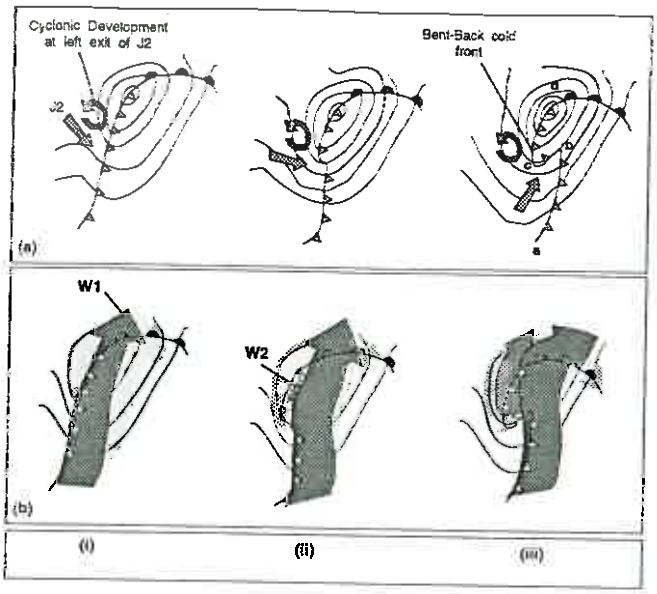

3) Cyclogenesis underway - the W2 flow

Associated with the left exit of J2 is a region of cyclonic development which starts to deform the northern part of the cold front into a 'bent back' structure.

In region ab the WCB rises in the classical ana type mode.

In region bcd the WCB is not forced to rise as steeply and ascends gradually in a shallow moist zone - the W2 flow.

4) Comma cloud formation

Once W2 reaches the surface cold front of cd, it is forced to rise abruptly over it forming a mid-level cloud extrusion. The vigorous ascent of the W2 flow results in large amounts of precipitation in the region of the cloud extrusion.

As the comma cloud develops, cold air just ahead of and beneath the warm front travels westward in the system relative co-ordinate system. The cold air is the developing 'cold conveyor belt' (CCB) which eventually emerges to west of the WCB. As the CCB ascends further, the flow bifurcates:

The northern branch ascends and turns anticyclonically, eventually merging with the WCB. The highest clouds of the CCB are found in this northern extremity.

The southern branch stops ascending (and may descend) and turns cyclonically towards the cyclone centre.

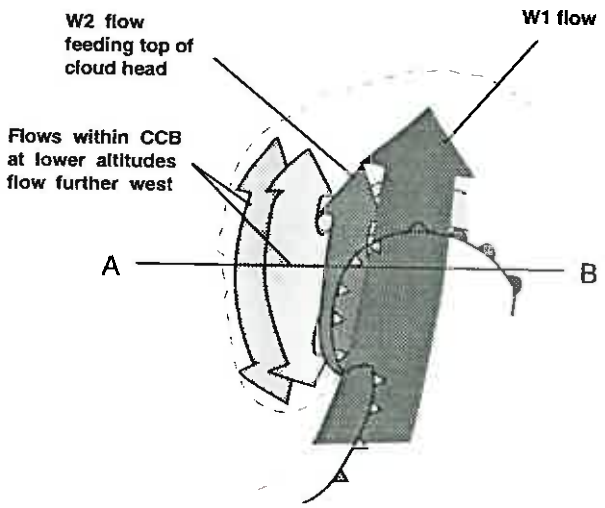

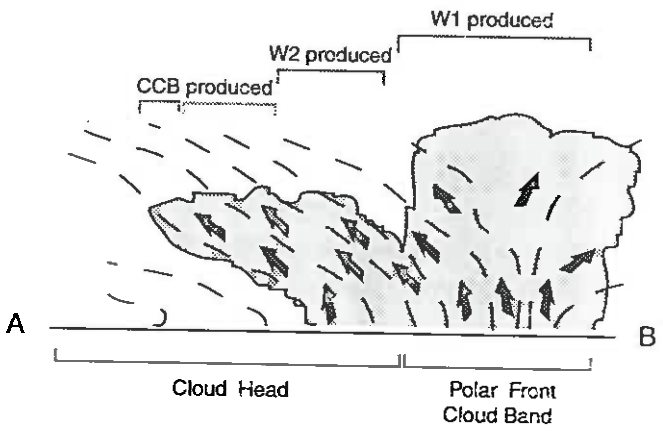

5) The mature cyclone

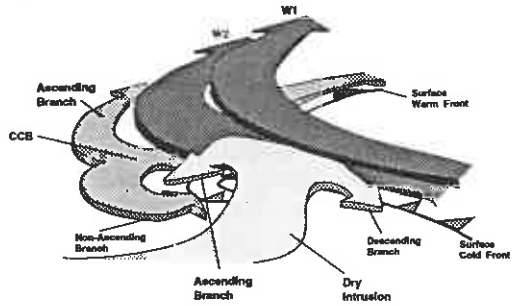

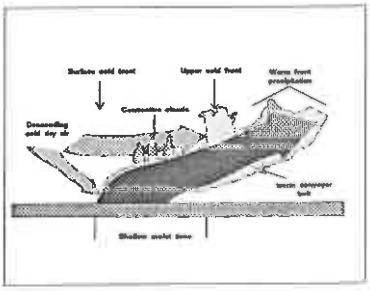

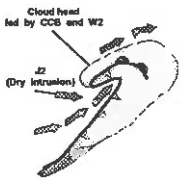

The bent-back structure of the cold front undergoes 'frontal-fracture' so that its northern part stays attached to the warm front and to the north west of J2, whilst the southern part is to the south east of J2.

By this stage, the dry intrusion airstream is drawn further into the circulation towards the cyclone centre and constitutes a cloud free region between the comma head and tail that is referred to as the dry slot.

The right hand edge of the dry intrusion can undercut the higher cloud of the polar front and produce an upper cold front often in line with, but further north than the surface cold front.

This situation, in which low θ_w air of the dry intrusion overlays relatively high θ_w air of the CCB and W2 flows is potentially unstable and convective clouds may develop into the dry intrusion airstream

6) The role of cold air features

Although the dry intrusion itself is a non-cloud producing airflow, its association with the cold air of the polar trough, its movement over relatively warm oceans, and the region of ascent associated with the upper level potential vorticity maximum combine to provide ideal conditions for convection to occur.

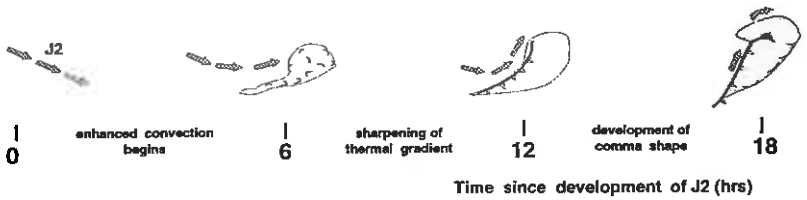

Although many factors will contribute to the likelihood of convection, a comma cloud may develop independently of the polar front in as little as 18 hours.

7) A cyclogenesis spectrum

Taking the degree of development of a cold air feature, C as a parameter which varies from zero to a fully developed comma cloud, it is clear that different modes of cyclogenesis are available depending at what stage C interacts with the polar front cloud band.

The figure presents this hypothesis within the context of a continuously evolving system.

To use the diagram, choose the appropriate distance between J2 and P in the top right hand corner (close, intermediate and far) and choose the degree of development of C (no convection, non-baroclinic, baroclinic, comma cloud) on the left hand side.

The intersection of the two paths then indicates the mode of cyclogenesis available for the developing storm.

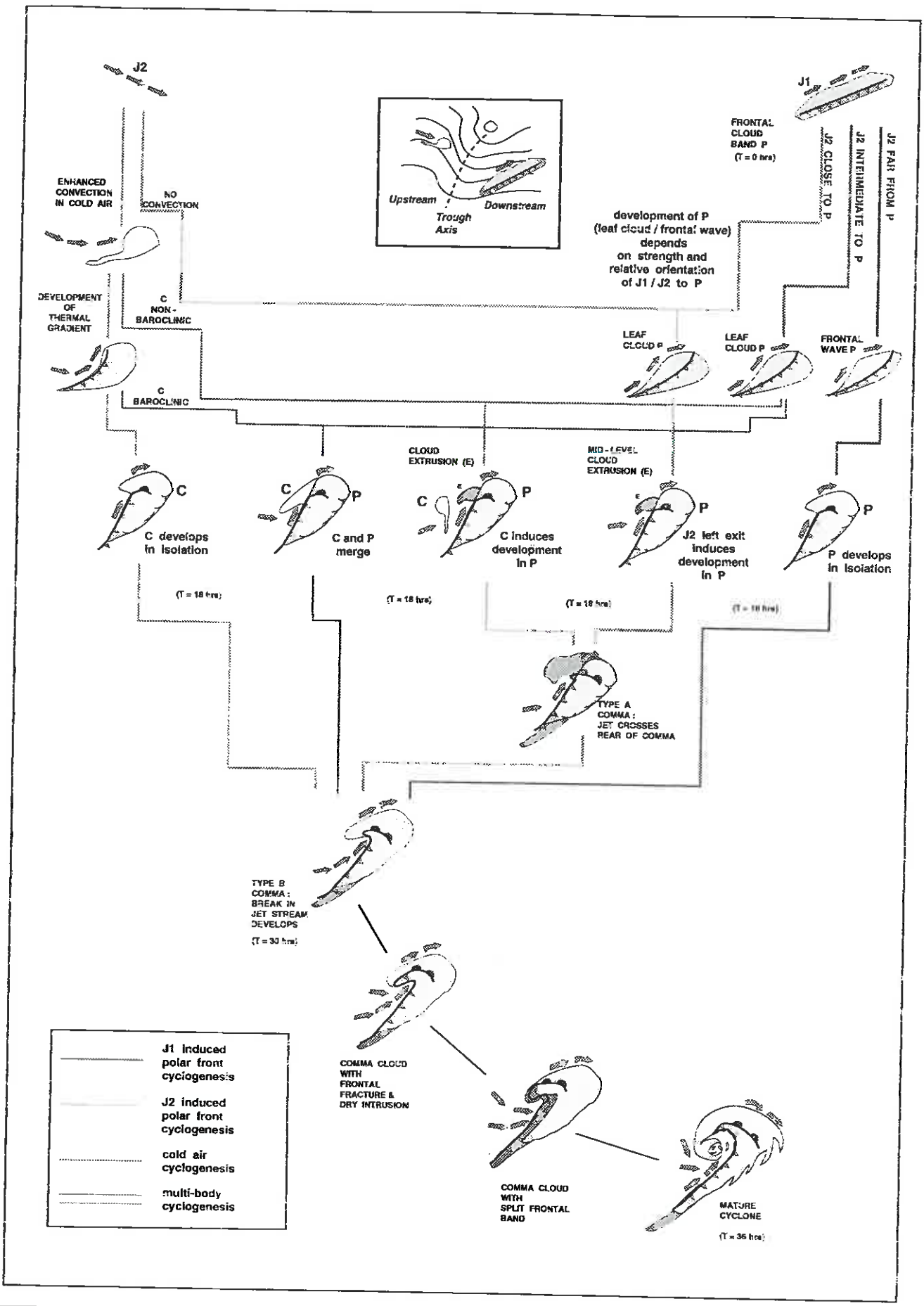

A complete treatment of the work presented in this poster may be found in the JCMM internal report 'Conceptual Models of Cyclogenesis'.

A CLASSIFICATION SCHEME FOR FASTEX CYCLONES

A.C.L. Deveson[1], K.A. Browning[1] & T.D. Hewson[2]

[1]*Dept. of Meteorology, University of Reading.* [2]*JCMM, UK Meteorological Office*

EXISTING CLASSIFICATION SCHEMES

Classification schemes of mid-latitude cyclogenesis have been used to increase the understanding of how cyclones develop, what causes variations in their development and what large-scale forcing features affect their structure.

IMAGERY BASED SCHEMES

Petterssen and Smebye (1971) outlined two types of cyclogenesis found from various observational studies. Type B was forced by an upper level trough while type A was a combination of upper and lower level forcing. Weldon (1979) used satellite imagery to define four flow patterns and their associated cloud structure, which were conducive to cyclogenesis over the USA. From this basis, many classification schemes for mid-latitude cyclogenesis have been developed.

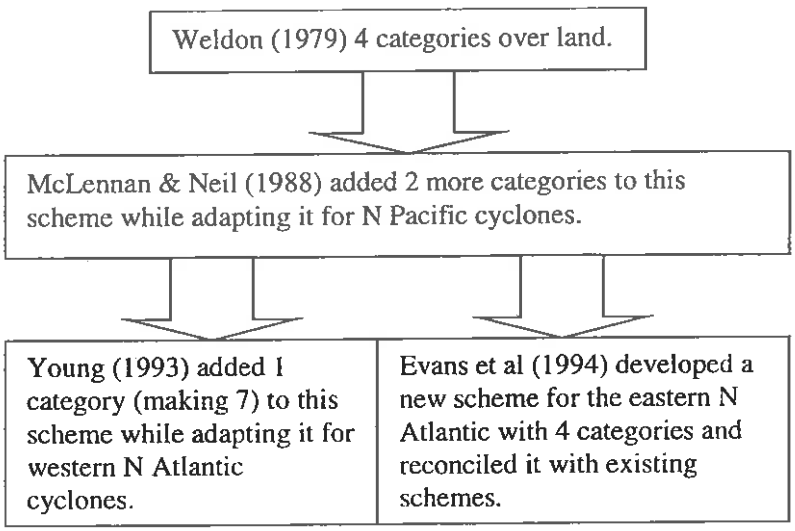

Figure 1. A flow chart showing how Weldon's scheme has been developed into synoptic classification schemes for N Atlantic cyclones.

These schemes are based on synoptic observations and satellite imagery and avoid using numerical model data so that they can be used as an alternative forecasting tool.

NWP-Based Schemes

Recently, an objective classification scheme for the N Atlantic region, based on tracking of relative vorticity maxima, has been developed (Aryault, 1998). Six categories have been defined using lower-level flow, frontal structure, upper-level jet location and cloud distribution from relative humidity distributions. This scheme has not yet been compared with any other scheme.

Idealised Schemes

Several numerical modelling experiments of idealised mid-latitude cyclogenesis have lead to the classification of idealised life cycles of cyclones (Thorncroft et al, 1993; Davies et al, 1991). These experiments have produced variations in cyclone development by applying a perturbation to idealised initial states. This enables large-scale differences in the cyclone development to be related to well-defined dynamical variations in the initial state prior to the disturbance developing.

	IMAGERY BASED SCHEMES	NWP-BASED SCHEMES	IDEALISED SCHEMES
ADVANTAGES	Use real data. Includes mesoscale features.	Data assimilation fills gaps in observational coverage. Application of the scheme can be automated.	A known perturbation is applied to produce the variations in the cyclogenesis.
DISADVANTAGES	Application can be subjective. Lack of observational data in some regions	There can be errors in model assimilation. No mesoscale features in the definitions of the categories.	Idealised initial states are used. No mesoscale structure in the model.

Table 1. The advantage and disadvantages of each type of classification scheme.

A New Approach To An Objective Classification Of Cyclones

A new NWP diagnostic for calculating vertical motion can be used to track cyclone development at various levels in the atmosphere. This parameter, known as 'Inv Lap Div Q', is a calculation of the vertical motion from the quasi-geostrophic omega equation (Clough and Davitt, 1994; Clough et al, 1996). The forcing for vertical velocity is calculated throughout the depth of the atmosphere and the vertical motion produced at each level is determined. The atmosphere can be partitioned into layers, allowing the vertical motion forced from only certain levels to be calculated. This enables a comparison of the strengths of the forcing from the upper and lower level troughs to be made.

Differences can be seen between cross-sections of actual vertical velocity and that implied by the total Inv Lap Div Q, due to the limitations of the quasi-geostrophic approximations and the omega equation. Small-scale features such as frontal structure can not be resolved and diabatically produced vertical motion is not explicitly included.

To develop an objective method of classifying cyclones, a method had to be developed to describe how the structure how the cyclone evolved. Various estimates of Inv Lap Div Q, hereafter referred to as QG forcing, were taken at the upper (600 – 100mb) and lower (1000 – 800mb) level. It was found that five 'ratios' summarised clearly the changes in the cyclone structure. They are of two types:

1. Ratios that describe the structure of the vertical motion at each level.
2. Ratios that describe how the levels of the atmosphere are interacting.

MEASUREMENTS ON A LEVEL	MEASUREMENTS BETWEEN THE LEVELS
PF & NF values – shows the intensity of the cyclone development.	U/L ratio – shows whether the upper or lower forcing is stronger.
PF/NF ratio – shows whether ascent or descent is dominating at each level.	Tilt – gives an estimate of the tilt of the system with height.
(PF-NF) distances – an estimate of the distance between the maximum ascent and descent on each level which gives an idea of the scale and the gradient of the forcing.	FU/FL ratio – shows the location of the low centre compared to the upper level trough. When the descent ratio is negative then the low centre is ahead of the upper level trough axis.

Table 2. A description of the estimates used to describe a cyclone's structure where PF is the maximum ascent associated with the low and NF is the maximum descent associated with the low at each level. FU is the vertical velocity at the upper level, located directly above PF and NF at the lower level (FL).

Plans For Developing An Overall Classification Scheme

The methods used to produce previous classification schemes will be combined in an attempt to minimise the impact of problems with each. To do this the scheme will be developed by:

- Use NWP analyses to provide good data coverage.
- Integrate this with satellite imagery and observations from the FASTEX experiment to limit errors in the NWP analyses.
- Use the FASTEX observations to examine the mesoscale structure of cyclones.
- Develop s classification scheme in which each category is defined using the new objective method together with the synoptic data and satellite imagery.
- The new scheme will be reconciled with existing ones.

Example Of One Category In The New Classification Scheme: Cold Air Cyclogenesis, FASTEX IOP4 & IOP18

The two cases, FASTEX IOP4 and IOP18 both developed other the Labrador Sea and were associated with a cold pool originating over northern Canada. Their structure developed in a similar manner though the IOP18 low intensified much more.

Figure 2 displays the QG diagnostic, used to classify cyclones, at the time of maximum intensification for IOP4 and IOP18. In both cases the upper level forcing for vertical motion dominates (grey shades), though both upper and lower-level forcing for vertical motion are much weaker in the IOP4 case. Figure 2 also shows that the tilt with height of the system is small as the upper level forcing dipole (representing the upper level trough) is nearly directly above the low centre. At later stages in the development both cases have no tilt or sometimes eastward tilt with height as the upper level trough moves directly over the low centre. This is one of the characteristics noted for this category.

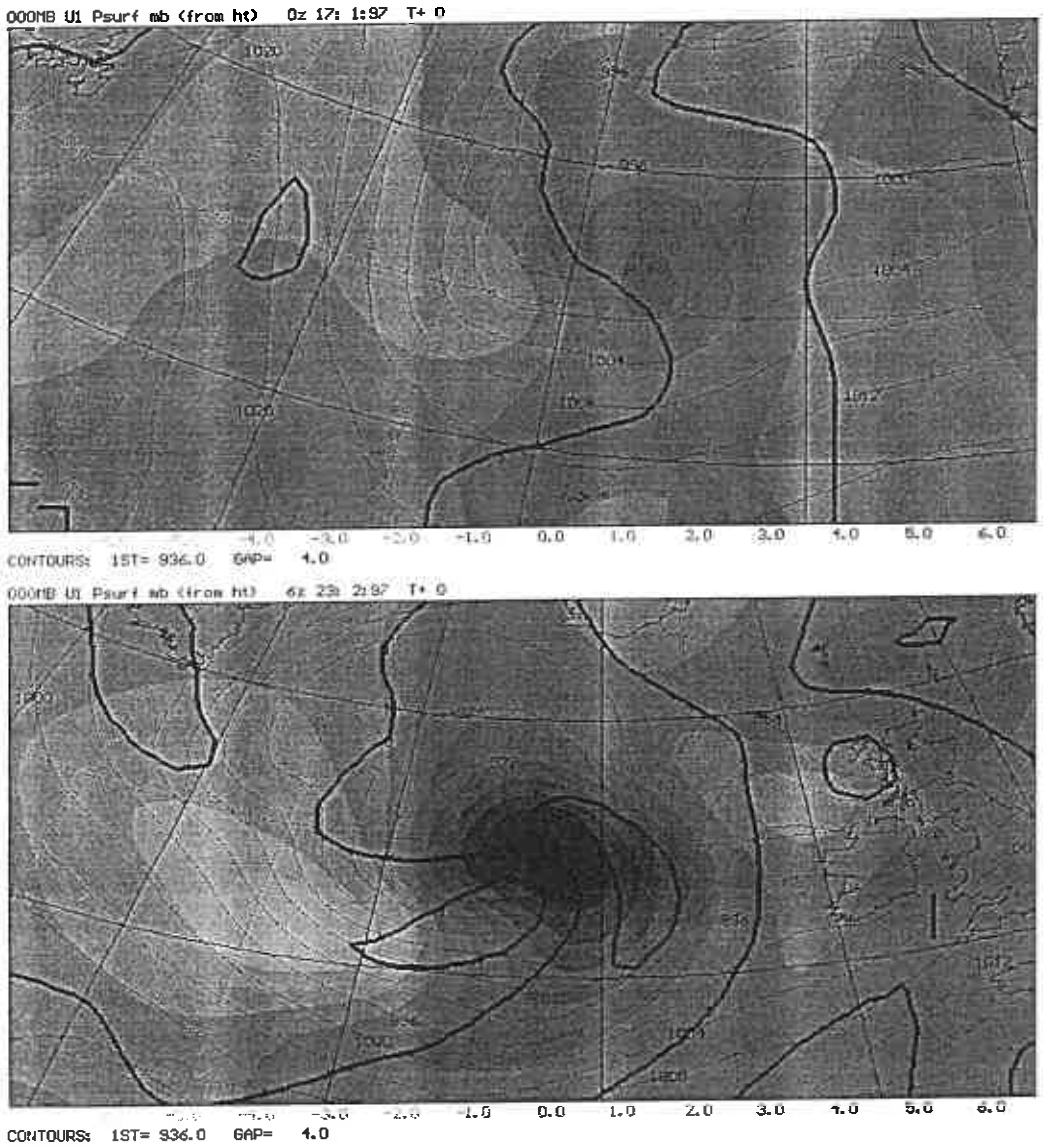

Figure 2. Th QG forcing for vertical motion at the time of maximum intensification for IOP4 (top) and IOP18 (bottom) where the grey shading represents is the upper level QG forcing, solid contours represent the lower level forcing and dashed contours the surface pressure contours.

Figure 3 displays an infrared satellite image for the time of maximum intensification for IOP18 (6z on 23/2/97). This image is overlaid with surface pressure contours (black) from the UKMO LAM data analysis. Objective θ_w fronts (Hewson, 1998) are plotted where light grey lines represents a cold front (thick line- standard front; thin line – weak front), dark grey a warm front, solid line a surface front (900mb) and dashed line an upper front (600mb). The thick dashed black lines represent jet cores of greater than 40 m/s at 300mb. These objective-plotting methods can reduce the subjectivity of relying solely on imagery-based classification schemes.

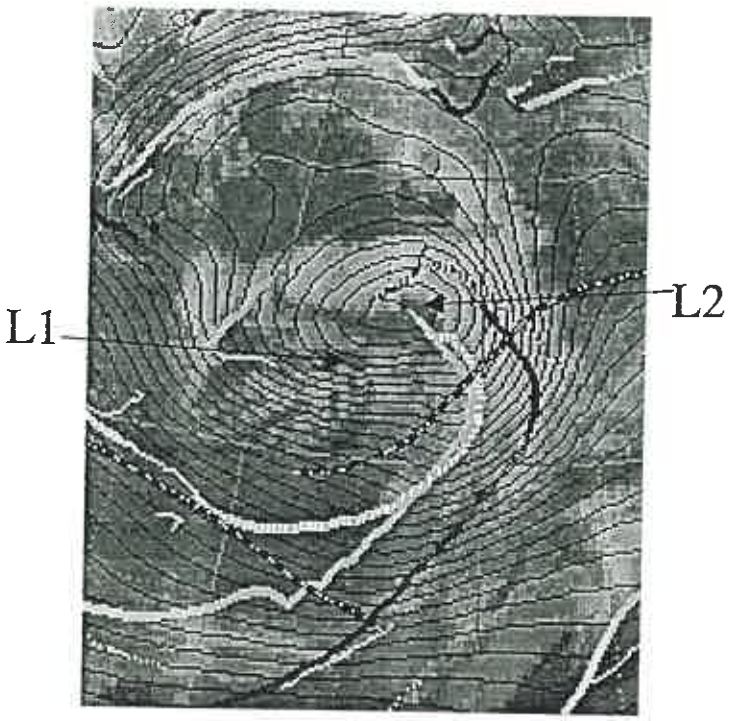

Figure 3. Infrared satellite image with objective fronts (Hewson, 1998) and upper level jet cores for the time of maximum intensification for IOP18. L1 and L2 are the location of the two vortices.

This satellite image gives some indication of two low centres within this system as two vortices can be identified within the convective cloud. This is an example of where the NWP model analysis is incorrect and the surface pressure pattern needs to be altered to be consistent with the cloud distribution. The convection is contributing to the development of the horizontal temperature gradient and the associated upper level jet. IOP4 has a similar convective cloud distribution but it is smaller in area and only weak fronts are present.

The main characteristics of the above cold air cyclogenesis category are:

- Large upper-level forcing for vertical motion.
- Associated with a deep tropopause fold.
- Abundant convective clouds.
- Complex frontal structure.
- Multiple vortices within the system centre.

REFERENCES

Aryult, F. (1998) Environement, structure et évolution des dépressions metéorologiques: réalité climalogique et modèles types. *PhD Thesis.*

Clough, S.A., Davitt, C.S.A. & Thorpe, A.J. (1996) Attribution concepts applied to the omega equation. *Q. J. R. Meteorol. Soc.* **122** 1943-1962

Davies, H.C., Shär, C.H. & Wernli, H. (1991) The palette of fronts and cyclones within a baroclinic wave development. *J. Atmos. Sci.* **48** 1666-1689

Evans, M.S. Keyser, D., Bosart, L.F. & Kackmann, G.M. (1994) A satellite derived classification scheme for rapid maritime cyclogenesis. *Mon. Weather Rev.* **122** 1381- 1416

Hewson, T.D. (1998) Objective fronts. *Mets. Apps* **5**, 37-65

McLennan, N. and Neil, L. (1988) Marine bombs program (phase II). Atmospheric Environment Service Pacific Region Tech. Rep. 88-002, 9pp

Petterssen, S. & Smebye, S.J. (1971) On the development of extratropical cyclones. *Q. J. R. Meteorol. Soc.* **97**, 457-482

Thorncroft, C.D., Hoskins, B.J. & McIntyre, M.E. (1993) Two paradigms of baroclinic-wave life cycle behaviour. *Q. J. R. Meteorol. Soc.* **119**, 17-55

Weldon, R. (1979) NWS satellite training course notes, part IV *Cloud Patterns and the Upper Wind Field,* Air Weather Service Tech. Rep. AWS/TR-79/003, 101pp

Young, M.V. (1993) Cyclogenesis: Interpretation of satellite and radar images for the forecaster. Forecasting Research Division Tech. Rep. No. 73 UKMO.

USE OF QUALITATIVE STRUCTURAL MODELS IN QUANTITATIVE WEATHER PREDICTION

Ian Roulstone, Adrian Semple and *Andy White* Met Office/JCMM

1. *Q.* WHAT IS A STRUCTURAL MODEL?

A. A structural (or conceptual) model of a weather system is a notional assembly of meteorologically significant component elements which describes the observed system in a concise and accurate way.

So a structural model is a rationalization of the 3D fields in a weather system – and of the thousands of numbers which represent them in a numerical model – into a small number of component structural elements (each of which may be quantified by a few parameters).

- A simple example of a structural model is shown at **A**
- A more complicated example is shown at **B**

Both **A** *and* **B** *refer to a developing/maturing mid-latitude cyclone. Air streams depicted are as seen in the system-relative frame.*

- At **C** is a list of some of the features that structural models identify; see, for example, Adrian Semple's poster in this session, and the book *Images in Weather Forecasting.*

2. DYNAMICAL INTERPRETATION

- *The components of structural models may be interpreted in various dynamical terms*

  For example, the **DRY INTRUSION** (see **B**) is (dry) air having high Potential Vorticity (PV), and the **WARM CONVEYOR BELT** (WCB, see **A** and **B**) is moist air having low PV – it may even be *negative.*

  Surface fronts are regions of large horizontal temperature gradient, and hence regions of concentration of PV in surface sheets.

  The PV interpretation of other elements
  (e.g. the **COLD CONVEYOR BELT,** CCB
  – see **A** *and* **B***) is less clear, and requires further study.*

- Dynamical interpretations in non-PV terms exist, of course; to some meteorologists they are more familiar, but are less concise.

  Structural models often feature air-stream elements (e.g. WCB, CCB) *which are identified by maxima of wind speed. Wind speed bears an analytically complicated but definite relation to the PV.* At **F** is an example of an isotach pattern and the corresponding PV field.

- Structural models raise many questions for the numerical modeller and the dynamicist – questions which are largely unaddressed as yet. For example: ***how well are the various elements described by various statements of balance?*** See **D** for discussion of this issue – in which the possibility of negative PV is key.

3. APPLICATIONS – CURRENT and FUTURE?

- Proxy data may be used to correct the upper level PV distribution in the initial conditions of an NWP run.

  Water vapour (WV) *satellite imagery is a useful proxy; it shows* (see the example at **G**) *the interleaving of deep regions of moist air* (blue shades) *and shallower regions of drier air* (yellow shades).

  Conceptual models such as the one shown at **B** allow the PV at a suitably chosen upper level to be conjectured from the WV imagery. *If NWP initial PV fields disagree with the suggestions of the WV imagery, then the model fields are likely to be in error.* Correction of the PV field, followed by inversion to give modified initial fields, may then lead to improved forecasts – see Sean Swarbrick's poster in this session, and hear Doug Mansfield's talk.

- *Structural models can be used in many ways to interpret satellite imagery.* For example, the visible and infra-red images shown at **E** strongly suggest the presence of a *kata cold front*. Such information could be invaluable in data assimilation for NWP.

- At a still more fundamental level regarding *the occurrence and structure of fronts*, it is clear that the influence functions used in some data assimilation schemes should respect the configuration of the flow, and not simply depend on physical distance. See **H** for discussion of the use of a *geostrophic coordinate transformation* to achieve this.

- Structural models could be used to appraise the performance of NWP models in a more illuminating way than that achieved by conventional skill scores (important though these are to gauge overall performance). Such *oriented verification* would enquire how the various structural elements were treated by the NWP models, and *would focus attention on their deficiencies in a way likely to suggest routes to improvement.*

- Finally, we recall that a structural model has already been used to achieve *dramatic improvements* in the forecasting of *tropical cyclones* by the UK Met Office; see the December 1994 edition of *NWP Gazette.*

A

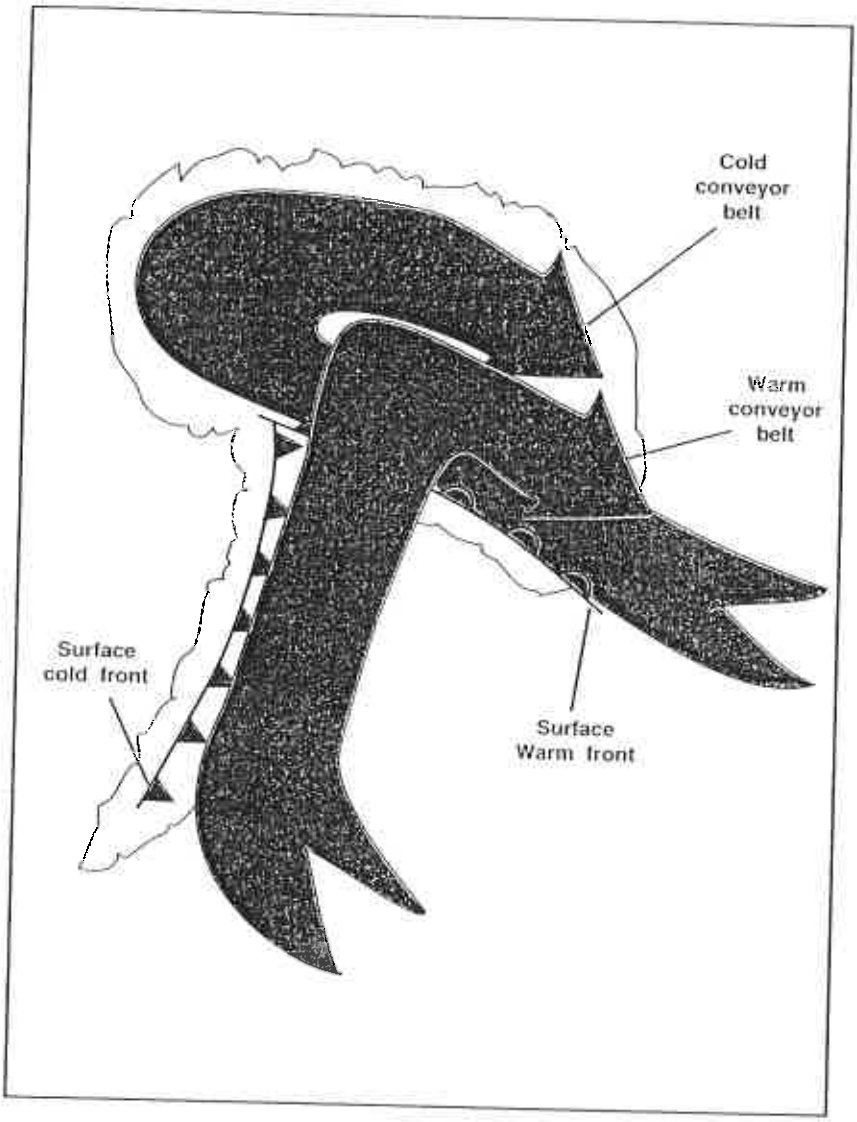
Cold
conveyor
belt
Warm
conveyor
belt
Surface
cold front
Surface
Warm front

B

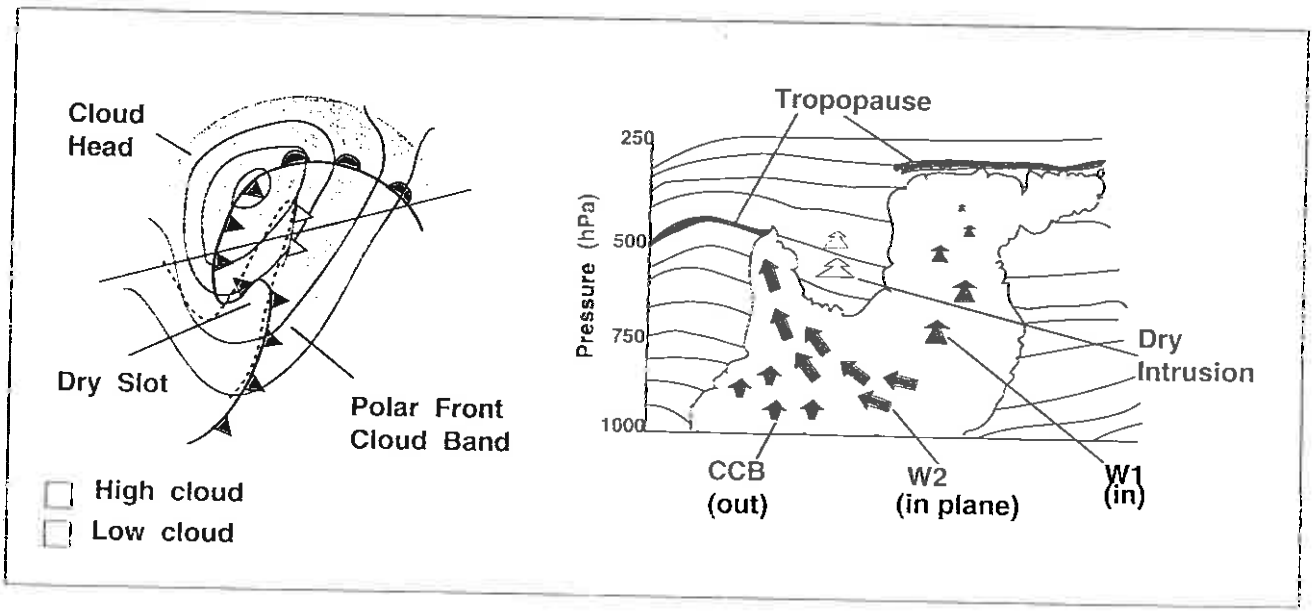
Cloud
Head
Dry Slot
Polar Front
Cloud Band
High cloud
Low cloud
Tropopause
250
500
750
1000
Pressure (hPa)
Dry
Intrusion
CCB
(out)
W2
(in plane)
W1
(in)

C *An incomplete list of structural model elements identified from observations of mid-latitude weather systems*

Ana cold front	Kata cold front
Warm conveyor belt	Cold conveyor belt
Dry intrusion	Frontal fracture
Cloud head	Leaf cloud
Cloud extrusion	Tropopause fold
Low-level jet	Shallow moist zone

D Potential vorticities in balanced models

- A Monge-Ampère equation is a relation of the form

$$A + B\phi_{xx} + 2C\phi_{xy} + D\phi_{yy} + E\left(\phi_{xx}\phi_{yy} - \phi_{xy}^2\right) = Q \qquad (1)$$

The coefficients A, B, C, D, E, Q may depend on $x, y, \phi, \phi_x, \phi_y$, where x and y are independent variables and $\phi = \phi(x, y)$ is an unknown function.

- The Monge-Ampère equation (1) is *elliptic* if

$$BD - C^2 - (A - Q)E > 0 \qquad (2)$$

- Monge-Ampère equations arise in many balanced models – e.g. semi-geostrophic theory, Salmon's L_1 (geostrophic) model, Charney balance equations .... In shallow-water versions of these models, we find the potential vorticity

$$Q = \frac{1}{h}\left[f + a\left(\frac{\partial v_g}{\partial x} - \frac{\partial u_g}{\partial y}\right) + \frac{\left(a^2 - c^2\right)}{f}\frac{\partial(u_g, v_g)}{\partial(x, y)}\right] \qquad (3)$$

Semi-geostrophic theory corresponds to the choice $a = 1, c = 0$

and L_1 dynamics corresponds to the choice $a = c = 1$

A 'new' balanced model (McIntyre and Roulstone 1996) has $a = 1, c = \sqrt{3}$, giving PV *accurate to two orders* in the Rossby number, that is, one order better than L_1 dynamics or semigeostrophy.

- The Monge-Ampère equation in semigeostrophic theory is elliptic if $Q > 0$; in the 'new' model it is elliptic if $Q < 3f/2h$.

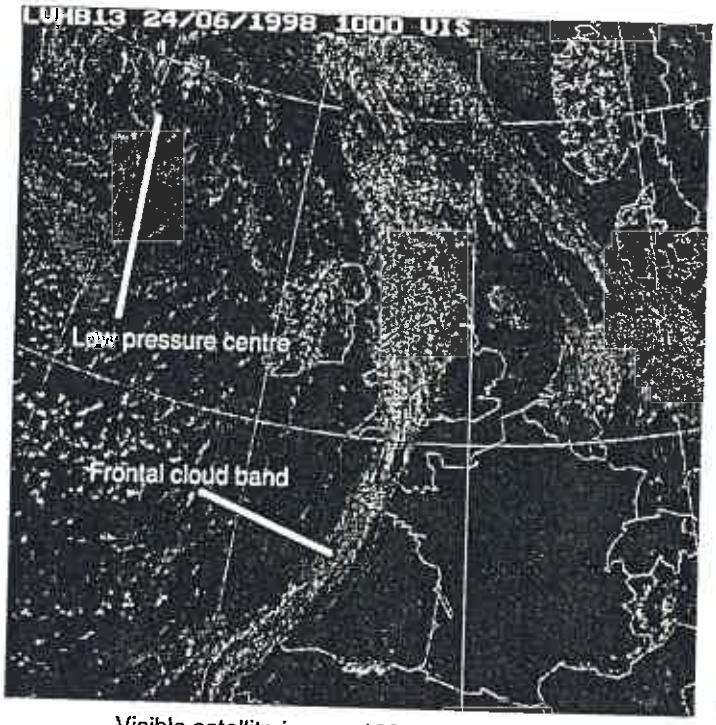

Visible satellite image, 1000am 24th June 1998

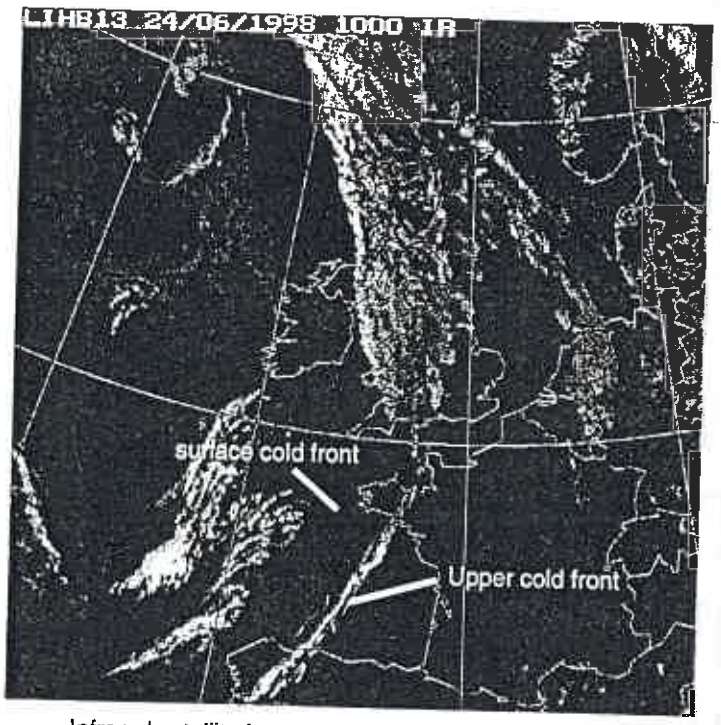

Infrared satellite image, 1000am 24th June 1998

E

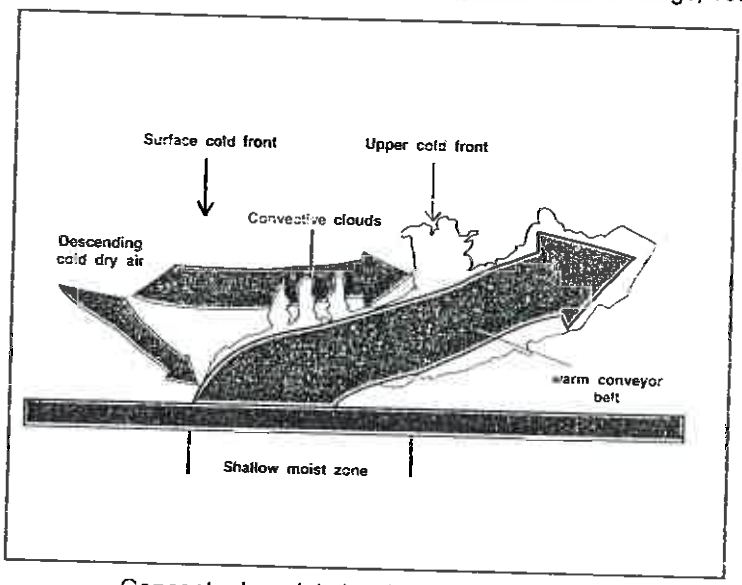

Conceptual model showing vertical profile

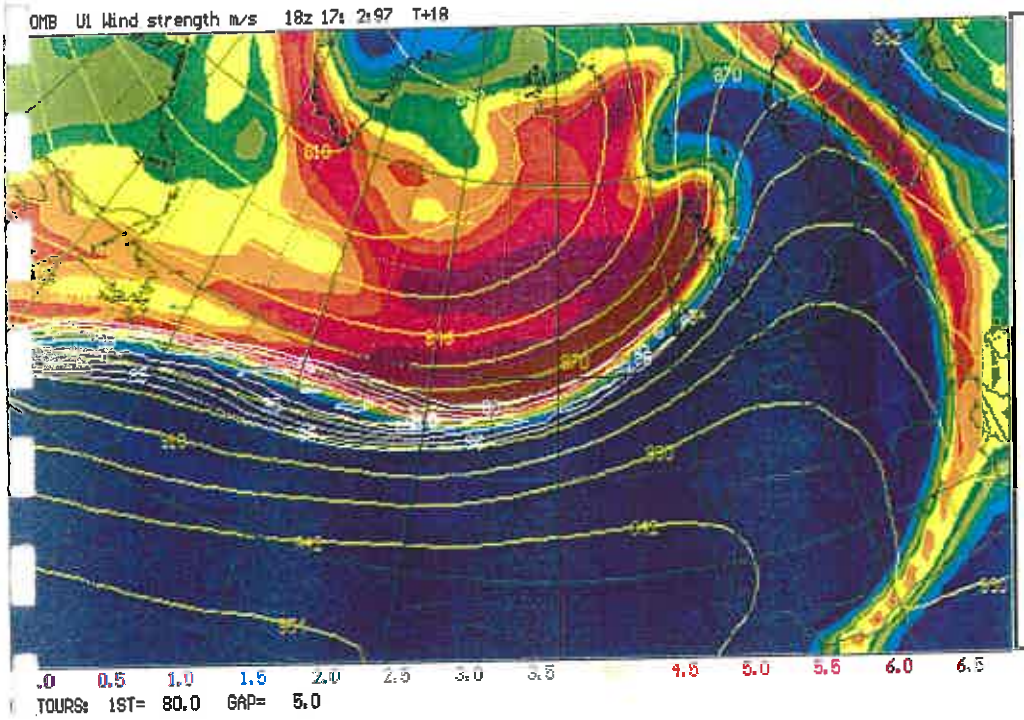

Colour field : PV on 300mb surface

yellow contours : 300mb Geopotentia height

white contours : wind speed > 80 m/s

F

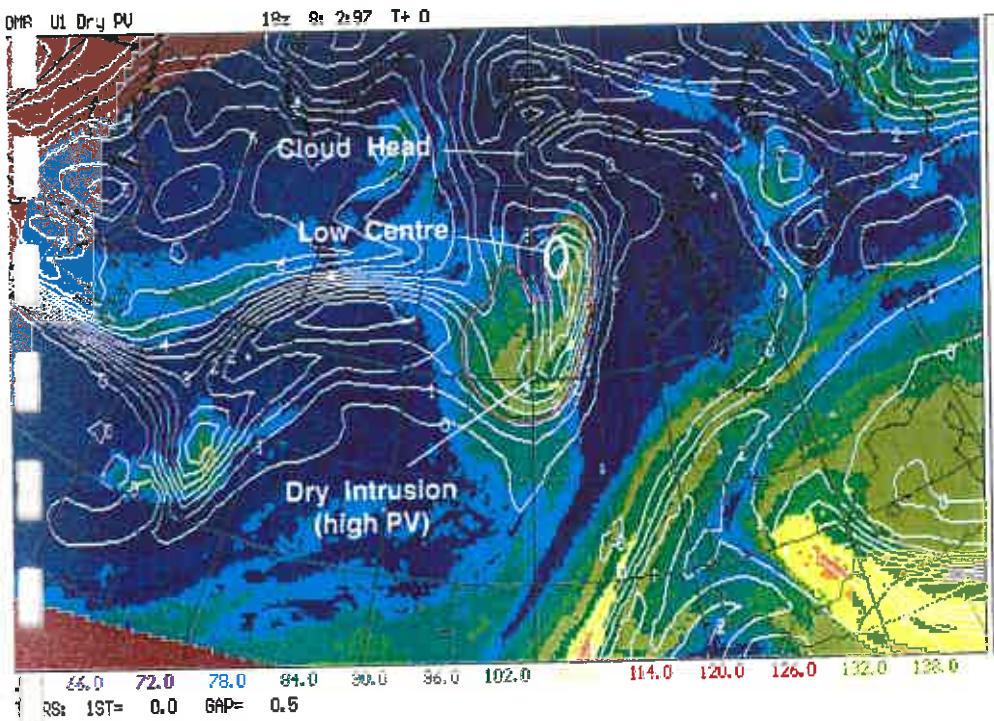

FASTEX IOP 11a
Water Vapor Satellite Image

white contours : PV on 300mb surface

G

H Applications of geostrophic coordinate transforms in data assimilation

Assimilation techniques used in NWP try to combine, in an optimal way, observations and forecasts. These techniques rely on a description of the statistics of forecast errors of the assimilating model.

- Flow-dependent forecast error correlations can be included by using the (flow-dependent) geostrophic transform of semi-geostrophic theory

$$X = x + \frac{g}{f^2}\frac{\partial h}{\partial x}, \qquad Y = y + \frac{g}{f^2}\frac{\partial h}{\partial y} \tag{4}$$

- Its purpose is to transform the homogeneous isotropic and barotropic correlations into structures more dynamically consistent with sloping frontal surfaces (Desroziers 1997). Note that

$$Q = \frac{f}{h}\frac{\partial(X,Y)}{\partial(x,y)} \tag{5}$$

and in terms of the transformation $(x,y)\mapsto(X,Y)$,

$$\text{cyclonic vorticity} \Rightarrow \frac{\partial(X,Y)}{\partial(x,y)} > 1$$

$$\text{anticyclonic vorticity} \Rightarrow \frac{\partial(X,Y)}{\partial(x,y)} < 1$$

Example (Hoskins 1975)

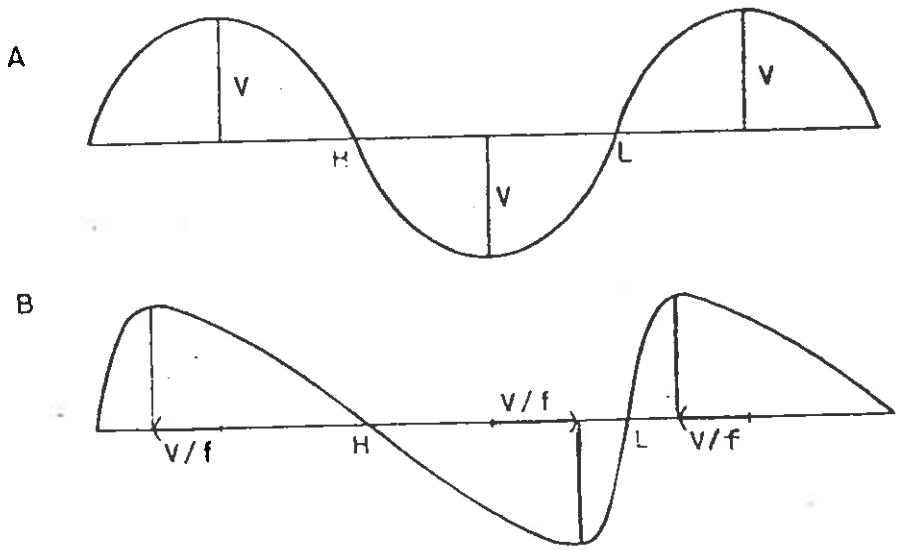

FIG. 1. A y-velocity pattern that is sinusoidal on quasi-geostrophic theory, or on semi-geostrophic theory in X space, is represented in A. In B is shown the physical space velocity pattern. The anticyclonic center H is broadened and weakened. The cyclonic center L is tightened and strengthened.

An example of the application of the geostrophic transformation (Desroziers 1997)

The situation presented here is the IOP 7 of FRONTS 87 (Thorpe and Clough 1991). Contour interval is 0.25; values > 1 are drawn with solid lines and values < 1 with dashed lines. The vorticity of the retrieved wind field (Fig. 2) can be compared with that of the initial field (Fig. 1). Notice that the bands of strong cyclonic vorticity remain almost unchanged.

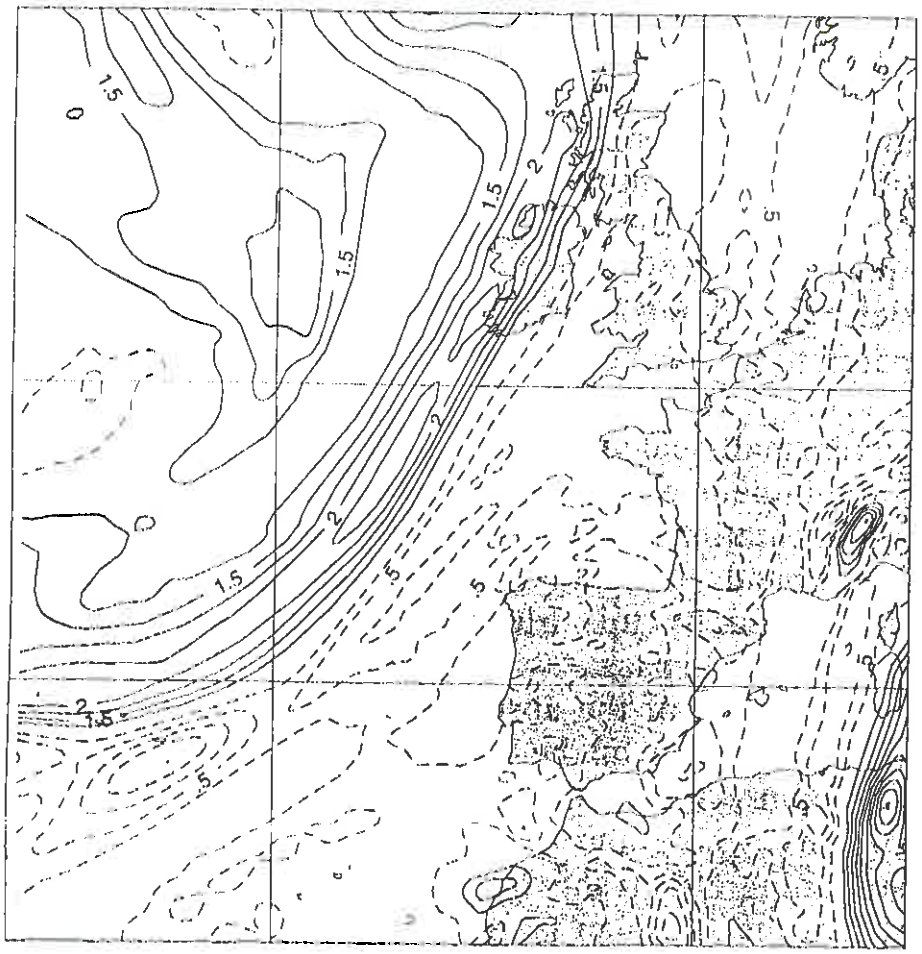

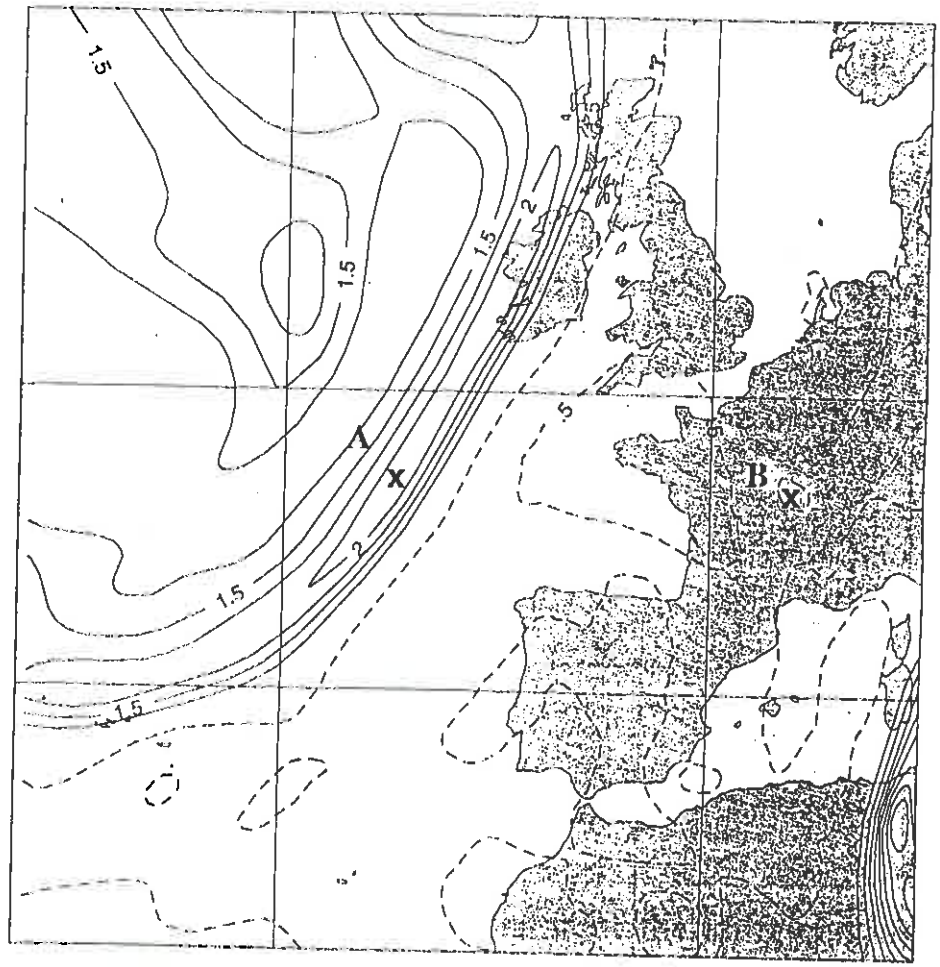

APPLICATION OF PV INVERSION AND WATER VAPOUR IMAGERY IN NWP

S.J.SWARBRICK UK Met. Office (JCMM)

Errors which occur in the numerical prediction of cyclonic development may be partly due to errors in the initial wind & temperature fields at upper tropospheric levels. Data assimilation sometimes fails to correct such errors. This project is investigating a method to detect such errors and make appropriate adjustments to the initial fields.

In general any cyclonic system can be associated with an intrusion of dry stratospheric air into the upper troposphere. Such dry intrusions show up on water vapour satellite images as regions of enhanced brightness temperature. They also correspond to anomalies in the potential vorticity (PV) fields at upper tropospheric levels, since stratospheric air has high PV.

It follows that there is a correspondence between anomalies in the model PV field at the tropopause level and anomalies in the satellite WV brightness temperature field. Errors in the model wind and temperature fields at upper tropospheric levels would give rise to mismatches between such PV anomalies and the WV image.

Climatology shows that isentropic surfaces in the 315K/330K range intersect the tropopause at latitudes corresponding to the N Atlantic cyclone track region. Comparison of model PV on such surfaces with the corresponding WV image thus provides a means of detecting errors in the model's initial state.

By using this principle in conjunction with PV inversion, the model's initial analysis may be improved. The PV inversion is carried out on pressure levels. In practice, the 300mb level may be used for PV adjustment, instead of the 315/330K isentropic surfaces. Related adjustments are also made on other pressure levels.

The method employed consists of the following steps:

- Compare the model initial PV field, at analysis time, on an appropriate isentropic or isobaric level (probably 300mb), with the corresponding satellite water vapour image. Hence decide how the PV field is to be modified.

- Carry out the PV modifications at 300mb, and perform related modifications on a range of other pressure levels (typically 250-500mb).

- Carry out a PV inversion on both the original PV field and on the modified PV field. Each PV inversion outputs wind and temperature fields. The difference of these two sets of fields gives wind and temperature increments.

- Use the wind and temperature increments to adjust the model wind and temperature fields at analysis time.

- Rerun the forecast from the adjusted analysis.

CASE STUDY : 12z 1/9/97 TO 12z 3/9/97

The UM LAM analyses show a cyclone E of Newfoundland at 12z 1/9/97, which fills and then deepens again as it travels eastwards. At 12z 2/9/97 it is at a mid-Atlantic location with central pressure about 1002mb. At 0z 3/9/97 it is located W of Ireland with central pressure about 996mb. At 12z 3/9/97 it is NW of Scotland and has deepened to about 988mb, having merged with an adjacent older cyclone.

The LAM forecast failed to develop the system sufficiently and also showed a slight position error. At T+24 (mid-Atlantic) the position is correct but the central pressure is 1006mb (4mb too high). At T+36 (W of Ireland) the central pressure is 1000mb (4mb too high) and the position is slightly too far S. At T+48, the central pressure is 992mb (4mb too high) and the position is about 5 deg too far E. The merger with the neighbouring cyclone is less developed.

The analysed PV field at 300mb shows a PV anomaly, maximum PV about 3.5 units, located just N of the corresponding brightness temp maximum in the WV image. A corresponding minor anomaly was evident at 400 & 500mb in the same horizontal position.

The adjustments made to the PV field were as follows. The anomaly at 300mb (and 250mb) was moved slightly S, to coincide with the BT maximum, and was enhanced to a PV maximum of 6 units. The anomaly enhancement was extended down to 500mb; the PV maximum created amounted to 2.5 units at 500mb. This downward extension was found to be necessary in order to influence surface development to the desired extent.

In the rerun forecast the intensity and position errors at T+24, T+36 and T+48 were found to be substantially reduced. Indeed, at T+36 the errors were virtually eliminated.

Initial analysis 12z 1/9/97 (PMSL)

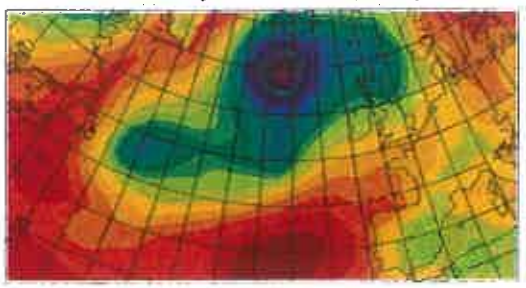

9940 9980 1002 1020 1060 1100 1140 1180 1220 1260 0

Analysis (PMSL) 12z 2/9/97

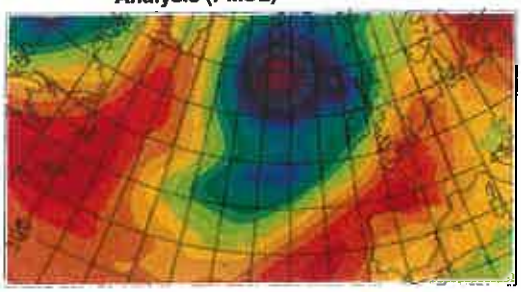

9940 9980 1002 1020 1060 1100 1140 1180 1220 1260 0

Original forecast (PMSL) 12z 2/9/97 T+ 24

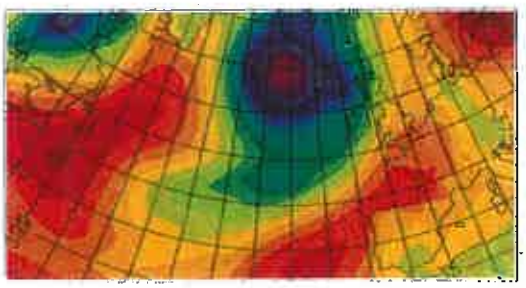

9940 9980 1002 1020 1060 1100 1140 1180 1220 1260 0

Rerun forecast (PMSL) 12z 2/9/97 T+ 24

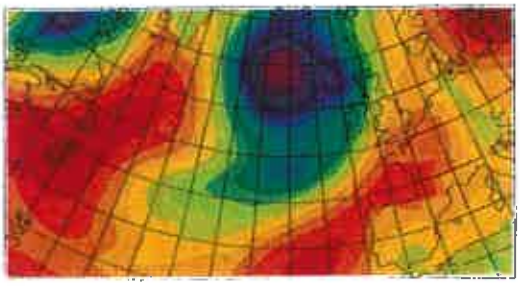

9940 9980 1002 1020 1060 1100 1140 1180 1220 1260 0

Analysis (PMSL) 0z 3/997

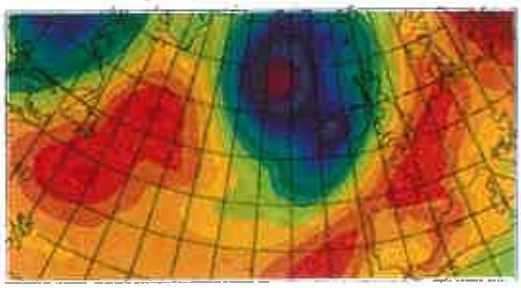

9940 9980 1002 1020 1060 1100 1140 1180 1220 1260 0

Original forecast (PMSL) 0z 3/997 T+ 36

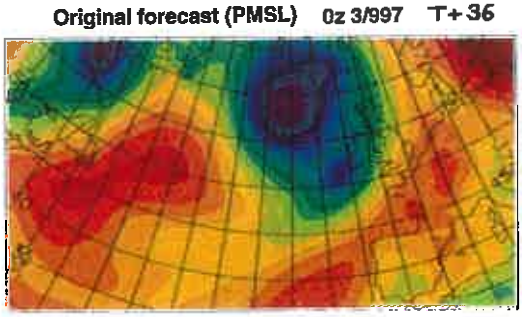

9940 9980 1002 1020 1060 1100 1140 1180 1220 1260 0

Rerun forecast (PMSL) 0z 3/997 T+ 36

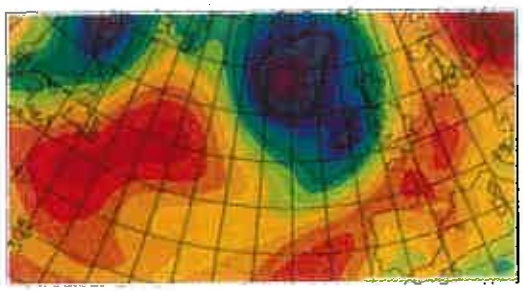

9940 9980 1002 1020 1060 1100 1140 1180 1220 1260 0

Analysis (PMSL) 12z 3/9/97

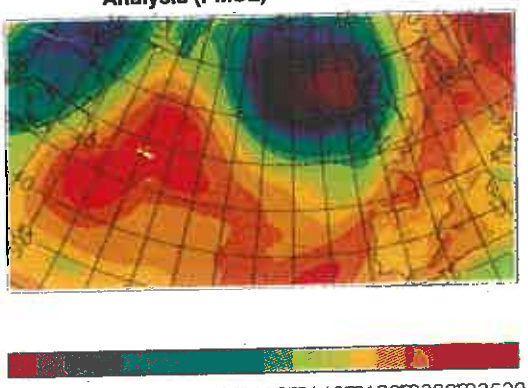

9940 9980 1002 1020 1060 1100 1140 1180 1220 1260

Original forecast (PMSL) 12z 3/9/97 T+48

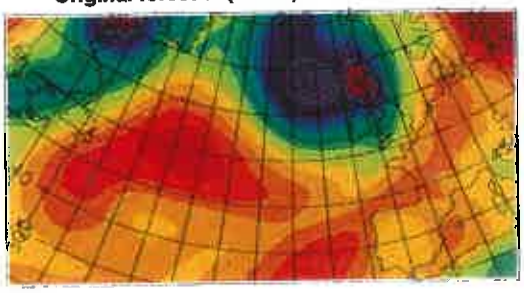

9940 9980 1002 1020 1060 1100 1140 1180 1220 1260

Rerun forecast (PMSL) 12z 3/9/97 T+48

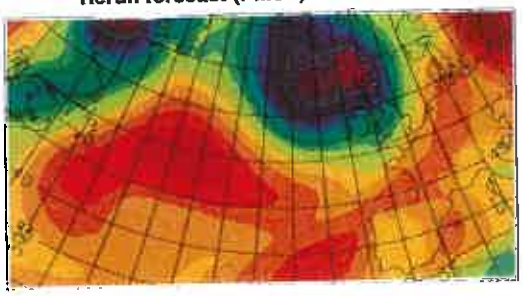

9940 9980 1002 1020 1060 1100 1140 1180 1220 1260

PV on 300mb & WV image - original forecast T+0

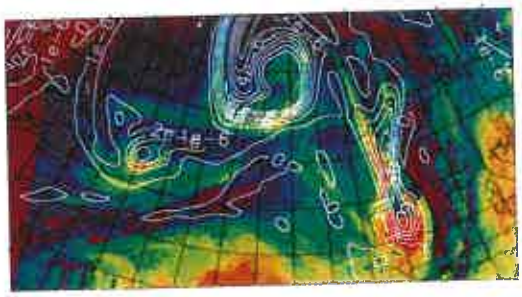

10 40 70 100 130 160 190 220 250

PV on 300mb & WV image - rerun forecast at T+0

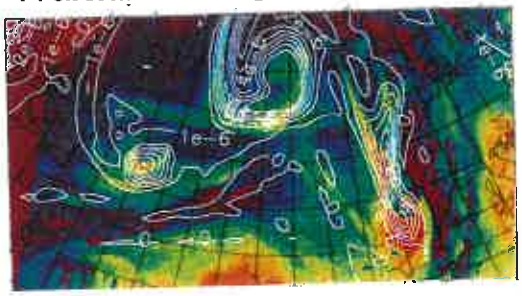

10 40 70 100 130 160 190 220 250

Control Tests of PV Inversion on the UM Global Grid

N. Keeley and A.A. White

The Meteorological Office, Joint Centre for Mesoscale Meteorology, The University of Reading, P.O. Box 243, Reading, Berkshire

Abstract

A series of "control tests" has been carried out to test the effect of PV inversion itself on UM model forecasts. The unmodified initial PV was inverted and the resultant wind and temperature fields inserted into the initial dump. The model forecast was then re-run out to three days and the result compared with that using the unchanged initial dump.

The results of this rather severe test of the PV inversion process have so far been most encouraging.

1 Introduction

• Improved Unified Model (UM) forecasts have been obtained by modifying the initial potential vorticity (PV) field so that it matches water vapour satellite imagery [see poster by S. Swarbrick].
• This technique requires inversion of the modified PV to give modified wind and temperature fields for input to the UM.
• How much (if any) of the improvement in forecast is due to the inversion process itself rather than the change in the PV?
• Forecast reruns using fields from inverted, unaltered, PV distributions are presented to check any change due to the inversion process itself.

2 The Tests

All tests were carried out using the global version of the Meteorological Office's Unified Model. PV was inverted over a sub-area of the global grid, corresponding to the North Atlantic. The tests were conducted as follows:
• Obtain PV field over sub-area. Invert using code developed by M. Griffiths to obtain winds and temperatures.

• Interpolate fields from pressure levels to model (η) levels and over-write initial dump using code developed by S. Swarbrick.
• Rerun forecast out to T+72 (no data assimilation).
• Compare rerun forecast with that using unmodified initial dump (also with no data assimilation).

3 Results

The figures show fractional difference fields (F_{orig}-F_{rerun}/F_{orig}) for the winds and temperatures from forecasts run using the original and over-written initial dumps. The forecasts ran from 00Z on 22/6/1998 with output every 24 hours.
• Any changes introduced by the inversion process are small.
• Largest changes are in the winds (these may be merely indicating areas of divergent flow).

4 Conclusions

This is a rather severe test of PV inversion. In the usual use of this technique, two PV inversions are carried out and increments in winds and temperatures are added to the initial dump rather than over-writing the entire field. Our results show that, for all cases investigated so far, the inversion process itself does not appear to have a significant effect on the rerun forecast. Thus, we can infer that any improvements in forecasts from the matching of PV with water vapour imagery are due to the changes in PV rather than to the inversion process.

Geopotential Height

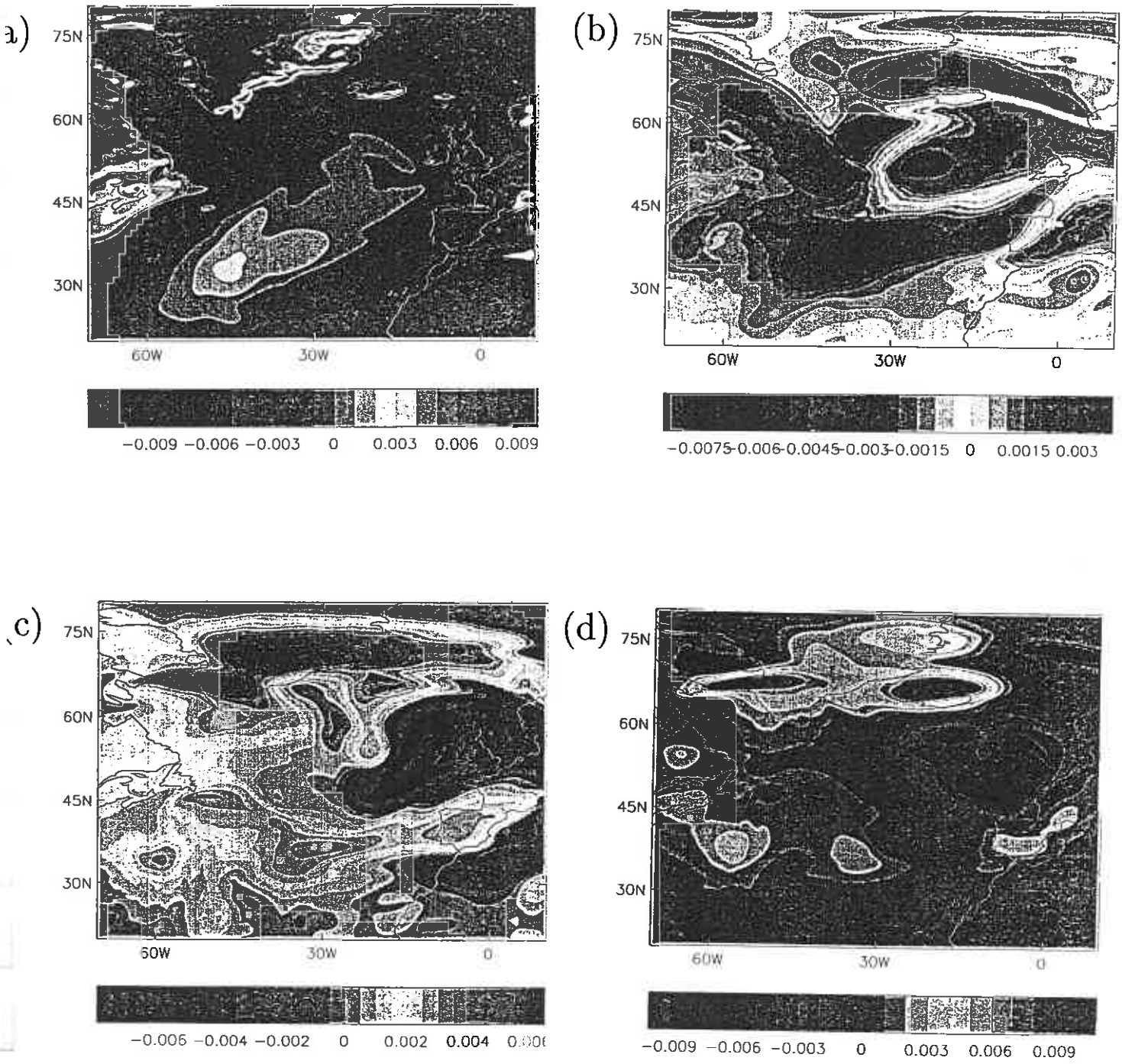

$\frac{\Phi_{\text{orig}} - \Phi_{\text{rerun}}}{\Phi_{\text{orig}}}$ on the 300 hPa level at: (a) 00Z on 22/6/1998 (T+0); (b) 00Z on 23/6/1998 (T+24); (c) 00Z on 24/6/1998 (T+48); (d) 00Z on 25/6/1998 (T+72)

u component of wind

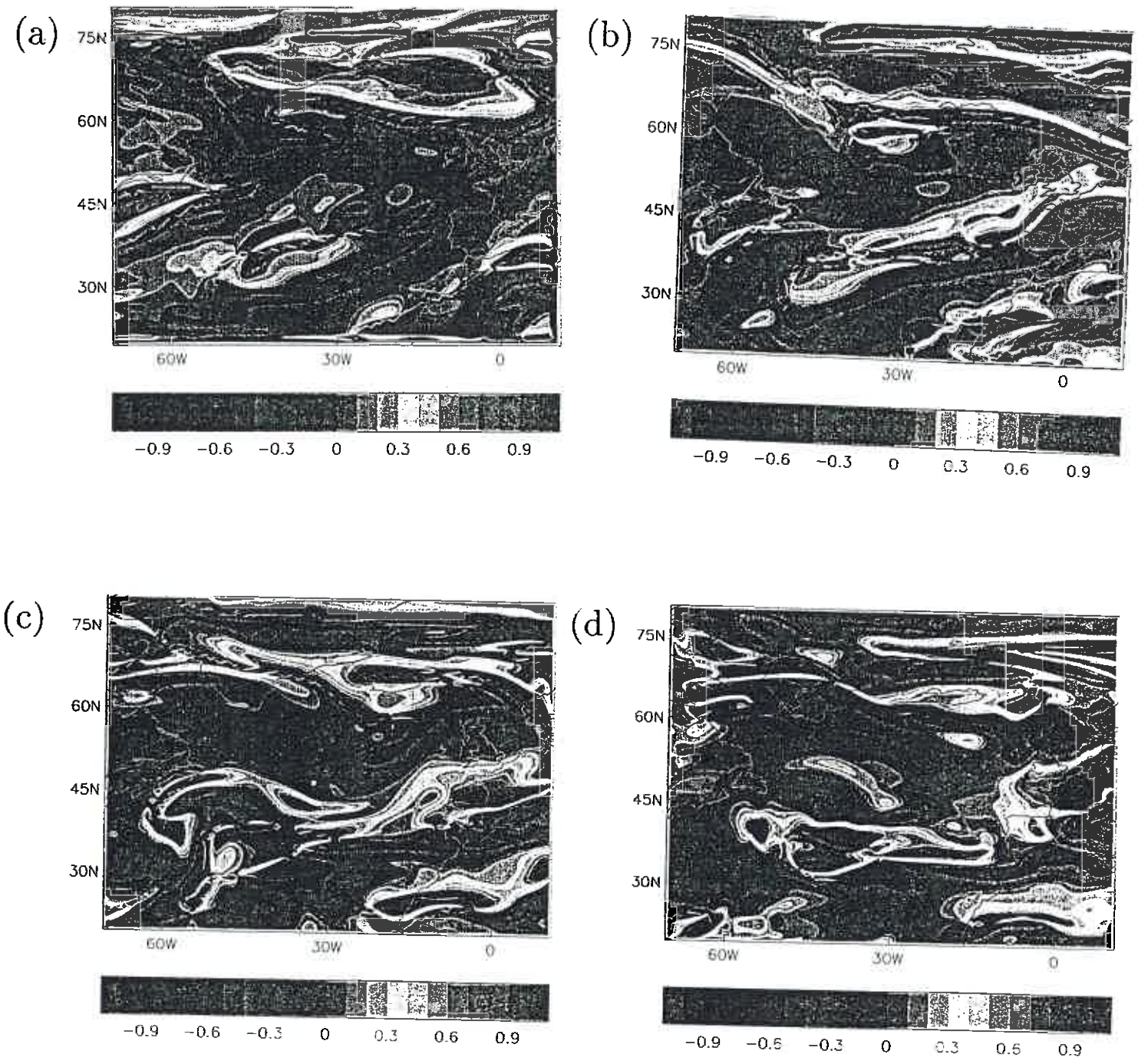

$\frac{u_{orig}-u_{rerun}}{u_{orig}}$ on the 300 hPa level at: (a) 00Z on 22/6/1998 (T+0); (b) 00Z on 23/6/1998 (T+24); (c) 00Z on 24/6/1998 (T+48); (d) 00Z on 25/6/1998 (T+72)

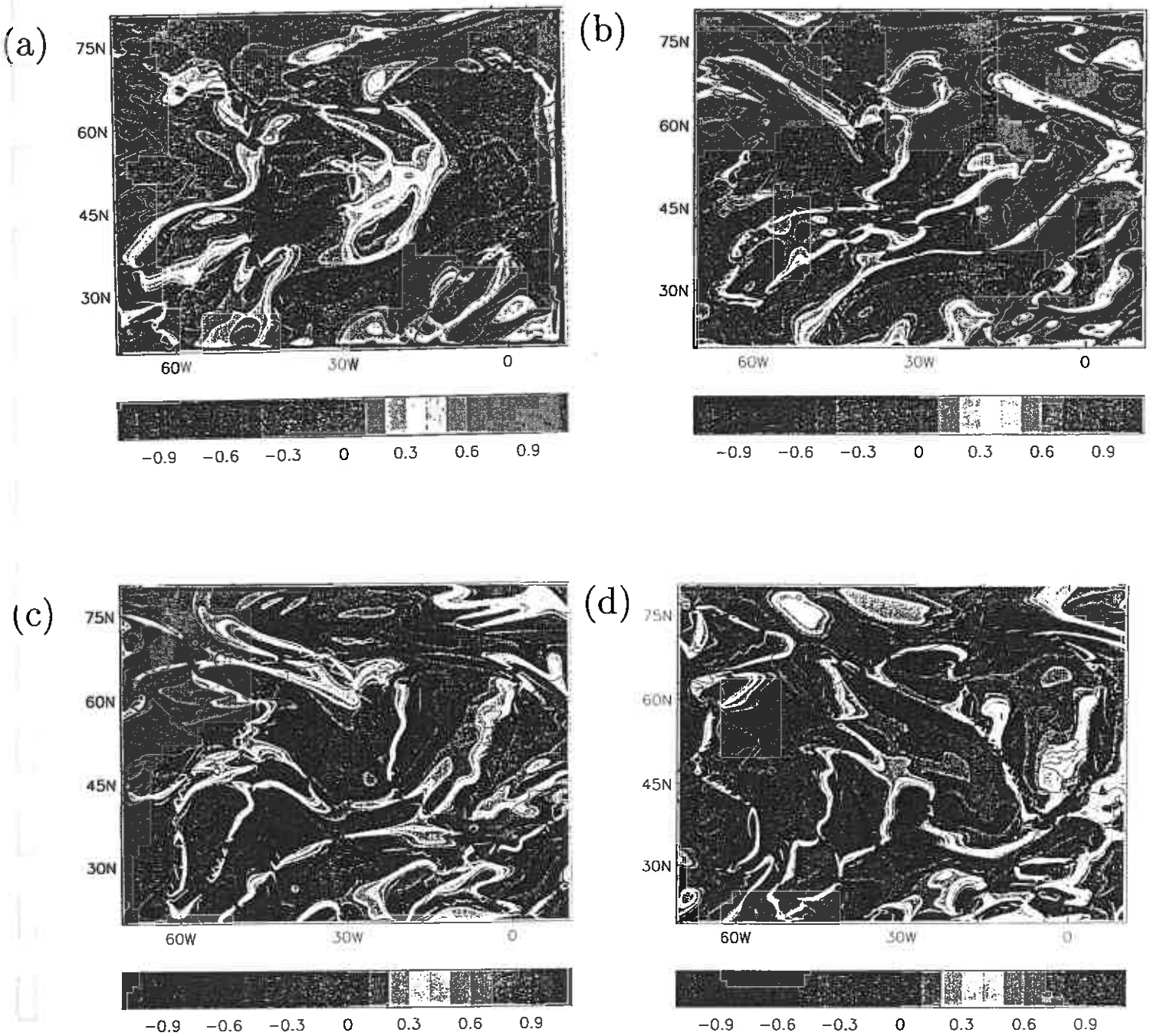

$\frac{v_{orig}-v_{rerun}}{v_{orig}}$ on the 300 hPa level at: (a) 00Z on 22/6/1998 (T+0); (b) 00Z on 23/6/1998 (T+24); (c) 00Z on 24/6/1998 (T+48); (d) 00Z on 25/6/1998 (T+72)

Temperature

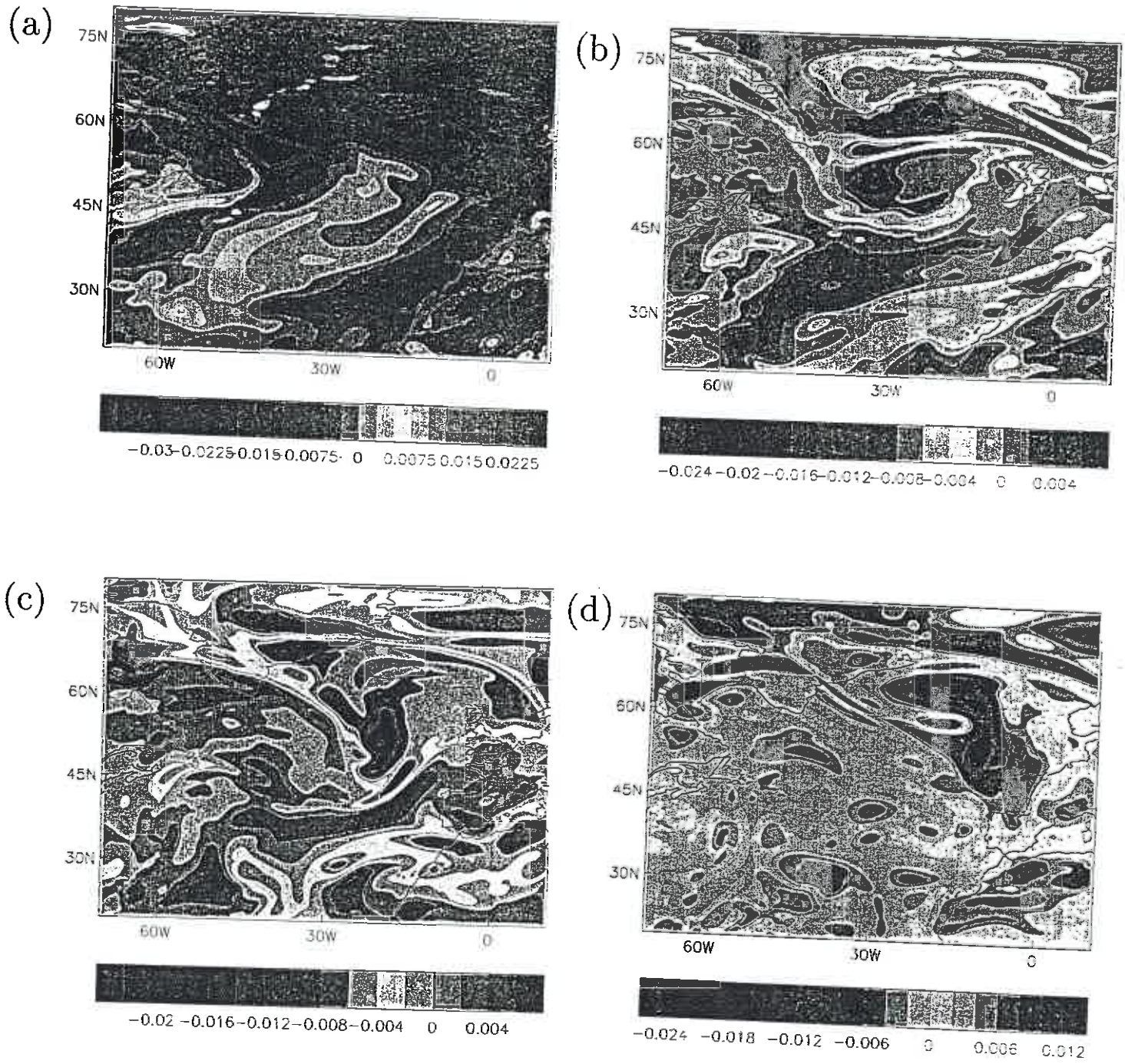

$\frac{T_{orig}-T_{rerun}}{T_{orig}}$ on the 300 hPa level at: (a) 00Z on 22/6/1998 (T+0); (b) 00Z on 23/6/1998 (T+24); (c) 00Z on 24/6/1998 (T+48); (d) 00Z on 25/6/1998 (T+72)

Mean sea level pressure

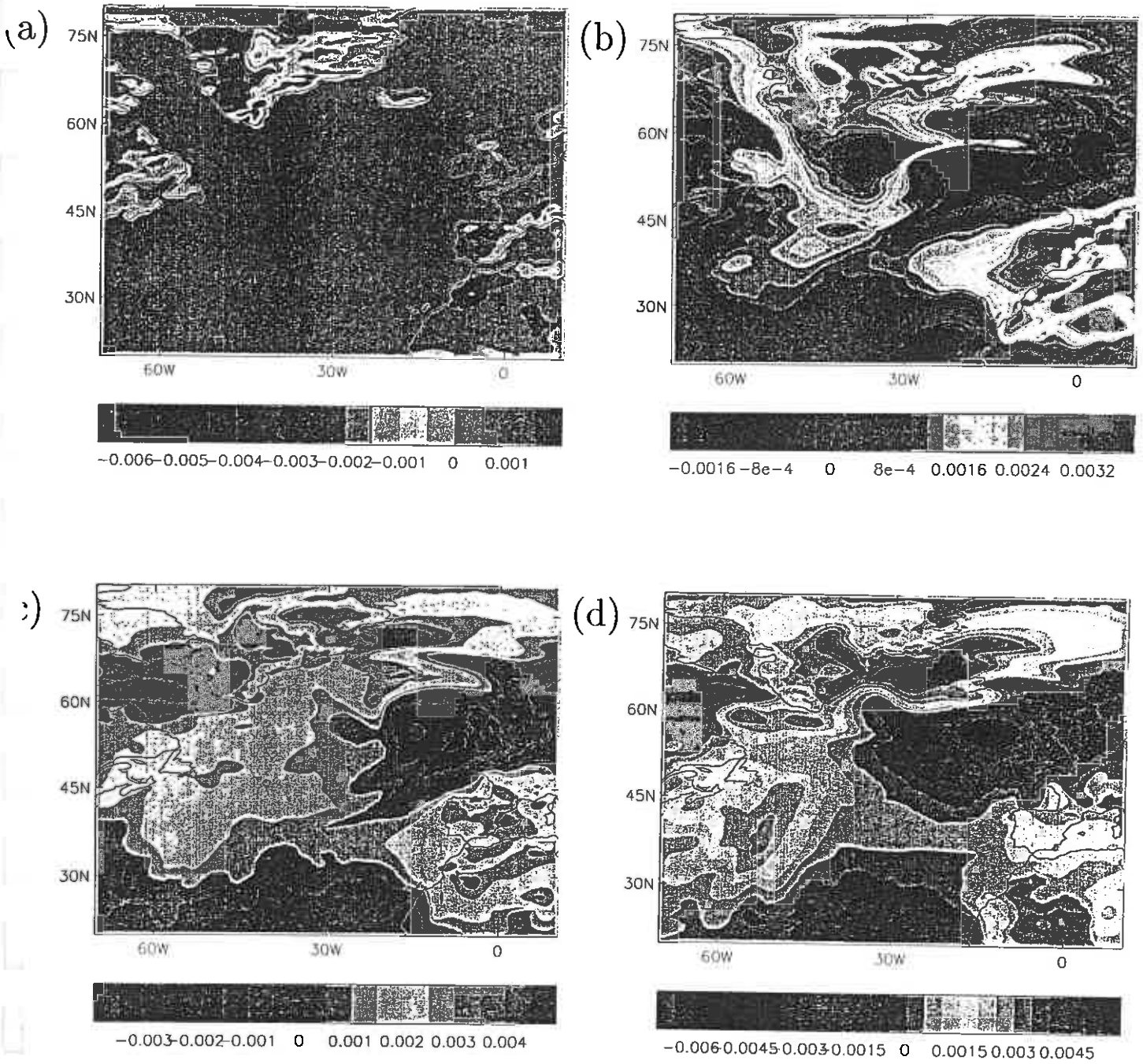

$\frac{\text{slp}_{\text{orig}} - \text{slp}_{\text{rerun}}}{\text{slp}_{\text{orig}}}$ on the 300 hPa level at: (a) 00Z on 22/6/1998 (T+0); (b) 00Z on 23/6/1998 (T+24); (c) 00Z on 24/6/1998 (T+48); (d) 00Z on 25/6/1998 (T+72)

USE OF ECMWF SINGULAR VECTORS FOR TARGETING DURING FASTEX

Andrea Montani and Alan J. Thorpe

Department of Meteorology, University of Reading, Reading RG6 6 BB, UK

INTRODUCTION

Why do forecast errors exist?

The true state of the atmosphere is known only approximately and uncertainties are especially larger where data coverage is poorer (for example in the oceanic storm–tracks). Fast growing features of analysis errors, responsible for the greatest forecast errors, are located in small *sensitive regions*, whose locations depend on the features on the flow.

Where are the sensitive regions?

In order to improve short and medium range weather forecasts, there is a need to make extra–observations in such sensitive regions (*targeting*), in order to reduce as much as possible those analysis errors which are going to grow eventually fastest with time.

How to look for sensitive regions?

Singular vector (SV) *technique* can locate sensitive regions by identifying fast growing perturbations, which are characterised by maximum growth of total energy over a time interval in a localised area. The SV technique was tested during the Fronts and Atlantic Storm–Track EXperiment (FASTEX), to target upstream observations of incipient cyclones.

CASE STUDIES

Calculations of SVs were performed using ECMWF forecasting model for the Intensive Observation Periods (IOPs) 9, 11, 12 and 17. For each case study, it was prepared:

- a control analysis, without any FASTEX data;
- a perturbed analysis, obtained by adding to the control one the data from those dropsondes deployed in regions highlighted as sensitive by SVs.

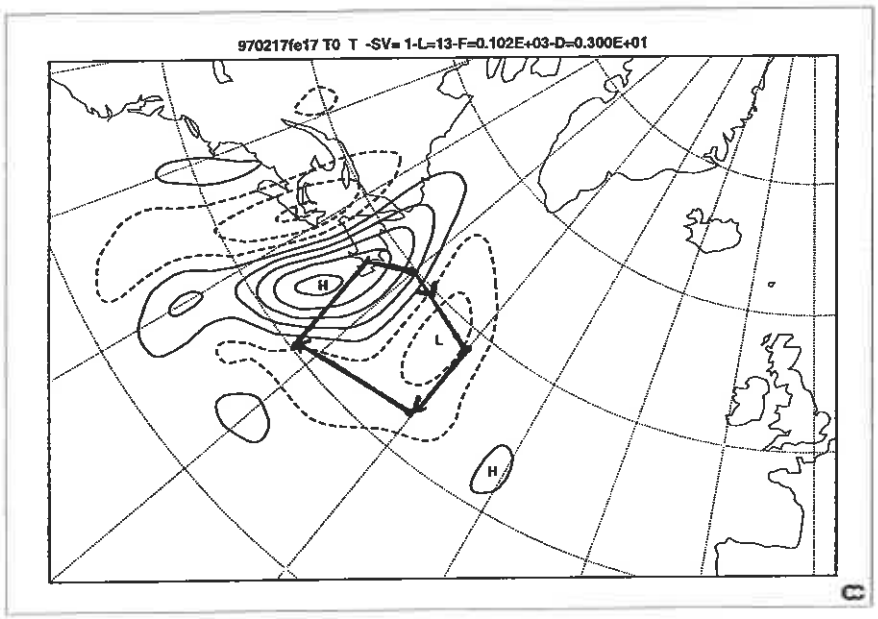

Figure 1: SV=1 valid at 18Z of 17 February 1997, plotted in terms of temperature (contour interval: 0.03 °C) at around 700 hPa (solid and dashed contours), overlapped with the flight track (thick black line) of the Gulfstream IV (take off at 15Z, landing at 20.30Z in St John's Newfoundland); the verification area extends between 50–65N and 0–20W.

Reruns of the model from both analysis were performed to assess the impact of the extra–data on forecast skill. Fig.1 shows, as an example, the sensitive region indicated by the most amplifying SV (SV=1), overlapped with the flight track of the research aircraft Gulfstream IV, during IOP 17. The data from the dropsonde deployed were used as extra–information to prepare the perturbed analysis.

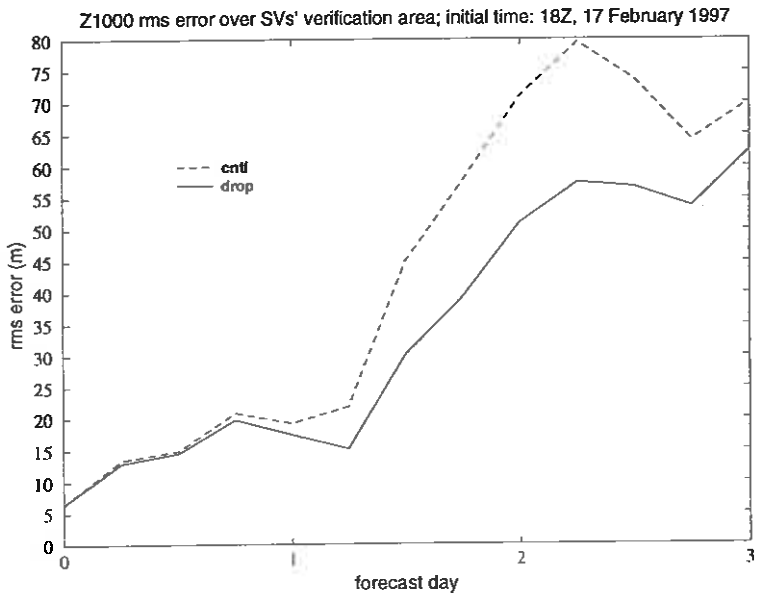

Figure 2: Root–mean–square errors of the 1000 hPa geopotential height (in metres) over the SVs' verification region (50–65N, 0–20 W), comparing the forecast without any FASTEX data (marked "cntl", dashed line) to the one with the Gulfstream IV data included (marked "drop", solid lines). Both forecasts start at 18Z of 17 February 1997.

The skill of each forecast is *objectively* assessed in fig.2, where the root–mean–square forecast errors in geopotential height at 1000 hPa are shown for the control case and for the dropsonde rerun.

The error is reduced when the dropsonde data are included in the initial analysis.

Fig.3 considers all the case studies and presents a scatter plot of the root–mean–square errors of the geopotential height at 1000 and 500 hPa for the forecasts without (y–axis) and with (x–axis) the inclusion of additional dropsondes. Although there are some negative impact points on the plot, the substantial positive impact of the dropsonde data released in sensitive regions (according to SVs) is evident.

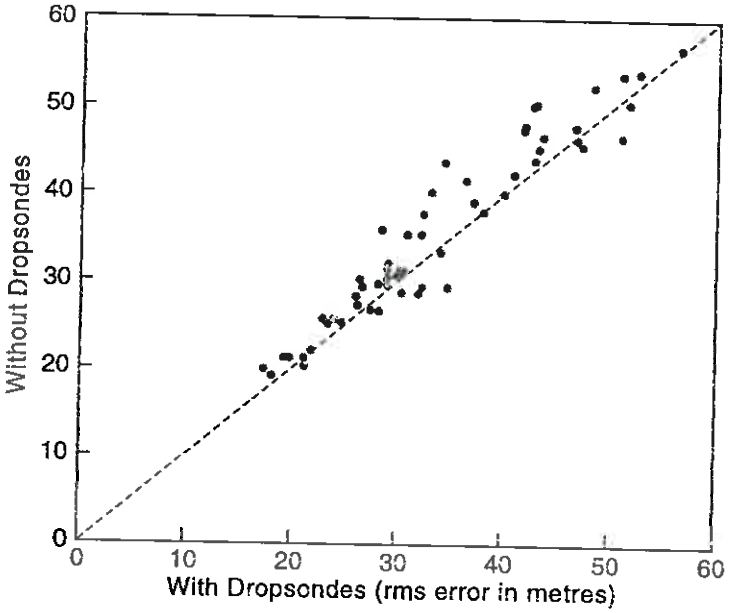

Figure 3: Scatter plots with all the rerun forecasts of the 1000 and 500 hPa root–mean–square errors (in metres). These are plotted to compare the errors for forecasts without (y–axis, marked "Without Dropsondes") and with (x–axis, marked "With Dropsondes") the inclusion of the additional dropsondes for forecast time–periods of 48, 60 and 72 hours, verifying over Europe and North Atlantic.

SV DYNAMICS

Are SVs well–balanced perturbations?

Vertical profiles of the ratio of the horizontal average of the modulus of divergence ($|D|$) to the horizontal average of the modulus of vorticity ($|V|$) show the balance properties of SVs.

Fig.4 shows that SVs have initially an intense component in divergence in the lower troposphere, indicating a lack of such balance. At final time, the evolved perturbations have a more balanced structure, with a vertical profile more similar to that of the basic state.

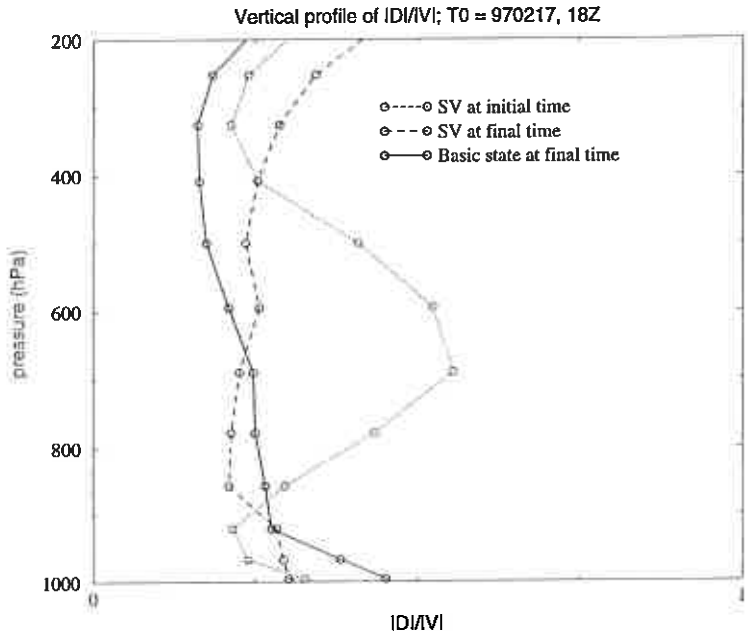

Figure 4: Vertical profiles of the ratio between the horizontal averages of the modulus of divergence and vorticity for SV=1 at initial time (valid at 18Z of 17 February 1997, dotted line), for the same SV at final time (12Z of 19 February 1997, dashed line) and for the basic state at final time (solid line).

Application of potential vorticity diagnostics to SV

Potential vorticity (PV) concepts have been applied to determine the most dynamically active regions for a perturbation to grow.

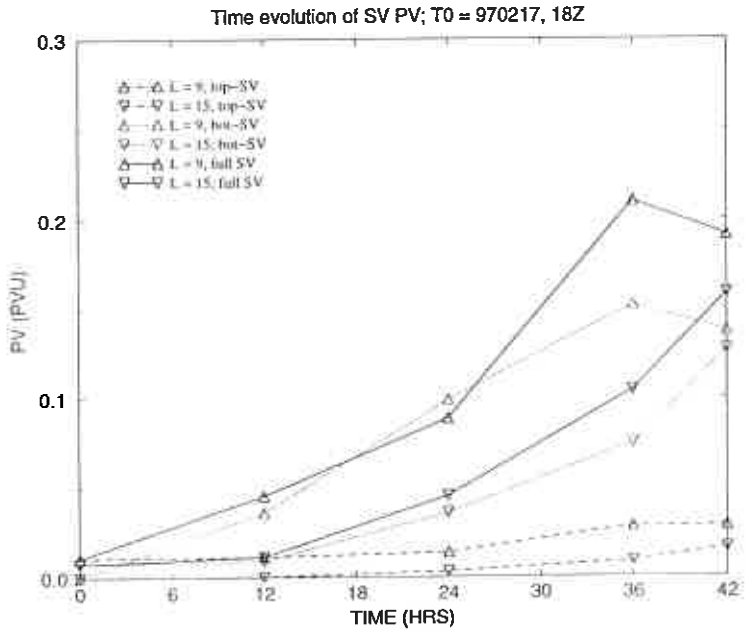

Figure 5: Time evolution (every 6 hours) of the modulus of PV maximum (in PVU) at model levels 9 (located approximately at 325 hPa, points denoted with Δ) and 15 (850 hPa, denoted with ∇) for the full SV (solid lines), for the "top–SV" (dashed lines) and for the "bot–SV" (dotted lines). Initial time: 18Z of 17 February; final time: 12Z of 19 February.

The time evolutions of the upper and lower parts (fig.5) indicate that SVs initially confined in the lower troposphere, grow behaving almost exactly as the full perturbation, increasing the amount of PV mainly at the tropopause. If a low–level PV anomaly in the basic state interacts with the SV, great perturbation growth in PV is experienced also in the lower troposphere (dotted trend). On the other hand, SVs initially confined in the upper troposphere (and stratosphere) propagate maintaining a nearly constant amplitude (dashed trend).

CONCLUSIONS

During FASTEX, additional observations were taken in target zones defined by SV calculation. These data, when included in ECMWF forecast reruns, provided a significant reduction in root–mean–square errors of the height of pressure surfaces.

SVs do not appear to be well-balanced perturbations at initial time, although, during their time evolution, they tend to achieve a more balanced configuration.

SVs, plotted in terms of PV, indicate that their lower–tropospheric portion is mainly responsible for the mechanisms of perturbation PV growth.

WHATEVER HAPPENED TO STABILITY THEORY?

Andy White Met Office/JCMM

• *STABILITY ANALYSES* of simple, steady flows have been an active area of theoretical fluid dynamics since the times of Reynolds and Rayleigh. To this day, the subject area attracts great interest amongst students and researchers in meteorology; the residence time of P G Drazin and W H Read's *Hydrodynamic Stability* in the Departmental library may be measured in hours rather than days.

• *THE GRAND ERA* of linear instability theory in meteorology followed publication of the famous papers by J G Charney (1947) and E T Eady (1949). Eady's paper was particularly influential because it addressed a problem which can be solved analytically in the quasi-geostrophic (QG) approximation. *A steady, stably-stratified, incompressible flow, in thermal-wind balance with a constant meridional temperature gradient, is subjected to wave-like, normal mode perturbations confined by two rigid, horizontal boundaries.* Eady's problem gave maximum instability to horizontal wavelengths of perturbation similar to those of mid-latitude, synoptic-scale weather systems, and with eigenstructures of a synoptically reasonable form. It also accounted convincingly for the transition from axisymmetric to wavy flow in the rotating annulus; see Hide and Mason (1975; Advances in Geophysics).

• *AN OUTPOURING* of papers followed Charney's and Eady's work; signs of decline became evident only after 30 years or so (see below). Amongst sophistications introduced to the basic problem were:

- *lateral shear and more realistic profiles of static stability in the unperturbed state;*
- Ekman or internal friction, and other physical processes, acting on the perturbations;
- *use of spherical geometry and more comprehensive dynamical equations (e.g. hydrostatic primitive equations instead of QG);*
- weak nonlinearities (studied analytically);
- *strong nonlinearities (studied numerically);*
- instability of wavy unperturbed states.

[See Hide and Mason (1975), Simmons and Hoskins (1978; *JAS*), Pedlosky (1987; *GFD*), Frederiksen (1989; *JAS*), Hartmann and Zuercher (1998; *JAS*)]

• ***In the 1980s and 1990s there was a perceptible decrease in the number of published papers on baroclinic instability***:

J Atmos Sci carried 15 papers on baroclinic instability in 1977, 10 in 1987, and only 7 in 1997.

WHY DID THIS HAPPEN ?

Read on for possible explanations !

THREE FACTORS OPERATED

1. **All done?** By the end of the 1970s a majority of the meteorologically-relevant instability problems had been solved (it was fondly supposed), so a fall-off in the rate of publication was only to be expected.

2. **So what?** It began to be appreciated that the implications of instability analyses could easily be overstated. Showing that a flow is highly unstable accounts for its non-occurrence in practice, but what else can you really deduce from the result that a particular wave grows with a short e-folding time? *How would the atmosphere in reality ever reach such a supercritical state?* Instability analyses are thought experiments in which a steady flow is set up, a perturbation is applied, and you ask what happens next. The real atmosphere, of course, does not work like this - it is in a state of continuous evolution (even when you are not thinking about it).

3. **A la mode?** Many workers had been aware during the 1960s and 1970s that the baroclinic (and barotropic) instability problems were not spanned by the *normal mode* solutions which most studies sought; a *continuous spectrum* of non-modal solutions exists too. This situation can be related to the *non-self-adjointness* of the relevant differential operators (at least within the usual Eulerian framework). The implications were not, however, widely appreciated until the 1980s. *Locally (in space and time) the fastest-growing perturbations may not be, and usually are not, of normal mode form;* only in the long-time limit - when linear theory is no longer applicable - do the normal modes dominate. B. Farrell made the importance of this point especially clear in a paper in *J Atmos Sci* in 1985: he found significant transient growth in a baroclinic instability problem in which (because of the influence of Ekman friction) *no unstable normal modes existed.* The ramifications have yet to be worked out fully. In general theoretical terms there are important issues to be confronted; in specific terms, the best that can be done about most of the instability analyses published in the 1960s and 1970s is to issue a retrospective health warning. [Farrell's many papers in *J Atmos Sci* give a comprehensive account of the situation; see North (1984) and especially Held (1985), both also in *JAS*, for theoretical background and insight.]

Factors 2 and 3 re-inforced one another to some extent. They made it clear that new approaches to instability theory were needed.

CURRENT USES OF INSTABILITY THEORY

• *Factors 1, 2, and 3 have led to a more restrained use of instability theory in meteorology since the headlong career of the 1950s, 1960s and 1970s.*

• *From* Factor 2 *has grown a line of study which seeks to demonstrate the zonal mean atmosphere's proximity to a threshold of stability, and to rationalize the behaviour of the atmosphere in these terms.* This began with P H Stone's baroclinic adjustment paper (1978; *JAS*) and has continued with work by R S Lindzen, P D Sardeshmukh and others (see *JAS*).

• *From Factor 3 has grown the application of the theory of non-self-adjoint operators to meteorology:*

♦ ECMWF use linear adjoint operator theory to define perturbed initial conditions for their Ensemble Prediction System (EPS). *The spatial pattern is sought that gives fastest* linearised *departure from the reference evolution according to some chosen norm.* Then the spatial pattern giving next fastest departure from the reference evolution is found by requiring orthogonality to the pattern found previously - and so on. See Buizza (1994; *QJ*).

♦ ECMWF (and other forecasting centres) use similar adjoint theory in *4D Variational Data Assimilation* (4DVar) to find the choice of initial conditions which minimises the departure of the time evolution from the observations during some time window, according to some chosen norm. The use of linear theory is evidently less critical in the 4DVar context than in the EPS context. See Errico (1997; *Bull AMS*).

• *In summary, the answer to the question in the title of this poster is:*

After a long and perhaps self-indulgent adolescence in meteorology, linear stability theory in its adult years is playing a more focused role in furthering understanding of the atmosphere's general circulation, and is being really useful in ensemble forecasting and data assimilation for NWP.

It is interesting to speculate on whether meteorology would have taken to adjoint theory more or less readily in the 1980s and 1990s if there had not been a tradition of linear stability analysis in the subject. *Did an incomplete view of instability theory help or hinder acceptance of adjoint methods ?*

CURRENT JCMM INTERNAL REPORTS

This series of JCMM Internal Reports, initiated in 1993, contains unpublished reports and also versions of articles submitted for publication. The complete set of Internal Reports is available from the National Meteorological Library on loan, if required.

1. **Research strategy and programme**
   K A Browning et al
   January 1993

2. **The GEWEX Cloud System Study (GCSS)**
   GEWEX Cloud System Science Team
   January 1993

3. **Evolution of a mesoscale upper tropospheric vorticity maximum and comma cloud from a cloud-free two dimensional potential vorticity anomaly**
   K A Browning
   January 1993

4. **The global energy and water cycle**
   K A Browning
   July 1993

5. **Structure of a midlatitude cyclone before occlusion**
   K A Browning and N Roberts
   July 1993

6. **Developments in systems and tools for weather forecasting**
   K A Browning and G Szejwach
   July 1993

7. **Diagnostic study of a narrow cold frontal rainband and severe winds associated with a stratospheric intrusion**
   K A Browning and R Reynolds
   August 1993

8. **Survey of perceived priority issues in the parametrizations of cloud-related processes in GCMs**
   K A Browning
   September 1993

9. **The effect of rain on longwave radiation**
   I Dharssi
   September 1993

10. **Cloud microphysical processes - a description of the parametrization used in the large eddy model**
    H Swann
    October 1993

11. **An appreciation of the meteorological research of Ernst Kleinschmidt**
    A J Thorpe
    May 1992

12. **Potential vorticity of flow along the Alps**
    A J Thorpe, H Volkert and Dietrich Heimann
    August 1992

13. **The representation of fronts**
    A J Thorpe
    January 1993

14. **A parametrization scheme for symmetric instability: test for an idealised flow**
C S Chan and A J Thorpe
February 1993

15. **The Fronts 92 Experiment: a Quicklook Atlas**
Edited by T D Hewson
November 1993

16. **Frontal wave stability during moist deformation frontogenesis**
Part 1: Linear wave dynamics
C H Bishop and A J Thorpe
May 1993

17. **Frontal wave stability during moist deformation frontogenesis**
Part 2. The suppression of non-linear wave development
C H Bishop and A J Thorpe
May 1993

18. **Gravity waves in sheared ducts**
S Monserrat and A J Thorpe
October 1993

19. **Potential vorticity and the electrostatics analogy: quasi-geostrophic theory**
C Bishop and A J Thorpe
November 1993

20. **Recent advances in the measurement of precipitation by radar**
A J Illingworth
April 1993

21. **Micro-physique et givrage: cloud microphysics and aircraft icing**
A J Illingworth
May 1993

22. **Differential phase measurements of precipitation**
M Blackman and A J Illingworth
May 1993

23. **Estimation of effective radius of cloud particles from the radar reflectivity**
N I Fox and A J Illingworth
May 1993

24. **A simple method of Dopplerising a pulsed magnetron radar**
A Hua, A J Illingworth and J Eastment
November 1993

25. **Radiation and polar lows**
George C Craig
February 1994

26. **Collected preprints submitted to the International Symposium on the Life Cycles of Extratropical Cyclones; Bergen, Norway, 27 June - 1 July 1994**
April 1994

27. **Convective frontogenesis**
Douglas J Parker and Alan J Thorpe
April 1994

28. **Improved measurement of the ice water content in cirrus using a total water evaporator**
Philip R A Brown and Peter N Francis
April 1994

29. **Mesoscale effects of a dry intrusion within a vigorous cyclone**
K A Browning and B W Golding
April 1994

30. **GEWEX Cloud System Study, Science Plan**
May 1994

31. **Parametrization of momentum transport by convectively generated gravity waves**
R Kershaw
May 1994

32. **Mesoscale Modelling Newsletter No 5**
May 1994

33. **Observations of the mesoscale sub-structure in the cold air of a developing frontal cyclone**
K A Browning, S A Clough, C S A Davitt, N M Roberts and T D Hewson
May 1994

34. **Longwave radiative forcing of a simulated tropical squall line**
Imtiaz Dharssi
July 1994

35. **On the nature of the convective circulation at a kata-cold front**
K A Browning
September 1994

36. **Collective preprints of papers submitted to the COST-75 International Seminar on Advanced Weather Radar Systems, Brussels, 20-23 September 1994**
November 1994

37. **Use of satellite imagery to diagnose events leading to frontal thunderstorms: Parts I and II of a case study**
K A Browning and N M Roberts
November 1994

38. **The role of spaceborne millimetre-wave radar in the global monitoring of ice cloud**
P R A Brown, A J Illingworth, A J Heymsfield, G M McFarquhar, K A Browning and M Gosset
December 1994

39. **Potential vorticity inversion**
Michal Ziemianski
October 1994

40. **Theory of mature tropical cyclones; a comparison between Kleinschmidt (1951) and Emanuel (1986)**
Suzanne L Gray
December 1994

41. **Dispersion and removal of pollutants during the passage of an atmospheric frontal system**
N R Gimson
December 1994

42. **The role of snow sublimation in frontogenesis**
D J Parker and A J Thorpe
December 1994

43. **Potential vorticity and the electrostatics Analogy: Ertel-Rossby formulation**
A J Thorpe and C H Bishop
December 1994

44. **Mesoscale aspect of extratropical cyclones: an observational perspective**
K A Browning
January 1995

45. **A polar low outbreak: evolution and mesoscale structures**
T D Hewson, G C Craig and C Claud
February 1995

46. **Generation of near-surface gusts of deep convection**
K Nakamura and R Kershaw
April 1995

47. **Attribution concepts applied to the Omega Equation**
S A Clough, C S A Davitt and A J Thorpe
June 1995

48. **Parametrization of mixed-phase cloud and precipitation**
Susan P Ballard and M Gerard Hutchinson
June 1995

49. **Short-range forecasting of stratocumulus: initialization prediction**
Susan P Ballard, Simon D Jackson and B Macpherson
June 1995

50. **Contributions of the JCMM/Dept of Meteorology Radar Group to the 27th AMS Radar Meteorology Conference, Vail October 1995**
June 1995

51. **Cold pools in shear**
Douglas J Parker
September 1995

52. **High-resolution analysis of frontal fracture**
K A Browning, S P Ballard and C S A Davitt
September 1995

53. **The albedo of broken cloud fields: calculations using a modified two stream radiation code**
Imtiaz Dharssi and Roy Kershaw
October 1995

54. **Parametrization of momentum transport by convection. I: theory and cloud modelling results**
R Kershaw and D Gregory
November 1995

55. **Variation of frontal structure along a cold front**
K A Browning and N M Roberts
November 1995

56. **Secondary frontal waves**
Douglas Parker
December 1995

57. **Objective fronts**
T D Hewson
March 1996

58. **Mesoscale analysis of the activation of a cold front during cyclogenesis**
K A Browning, N M Roberts and A J Illingworth
June 1996

59. **Investigation of different representations of rain in a 1-d evaporation model**
H Swann
May 1996

60. **Parametrization of diabatic processes in the inversion of the omega-equation**
M Athanassiadou and A J Thorpe
June 1996

61. **The role of the environmental flow in the development of secondary frontal cyclones**
I A Renfrew, A J Thorpe and A Joly
June 1996

62. **Consequences of the geostrophic momentum approximation on barotropic instability**
S Malardel, A J Thorpe and A Joly
June 1996

63. **Contributions to the AMS/RMS Conference on Mesoscale Processes**
Reading, 9-13 September 1996

64. **Vorticity and potential vorticity in stratified flows interacting with an isolated obstacle**
Jorge A Gutiérrez and A J Thorpe
September 1996

65. **Triple point development: two case studies**
Douglas Parker
September 1996

66. **Radar observations of wind-shear splitting within evolving atmospheric Kelvin-Helmholtz billows**
D Chapman and K A Browning
April 1997

67. **Cold frontal structure derived from radar wind profilers**
K A Browning, D Jerrett, J Nash, T Oakley and N M Roberts
May 1997

68. **The dry intrusion and its effect on the frontal, cloud and precipitation structure of extratropical cyclones**
K A Browning - Text of invited special lecture at the Spring Conference
of the Meteorological Society of Japan, University of Tsukuba, 22 May 1997

69. **Met. Office Unified Model data, diagnostics, graphics programs, and other observational data available from the JCMM through the aegis of the Universities Weather Research Network (UWERN).** (Plus supplement)
Peter Panagi and Ed Dicks
June 1997

70. **Contributions of the JCMM/Dept of Meteorology Radar Group to the 28th AMS Radar Meteorology Conference.** Austin, Texas
September 1997

71. **Sensitivity of short-range weather forecasts to local potential vorticity modifications**
Meral Demirtas and Alan Thorpe
July 1997

72. **Objective identification of frontal wave cyclones**
T D Hewson
August 1997

73. **Attribution and its application to mesoscale structure associated with tropopause folds**
A J Thorpe
September 1997

74. **The role of the environmental flow in the development of secondary frontal cyclones**
Ian A Renfrew, Alan J Thorpe and Craig H Bishop
September 1997

75. **Potential vorticity: a short history of its definitions and uses**
Alan J Thorpe and Hans Volkert
September 1997

76. **Superposing semi-geostrophic potential vorticity anomalies**
H R Birkett and A J Thorpe
September 1997

77. **Short period forecasting of catchment-scale precipitation.**
Part 1: the role of Numerical Weather Prediction
M A Pedder, M Haile and A J Thorpe
September 1997

78. **Verification of the tracking technique used in an experimental cloud motion wind inferring system**
Z Wang, K A Browning and G A Kelly
October 1997

79. **A preliminary study of Fourier series analysis for cloud tracking with GOES high temporal resolution images**
Z Wang
October 1997

80. **Analysis of an ex-tropical cyclone after reintensifying as a warm-core extratropical cyclone**
K A Browning, G Vaughan and P Panagi
November 1997

81. **A JCMM overview of FASTEX IOPs**
S A Clough, H W Lean, N M Roberts, H Birkett, J-P Chaboureau, R Dixon, M Griffiths, T D Hewson and A Montani
January 1998

82. **Programs for PV inversion and modification**
Meral Demirtas
December 1997

83. **Release of potential shearing instability in warm frontal zones**
D Chapman and K A Browning
February 1998

84. **The European Cloud-Resolving Modelling Programme (EUCREM)**
Summary Report from the coordinator
P W White
April 1998

85. **A frontal wave database**
T D Hewson
April 1998

86. **Layering observed in dropsoundings from IOP 1 of Fronts 92**
S A Clough
May 1998

87. **Use of wind-shear displays for Doppler radar data**
D Chapman and K A Browning
May 1998

88. **Radar estimates of rainfall rates at the ground in bright band and non-bright band events**
T J Smyth and A J Illingworth
June 1998

89. **Correction for attenuation of radar reflectivity using polarisation data**
T J Smyth and A J Illingworth
June 1998

90. **The effects of convection on chemical reactions and precipitation scavenging**
Neil R Gimson
July 1998

91. **How to use the display program DISP**
Nigel Roberts
August 1998

92. **Conceptual models of cyclogenesis**
Adrian T Semple
August 1998

93. **Observations of oblate hail using dual polarisation radar and implications for hail detection schemes**
T J Smyth, T M Blackman and A J Illingworth
September 1998

94. **The semigeostrophic diagnosis of vertical motion. Part I: Formulation and co-ordinate transformations**
Mike A Pedder and Alan J Thorpe
September 1998

95. **The semigeostrophic diagnosis of vertical motion. Part II: Results for an idealised baroclinic wave life cycle**
Alan J Thorpe and Mike A Pedder
September 1998

96. **Convective destabilisation by a tropopause fold diagnosed using potential vorticity inversion**
Morwenna Griffiths, Alan Thorpe and Keith Browning
October 1998

97. **Forecast skill of the ECMWF model using targeted observations during FASTEX**
A Montani, A J Thorpe, R Buizza and P Unden
October 1998

98. **Observations and model simulations of the FASTEX IOP 16 frontal wave - effects of sublimation**
Sid A Clough, Humphrey W Lean, Nigel M Roberts and Richard M Forbes
December 1998

99. **The application of conceptual models in NWP**
Adrian T Semple
January 1999

100. **Mesoscale analysis of arc rainbands in a dry slot**
K A Browning and N M Roberts
January 1999

101. **Interaction of mesoscale tropopause depressions with a warm-core cyclone: observational and model analyses, and sensitivity to analysis errors**
K A Browning, A J Thorpe, A Montani, D Parsons, M Griffiths, P Panagi and E M Dicks
February 1999

102. **Use of water vapour imagery and PV inversion to adjust initial conditions in NWP**
Sean J Swarbrick
February 1999

103. **Summary notes for a lecture course on Waves in the Atmosphere and Ocean**
A A White
March 1999

104. **Results of a questionnaire on the operational value of conceptual models (CMs) of fronts and cyclones**
N M Roberts & M V Young
July 1999

105. **Contributions to the Poster Session at the 1998 UWERN Annual Science Meeting**
assembled by A A White
August 1999

Met Office Joint Centre for Mesoscale Meteorology Department of Meteorology
University of Reading PO Box 243 Reading RG6 6BB United Kingdom
Tel: +44 (0)118 931 8425 Fax: +44 (0)118 931 8791
www.metoffice.com